

A Novel Role for RalA in Regulating Lipid Droplets during Nutrient Starvation

Syed Saad Hussain  
Chantilly, VA

B.A. in Biology and Economics, University of Virginia, 2014

A dissertation presented to the Graduate Faculty of the University of Virginia in Candidacy  
for the Degree of Doctor of Philosophy

Department of Microbiology, Immunology and Cancer Biology

University of Virginia

August 2021

## Abstract

The Ras-related small-GTPase RalA is involved in a number of cellular processes including membrane dynamics, vesicular trafficking, and filipodia formation. When membrane associated, RalA localizes to a number of cellular compartments including the plasma membrane, endosomes, mitochondria and lipid droplets. Unlike with the rest of these organelles, the functional relationship between RalA and lipid droplets remains unexplored. Lipid droplets are organelles that store excess cellular fatty acids (FAs) in the form of triacylglycerides and cholesterol esters. Far from being mere intracellular depots, lipid droplets are dynamic organelles and recent studies have highlighted their important role during nutrient deprivation. Amino acid starvation in MEFs and HeLa cells results in the induction of autophagy, a process that cells utilize to recycle their metabolic and structural building blocks. Autophagy liberates fatty acids from unwanted membranes for use as energy through  $\beta$ -oxidation. These fatty acids are cytotoxic if left in the cytosol and, therefore, are temporarily sequestered into lipid droplets that accumulate without harming the cell. Thus, lipid droplets play the critical role of protecting the cell from the cytotoxic effects of fatty acids while concurrently facilitating quick access to an energy source. Lipid droplets are found in most eukaryotic cells, all of which must be able to store excess FAs and utilize them on demand. However, the regulation of lipid droplets, including the mechanism of formation and growth is not fully understood.

The work in this dissertation identifies RalA as an important regulator of lipid droplets. RalA is required for lipid droplet growth during nutrient depletion. We find that RalA acts downstream of autophagy during nutrient starvation to directly facilitate lipid droplet growth. Mechanistically, RalA performs this function through phospholipase D1 (PLD1), an enzyme that converts phosphatidylcholine (PC) to phosphatidic acid (PA). We report that PLD1 is recruited to lysosomes during nutrient stress in a RalA-dependent fashion. Our data indicate

that PLD1 is necessary for local PA production at the lysosome, a function necessary for lipid droplet growth during nutrient starvation. Additionally, we find that RalA promotes lipid droplet growth by facilitating the recruitment of the lipid droplet associated protein, perilipin 3, onto growing droplets. RalA and PLD1 inhibition prevents perilipin 3 recruitment onto lipid droplets, which associates with membranes in a PA-dependent fashion and is required for LD growth. Collectively, the data presented in this thesis support a model in which RalA recruits PLD1 to lysosomes during nutrient deprivation to promote the localized production of phosphatidic acid and the subsequent recruitment of perilipin 3 to expanding lipid droplets.

## **TABLE OF CONTENTS**

<b>CHAPTER 1: INTRODUCTION TO RALA, PLD1 AND LIPID DROPLETS</b> .....	<b>13</b>
<b>1.1 DISCOVERY OF RAL</b> .....	<b>13</b>
<b>1.2 RAL PROTEIN STRUCTURE</b> .....	<b>14</b>
<b>1.3 RAL LOCALIZATION</b> .....	<b>14</b>
<b>1.4 REGULATION OF RAL ACTIVITY</b> .....	<b>15</b>
<b>1.5 RAL EFFECTORS AND INTERACTING PARTNERS</b> .....	<b>17</b>
<b>1.5.1 RalBP1</b> .....	<b>17</b>
<b>1.5.2 Sec5 and Exo84</b> .....	<b>18</b>
<b>1.5.3 Phospholipase D1</b> .....	<b>19</b>
<b>1.5.4 Other Interactors</b> .....	<b>21</b>
<b>1.6 RAL POSTTRANSLATIONAL MODIFICATIONS</b> .....	<b>22</b>
<b>1.6.1 CAAX Motif</b> .....	<b>23</b>
<b>1.6.2 Phosphorylation</b> .....	<b>24</b>
<b>1.6.3 Ubiquitination</b> .....	<b>25</b>
<b>1.7 RAL CELLULAR FUNCTIONS</b> .....	<b>26</b>
<b>1.8 LIPID DROPLET BACKGROUND</b> .....	<b>28</b>
<b>1.8.1 LD Biogenesis and Growth</b> .....	<b>28</b>
<b>1.8.2 LD breakdown</b> .....	<b>33</b>
<b>1.9 LIPID DROPLET CONTACT SITES WITH OTHER ORGANELLES</b> .....	<b>35</b>
<b>1.10 LIPID DROPLETS AND RALA</b> .....	<b>38</b>
<b>1.11 LIPID DROPLETS AND PLD1</b> .....	<b>39</b>
<b>1.12 LIPID DROPLETS AND THE CELLULAR STRESS RESPONSE</b> .....	<b>41</b>
<b>1.12.1 Oxidative stress</b> .....	<b>42</b>
<b>1.12.2 Pathogen infection</b> .....	<b>43</b>
<b>1.12.3 Nutrient stress</b> .....	<b>44</b>
<b>CHAPTER 2: RALA AND PLD1 PROMOTE LIPID DROPLET GROWTH IN RESPONSE TO NUTRIENT WITHDRAWAL</b> .....	<b>52</b>
<b>2.1 INTRODUCTION</b> .....	<b>52</b>
<b>2.2 RESULTS</b> .....	<b>53</b>
<b>2.2.1 RalA is required for starvation-induced lipid droplet accumulation</b> .....	<b>53</b>
<b>2.2.2 Triacylglyceride levels increase in a RalA dependent manner during nutrient starvation</b> .....	<b>54</b>
<b>2.2.3 RalA acts downstream of autophagy in starvation-induced LD accumulation</b> .....	<b>55</b>

2.2.4	<i>PLIN3 recruitment to LDs during nutrient starvation is dependent on RalA</i>	57
2.2.5	<i>PLD1 is required for RalA dependent starvation-induced LD accumulation</i>	59
2.2.6	<i>RalA recruits PLD1 to lysosomes during nutrient stress</i>	62
2.2.7	<i>Enrichment and depletion of PA at lysosomes impacts LD accumulation and PLIN3 redistribution</i>	64
2.3	DISCUSSION	66
2.4	MATERIALS AND METHODS	71
2.4.1	<i>Chemicals</i>	71
2.4.2	<i>Cell Culture</i>	71
2.4.3	<i>Western Blotting</i>	71
2.4.4	<i>Immunofluorescence</i>	72
2.4.5	<i>Image Analysis</i>	73
2.4.6	<i>Transfection and Constructs</i>	73
2.4.7	<i>Knockdowns and Knockouts</i>	74
2.4.8	<i>Fatty Acid Pulse Chase Assay</i>	75
2.4.9	<i>Oleic Acid Stimulation</i>	75
2.4.10	<i>Ral GTP Pulldown</i>	76
2.4.11	<i>Lipid Extraction</i>	76
2.4.12	<i>LC-MS/MS Analysis of Lipid Extracts</i>	77
2.4.13	<i>Lipid Species Identification from LC-MS/MS Analysis</i>	77
2.4.14	<i>Electron Microscopy</i>	78
2.4.15	<i>Quantification and Statistical Analysis</i>	78
CHAPTER 3:	PERSPECTIVES AND FUTURE DIRECTIONS	106
3.1	INTRODUCTION	106
3.2	IDENTIFYING HOW RALA SENSES NUTRIENT STARVATION	106
3.3	UNCOVERING MECHANISM OF RALA TRAFFICKING TO ENDOSOMAL SYSTEM	111
3.4	ELUCIDATING THE ROLE OF PA IN STARVATION-INDUCED LD ACCUMULATION	113
3.4.1	<i>Understanding the precise function of PA in LD accumulation</i>	114
3.4.2	<i>Determining the localization of PA during nutrient starvation</i>	115
3.4.3	<i>Understanding the rationale for PA production at the lysosome</i>	117
3.4.4	<i>Determining how PA is trafficking from the lysosome to its final destination</i>	117
3.5	INVESTIGATING THE PHYSIOLOGICAL RELEVANCE OF RALA MEDIATED LD ACCUMULATION	120
3.6	INVESTIGATING THE RELEVANCE OF RALA MEDIATED LD ACCUMULATION IN CANCER CELLS	120
3.7	INVESTIGATING THE PHYSIOLOGICAL RELEVANCE OF STARVATION-INDUCED LD ACCUMULATION IN A SKELETAL MUSCLE MOUSE MODEL	123

**REFERENCES .....132**

# LIST OF FIGURES

## Chapter 1

FIGURE 1.1 RAL PROTEIN STRUCTURE.....	47
FIGURE 1.2 RAL GTP CYCLING AND REGULATORS.....	48
FIGURE 1.3 LIPID DROPLET BIOGENESIS.....	49
FIGURE 1.4 LIPID DROPLET BREAKDOWN.....	50
FIGURE 1.5 LIPID DROPLETS DURING CELLULAR STRESS.....	51

## Chapter 2

FIGURE 2.1 RALA IS REQUIRED FOR STARVATION-INDUCED LIPID DROPLET ACCUMULATION.....	80
FIGURE 2.2 WT RALA IS SUFFICIENT TO RESCUE LD ACCUMULATION IN RALA KO MEFS.....	82
FIGURE 2.3 OLEIC ACID-INDUCED LD ACCUMULATION IS NOT RALA-DEPENDENT.....	83
FIGURE 2.4 ANALYSIS OF LIPID COMPOSITION IN NUTRIENT STARVED MEFS.....	84
FIGURE 2.5 ANALYSIS OF PHOSPHOLIPID COMPOSITION IN NUTRIENT STARVED MEFS.....	85
FIGURE 2.6 AUTOPHAGY IS NECESSARY FOR RALA-DEPENDENT LD ACCUMULATION.....	86
FIGURE 2.7 AUTOPHAGY IS NOT IMPAIRED IN RALA KO MEFS.....	88
FIGURE 2.8 FATTY ACID TRAFFICKING TO THE MITOCHONDRIA IS NOT RALA-DEPENDENT.....	89
FIGURE 2.9 PLIN3 RECRUITMENT TO LDS DURING NUTRIENT STARVATION IS DEPENDENT ON RALA.....	91
FIGURE 2.10 PLIN3 IS NECESSARY FOR LD ACCUMULATION DURING NUTRIENT STARVATION.....	92
FIGURE 2.11 RALA IS NOT FUNCTIONING IN A NUCLEOTIDE-DEPENDENT MANNER DURING HBSS STARVATION.....	93
FIGURE 2.12 PLD IS REQUIRED FOR RALA-DEPENDENT STARVATION INDUCED LD ACCUMULATION.....	95
FIGURE 2.13 PLD1 RESCUES LD ACCUMULATION IN RALA KD HELA.....	96
FIGURE 2.14 RALA RECRUITS PLD1 TO LYSOSOMES DURING HBSS STARVATION.....	98
FIGURE 2.15 ER, LDS, AND LYSOSOMES COME INTO CLOSE PROXIMITY DURING HBSS STARVATION.....	100
FIGURE 2.16 FORCED PLD1 LOCALIZATION TO LDS RESCUES LD ACCUMULATION AND PLIN3 RECRUITMENT.....	102
FIGURE 2.17 ENRICHMENT AND DEPLETION OF PA AT LYSOSOMES IMPACTS LD ACCUMULATION AND PLIN3 REDISTRIBUTION.....	103
FIGURE 2.18 MODEL FOR RALA-DEPENDENT STARVATION INDUCED LD ACCUMULATION.....	105

## Chapter 3

FIGURE 3.1 KENNEDY PATHWAY FOR TRIACYLGLYCERIDE SYNTHESIS.....	123
FIGURE 3.2 MODEL FOR PHOSPHATIDIC ACID TRAFFICKING DURING NUTRIENT STARVATION.....	124
FIGURE 3.3 SKELETAL MUSCLE CONDITIONAL KO OF RALA IN MICE.....	125

TABLE 3.1 PREDICTED RALA PHOSPHORYLATION SITES AND KINASES.....	126
TABLE 3.2 PREDICTED OUTCOME OF CONDITIONAL RALA OR PLIN3 KNOCKOUT IN MICE SKELETAL MUSCLE DURING 24 HOURS OF FASTING.....	128

## LIST OF ABBREVIATIONS

AAK	Aurora-A Kinase
ACAT1	Acyl-CoA cholesterol acyltransferases 1
ACAT2	Acyl-CoA cholesterol acyltransferases 2
AGPAT	1-Acylglycerol-3-Phosphate O-Acyltransferase 3
ATGL	Adipose triglyceride lipase
BHT	Butylated hydroxy toluene
CAAX motif	C = cysteine, A = aliphatic amino acid, X = any amino acid
CaMKII	Ca <sup>2+</sup> /calmodulin-dependent protein kinase II
CCT1	Choline-phosphate cytidyltransferase 1
CE	Cholesterol Ester
CER	Ceramide
CIDE	Cell death-inducing DFFA-like effector
CMA	Chaperone-mediated autophagy
CME	Clatherin-mediated endocytosis
CST	Cell Signaling Technology
DAG	Diacylglycerides
DGAT1	Diacylglycerol acyltransferases 1
DGAT2	Diacylglycerol acyltransferases 2
DMEM	Dulbecco's modified eagle medium
eLD	Expanding LD
ER	Endoplasmic reticulum
FA	Fatty Acid
FBS	Fetal bovine serum
FIT2	Fat storage-inducing transmembrane 2
GGTaseI	Geranylgeranyltransferase-I
GPAT	Glycerol-3-phosphate acyltransferase
GSK3	Glycogen synthase kinase 3

HBSS	Hank's balanced salt solution
HCV	Hepatitis C virus
HIF	Hypoxia-inducible factor
HIG2	Hypoxia-inducible protein 2
HSL	Hormone sensitive lipase
ICMT	Isoprenylcysteine carboxyl methyltransferase
iLD	Initial LD
IPTG	Isopropyl $\beta$ - d-1-thiogalactopyranoside
KO	Knockout
LAL	Lysosomal acid lipase
LC-MS	Liquid chromatography-mass spectrometry
LD	Lipid Droplet
LIMP2	Lysosomal integral membrane protein-2
LPA	Lysophosphatidic acid
LTP	Lipid transfer protein
MAG	Monoacylglyceride
MCK	Muscle creatine kinase
MCS	Membrane contact sites
MFN2	Mitofusin 2
MGL	Monoacylglycerol lipase
MIGA2	Mitoguardian 2
MVB	Multivesicular bodies
NSCLC	Non-small cell lung cancer
NVJ	Nucleus-vacuole junction
OSBP	Oxysterol binding protein
PA	Phosphatidic Acid
PC	Phosphatidylcholine
PE	Phosphatidylethanolamine
PH	Pleckstrin homology

PI	Phosphatidylinositol
PKA	Protein Kinase A
PKC $\alpha$	Protein kinase C $\alpha$
PLD1	Phospholipase D1
PLD2	Phospholipase D2
PLIN1	Perilipin 1
PLIN2	Perilipin 2
PLIN3	Perilipin 3
PS	Phosphatidylserine
PTM	Post-translational modification
PX	Phos homology
RA	Ras association
RalA	Ras related protein A
RalB	Ras related protein B
RalBP1	Ral binding protein 1
RalGAP	Ral-specific GTPase activating protein
RalGEF	Ral-specific guanine exchange factor
RCE1	Ras converting enzyme 1
Red C12	BODIPY 558/568
REM	Ras exchanger motif
SE	Sterol Ester
sgRNA	Single guide RNA
shRNA	Short hairpin RNA
SI	Switch I
SII	Switch II
siRNA	Small interfering RNA
SM	Sphingomyelin
STARD3	StAR-related lipid transfer domain-3
STR	Short tandem repeat

STX17	Syntaxin17
TAG	Triacylglycerides
VAP	Vamp-associated proteins
VPS13	Vacuolar protein sorting-associated protein 13A
WAT	White adipose tissue
WT	Wild-type

## **Chapter 1: Introduction to RalA, PLD1, and Lipid Droplets**

The primary aim of this thesis is to characterize a newly discovered role for the small GTPase RalA in regulating lipid droplets (LD, LDs for plural) during nutrient stress. I will begin this chapter by providing background on RalA and, when necessary, its paralog RalB. Next, I will provide background on an interacting partner of RalA, Phospholipase D1 (PLD1), which has been identified in this thesis to work together with RalA in regulating LDs. Subsequently, I will discuss background on LDs and follow that with a review of the cellular response to stress. I will conclude this chapter with an overview of the goals and significance of this thesis dissertation.

### **1.1 Discovery of Ral**

RalA and RalB are closely related proteins that comprise the Ras-like (Ral) branch of the Ras superfamily of small GTPases. The *Ral* gene was initially discovered in 1986 in a simian cDNA library screen used to identify new *Ras* family members (Chardin and Tavitian, 1986). Chardin and Tavitian used seven amino acids that were conserved across known Ras proteins to design a 20-mer oligonucleotide used to probe a simian B-lymphocyte cDNA library (Chardin and Tavitian, 1986). The human *RalA* and *RalB* genes were discovered three years later when Chardin and Tavitian used simian Ral cDNA to probe a human pheochromocytoma cDNA library (Chardin and Tavitian, 1989). Both Ral proteins share more than >50% sequence homology with Ras. *Ral* is highly conserved across all species and the two isoforms (RalA and RalB) are found in all vertebrates (Dam et al., 2011). Single Ral orthologs have been discovered in *C. elegans* (Frische et al., 2007) and *D. melanogaster* (Sawamoto et al., 1999). No Ral orthologues have been found in unicellular organisms such as yeast.

## 1.2 Ral Protein Structure

RalA and RalB share 82% protein sequence identity. Ral protein structure consists of an 11-amino acid N-terminal, a G domain, and a C-terminal hypervariable region and terminates with a CAAX motif (Figure 1.1). The 11-amino acid N-terminal of Ral is not found in Ras and is proposed to be involved in Ral binding to its interacting partner, PLD1 (Jiang et al., 1995). Like Ras, Ral contains a G domain involved in GTP/GDP binding and cycles between inactive GDP and active GTP bound states (Figure 1.2). The G domain contains switch I (SI) and switch II (SII) regions that share 100% sequence identity between RalA and RalB and change conformation based on the bound nucleotide (Fenwick et al., 2009; Nicely et al., 2004). The switch regions are important for Ral regulator and effector recognition. Ral is inefficient in exchanging GDP for GTP and hydrolyzing GTP to GDP and, thus, requires Ral-specific guanine exchange factors (RalGEFs) and GTPase activating proteins (RalGAPs) that expedite this process (Figure 1.2). When GTP bound, RalA and RalB interact with the same set of downstream effector proteins through the SI and SII regions (Fenwick et al., 2010; Gentry et al., 2014). The Ral C-terminal is termed the hypervariable region because it has 50% sequence divergence between RalA and RalB (Figure 1.1). The hypervariable region contains a number of post-translational modification (PTMs) sites including phosphorylation and ubiquitination (Figure 1.1). These PTMs regulate Ral subcellular localization and function. Ral ends with a C-terminal CAAX motif that undergoes a series of PTMs and is important for proper membrane association and trafficking. The CAAX motif of RalA and RalB are CCIL and CCLL, respectively.

## 1.3 Ral Localization

The diversity in RalA's cellular functions is highlighted by its ability to localize to a variety of cellular compartments. RalA is found on early, recycling, and late endosome (Chen et al., 2006; Gentry et al., 2015; Shipitsin and Feig, 2004). Chen and coauthors found that

RalA cofractionated with the early endosomal protein Rab4 but not with EEA1, another early endosomal marker (Chen et al., 2006). This finding is interesting because it suggests that RalA is able to differentiate between different populations of early endosomes within the cell. RalA is also found to colocalize with Rab9, a late endosomal marker as well as the lysosome (Corrotte et al., 2010; Gentry et al., 2015). RalA is also found on secretory vesicles, such as GLUT4 vesicles (Chen et al., 2007), dense core granules (Li et al., 2007; Wang et al., 2004), and synaptic vesicles (Bielinski et al., 1993; Mark et al., 1996). Additionally, RalA is commonly observed at the plasma membrane in a variety of cell types (Corrotte et al., 2010; Hazelett et al., 2011; Neyraud et al., 2012; Shipitsin and Feig, 2004). RalA can localize to the mitochondria (Kashatus et al., 2011; Pollock et al., 2019). Similar to RalA, RalB has multiple cellular localizations which include the endosome, mitochondria, plasma membrane, and autophagosomes (Bodemann et al., 2011; Corrotte et al., 2010; Martin et al., 2012; Pollock et al., 2019; Singh et al., 2019).

RalA localization is dynamic and sensitive to cellular signals and stimulation. RalA undergoes cell cycle-dependent relocalization from the endosomal pathway to cytokinetic structures including the cleavage furrow and abscission site (Chen et al., 2006). During mitosis, RalA is phosphorylated by Aurora-A Kinase, which promotes its relocalization to the mitochondria (Kashatus et al., 2011). Mitochondrial depolarization also triggers RalA recruitment (Pollock et al., 2019). RalA relocalizes to phagocytic cups upon phagocytic stimulation in macrophages (Corrotte et al., 2010).

#### **1.4 Regulation of Ral Activity**

Ral GTPases cycle between inactive GDP and active GTP bound states (Figure 1.2). As with most GTPases, Ral GDP-GTP cycling is expedited by Ral guanine nucleotide exchange factors (RalGEFs) and GTPase activating proteins (RalGAPs) (Figure 1.2). Intracellular levels of GTP are significantly higher than GDP and thus favor Ral in a GTP

bound state. RalGEFs facilitate GTP bound Ral by releasing GDP from Ral, thereby freeing up Ral G domains to bind to GTP. There are currently 7 known RalGEFs, all of which contain the consensus CDC25 homology domain found in most GEFs of the Ras G protein family (Quilliam et al., 2002). RalGEFs can be subdivided into two categories based on whether they contain a Ras association (RA) or pleckstrin homology (PH) domain. The first subcategory of RalGEFs include RalGDS, RGL1, RGL2, and RGL3, which share a common domain structure consisting of a Ras exchanger motif (REM), CDC25 homology domain and RA domain. The REM and RA domain allow RalGEFs to bind to active Ras and thus directly link Ras activity to Ral GTPases. RalGDS was the first Ral effector to be discovered in a yeast two-hybrid screen and its activity is specific to RalA and RalB (Albright et al., 1993). RGL1, RGL2, and RGL3 were subsequently discovered using similar yeast two-hybrid screens (Isomura et al., 1996; Kikuchi et al., 1994; Shao and Andres, 2000; Wolthuis et al., 1996). The second subcategory of RalGEFs include RalGPS1 and RalGPS2 which contain a CDC25 domain but lack the REM and RA domain, and thus function independent of Ras (Bruyn et al., 2000; Ceriani et al., 2007; Rebhun et al., 2000). RalGPS1 and RalGPS2 contain a PH domain that is hypothesized to be important for Ral activation. The last RalGEF, RGL4 contains the consensus CDC25 domain but lacks both the RA and PH domain (D'Adamo et al., 1997).

RalGAPs inactivate Ral activity by binding to and hydrolyzing GTP to GDP. Two RalGAPs have currently been identified, RalGAP1 and RalGAP2 (Shirakawa et al., 2009). Both RalGAPs are heterodimers consisting of a regulatory and catalytic subunit and share structural similarity to the Tsc1/Tsc2 complex, which is a GAP for Rheb GTPases. Both RalGAP1 and RalGAP2 appear to be specific for RalA and RalB (Martin et al., 2014; Shirakawa et al., 2009).

## 1.5 Ral Effectors and Interacting Partners

Ral GTPases carry out their cellular functions by interacting with downstream effectors and interacting proteins. Given that RalA and RalB share perfect sequence homology in their effector binding SI and SII region, they are able to bind to the same set of effector proteins. However, differences in Ral subcellular localization dictates which effectors each isoform is able to interact with. Ral is able to interact with its effectors when bound to GTP but can bind to other interacting proteins irrespective of its GTP status. The following will outline well-known Ral effectors and other interacting proteins.

### 1.5.1 RalBP1

Ral binding protein 1 (RalBP1) was the first Ral effector to be discovered with both a yeast two-hybrid screen as well as cDNA library screen (Cantor et al., 1995; Jullien-Flores et al., 1995). RalBP1 contains a Ral binding domain and binds to both the SI and SII region of GTP-bound Ral (Fenwick et al., 2010). Additionally, RalBP1 contains a catalytic RhoGAP domain and has GAP activity for CDC42 and Rac1 (Park and Weinberg, 1995). Ral binding to RalBP1 does not impact the RhoGAP activity *in vitro* (Park and Weinberg, 1995), however active-RalA leads to increased RalBP1 activity in cultured cells (Lim et al., 2010).

RalBP1 acts as a key effector in a number of Ral dependent cellular processes. RalA recruits RalBP1 to mitochondria during mitosis to facilitate CDK1 phosphorylation of DRP1 and subsequently promote mitochondrial fission (Kashatus et al., 2011). RalB-RalBP1 mediate invadopodium formation in pancreatic ductal adenocarcinoma cell lines through the ATPase function of RalBP1 (Neel et al., 2012). Recently, both Ral isoforms and RalBP1 were identified to be crucial for intestinal stem cell maintenance and regeneration (Johansson et al., 2019). In this study, Ral and RalBP1 were identified to promote endocytosis of the Wnt receptor and thereby lead to activation of the Wnt signaling pathway (Johansson et al., 2019). Ral-RalBP1 signaling is important for blocking endocytosis during mitosis. The mitosis

regulatory protein Cyclin B1 binds to RalBP1 during mitosis and forms a complex with Cdk1, which in turn phosphorylates Epsin and prevents endocytosis (Rossé et al., 2003). Additionally, RalBP1 is able to interact with multiple proteins involved in endocytosis, including the AP2 adapter complex and Reps1/Reps2. RalBP1 regulates NMDA receptor-dependent endocytosis of AMPA receptors during long-term depression in neurons by interacting with RalA and PSD-95 (Han et al., 2009).

RalBP1 has displayed tumorigenic and metastatic properties in a variety of cancer cells ranging from cancer cell migration, invasion, angiogenesis, and metastasis (Lee et al., 2012; Neel et al., 2012; Wu et al., 2010). RalBP1 is upregulated in various cancers including ovarian, bladder, and glioblastoma (Hudson et al., 2007; Smith et al., 2007; Wang et al., 2013). A recent study showed that RalBP1 is a target of and is negatively regulated by the microRNA mir-143-3p in A2780 ovarian cancer cells (Zhang and Li, 2016). In this study, A2780 cells were found to have elevated RalBP1 mRNA and protein expression alongside suppressed mir143-3p expression, suggesting that the negative regulation of RalBP1 is needed to prevent tumorigenesis (Zhang and Li, 2016). Knockdown or depletion of RalBP1 suppresses tumor growth in a number of cancer models (Awasthi et al., 2018; Bose et al., 2020; Lee et al., 2012; Singhal et al., 2011). Thus, RalBP1 has the potential to be an important therapeutic target for multiple different cancer therapies.

### **1.5.2 Sec5 and Exo84**

Sec5 and Exo84 are two components of the exocyst complex and well-known Ral effectors (Moskalenko et al., 2002, 2003; Sugihara et al., 2001). The exocyst complex contains eight total subunits that together mediate tethering of secretory vesicles to the target membrane. Many of Ral's vesicular trafficking and exocytosis functions are thought to be mediated through its interaction with sec5 and exo84. Both RalA and RalB controls the subcellular localization of the exocyst complex to cell protrusions through sec5-paxillin

interaction (Spiczka and Yeaman, 2008). RalA facilitates polarized delivery of membrane proteins in epithelial cells through engagement with the exocyst complex (Shipitsin and Feig, 2004). In a metastatic tumor cell model, RalA engages with the exocyst complex to mediate integrin-dependent exocytosis of membrane rafts (Balasubramanian et al., 2010). Neuronal polarization, which involves polarized membrane trafficking, is also dependent on RalA and the exocyst complex (Lalli, 2009).

In addition to exocytosis, Ral GTPases engage with Sec5 and Exo84 to carry out other cellular functions. Upon nutrient starvation, RalB and Exo84 initiate autophagy by promoting autophagosome formation (Bodemann et al., 2011). RalB and Sec5 participate in innate immune signaling in response to viral infection. RalB is activated upon viral infection and engages with Sec5, which subsequently binds to and activates TBK1 to initiate the host defense response (Chien et al., 2006).

### **1.5.3 Phospholipase D1**

PLD1 is a member of the phospholipase D (PLD) superfamily, which are transphosphatidylases that carry out a headgroup exchange on glycerophospholipids to generate either phosphatidic acid (PA) or phosphatidyl alcohols and a free head group. The classical members of the family, PLD1 and PLD2, are isozymes that are best known for catalyzing the conversion of phosphatidylcholine (PC) into PA and choline. PLD1 and PLD2 share roughly 50% protein sequence similarity. Both isozymes contain two HKD motifs (HxKxxxxD; H = histidine, x = any amino acids, K = lysine, D = aspartic acid), which are critical for PLD enzymatic activity (Sung et al., 1997). Additionally, PLD isozymes contain conserved phos (PX), pleckstrin homology (PH), and PI(4,5)P2 binding domain, which regulate cellular localization (Du et al., 2003; Sciorra et al., 2002; Sugars et al., 2002). PLD1 also contains an auto inhibitory loop domain that is not found in PLD2 (Sung et al., 1999).

Unlike its effectors, Ral is able to bind to phospholipase D1 (PLD1), independent of its GTP-status and G Domain. The functional link between RalA and PLD1 was first reported in 1995, when Jiang et al. discovered that the Ras/Ral signaling pathway mediated PLD activation (Jiang et al., 1995). In that study, PLD activity was precipitated from cell lysates by both immobilized RalA protein as well as a Ral antibody (Jiang et al., 1995). Importantly, the authors showed that GTP or GDP loaded GST-RalA as well as effector domain mutant forms of RalA could precipitate PLD activity, suggesting that RalA influenced PLD activity independent of its GTP status and effector domain (Jiang et al., 1995). Instead, it was discovered that the first 11 amino acids of RalA were necessary for precipitating PLD activity (Jiang et al., 1995). Although the authors did not specify which PLD protein was precipitated by RalA, a follow-up study demonstrated that it was PLD1 (Luo et al., 1997). RalA has been shown to directly interact with both PLD1 and PLD2 in multiple cell types (Corrotte et al., 2010; Vitale et al., 2005). While there is strong evidence to support that RalA and PLD1 interact together, the domains of each protein involved in this interaction are still poorly defined. It is currently hypothesized that the first 11 amino acids of RalA mediate this interaction as a mutant with deletion of these amino acids is unable to precipitate PLD1 activity. However, there have been no reported studies showing loss of interaction between RalA and PLD1 following the deletion of the first 11 amino acids of RalA. Furthermore, RalA does not directly impact PLD1 activity upon binding (Luo et al., 1998). Instead, RalA forms a complex with Arf and PLD1 and Arf is required in this complex to stimulate PLD1 activity (Luo et al., 1998). Interestingly, Arf can also interact with RalA and does so via the first 11 amino acids of RalA (Luo et al., 1998). Future studies identifying the precise domains of each protein that are required for direct interaction between RalA and PLD1 will prove valuable.

Together, RalA and PLD1 carry out a number of cellular processes ranging from endocytosis and exocytosis to oncogenic signaling. RalA facilitates phagocytosis in macrophages; RalA interacts and colocalizes with PLD at phagocytic cups and stimulates

PLD1 activity (Corrotte et al., 2010). RalA and PLD1 interact together and are required for calcium-regulated exocytosis of secretory granules in PC12 cells (Vitale et al., 2005). Additionally, RalA controls PLD1 activation in its regulation of the secretory pathway in B-cells (Ljubicic et al., 2009). Both RalA and PLD1 have been implicated in a variety of cancer studies, although their tumorigenic functions working together have been limited. PLD1 and RalA were reported to promote transformation of rat fibroblasts (Lu et al., 2000). Recently, it was reported that Ral GTPases promote breast cancer metastasis by regulating pro-metastatic extracellular vesicle formation and secretion through PLD1 (Ghoroghi et al., 2021).

RalA can also interact with Phospholipase C- $\delta$ , although the biological function of this interaction has not been fully developed (Grujic and Bhullar, 2009; Sidhu et al., 2005a).

#### **1.5.4 Other Interactors**

Both Ral isoforms are able to interact with the calcium-binding protein calmodulin (Clough et al., 2002; Wang et al., 1997). RalA was initially found to bind to calmodulin in a  $Ca^{2+}$  dependent manner and is hypothesized to bind through amino acids 183-200 of RalA, which was identified as a putative calmodulin-binding domain (Wang et al., 1997). RalB, via its C terminus, was later discovered to also bind to calmodulin, although at a lower affinity compared to RalA (Clough et al., 2002). RalA binding to calmodulin is dependent on prenylation of its CAAX motif (Sidhu et al., 2005b). Ral truncation mutation studies demonstrate that Ral likely has an additional calmodulin binding domain in its N-terminus (Clough et al., 2002). Further,  $Ca^{2+}$ -dependent calmodulin can stimulate RalA activity (Clough et al., 2002; Wang and Roufogalis, 1999). Moreover,  $Ca^{2+}$  also appears activate RalA and is hypothesized to be able to do so by direct interaction (Hofer et al., 1998; Park, 2001). The biological functions of RalA and  $Ca^{2+}$ /calmodulin have yet to be identified and remain an open and interesting area for future studies.

RalA is able to bind to filamin, an actin filament crosslinking protein, in a GTP-dependent manner to aid in filopodia formation in fibroblasts (Ohta et al., 1999). Another cellular function of filamin is to regulate the cellular trafficking of receptors such as androgen and dopamine D<sub>2</sub> and D<sub>3</sub> receptors (Ozanne et al., 2000; Zheng et al., 2016a). Interestingly, active RalA has been shown to inhibit trafficking of dopamine D<sub>2</sub> receptors (Zheng et al., 2016b). Zheng and coauthors report this intriguing interplay between filamin-A and RalA in which filamin-A regulates the trafficking and signaling of D<sub>2</sub>R and D<sub>3</sub>R by controlling and downregulating RalA activity (Zheng et al., 2016a). How filamin-A is able to decrease RalA activity is currently unknown but this finding provides insight into additional ways in which RalA activity is regulated.

RalA is reported to interact with the transcription factor ZONAB in a GTP-dependent and cell-density dependent manner (Frankel et al., 2005). This interaction alleviates transcriptional repression of a ZONAB-regulated promotor; however, it is not known which genes are upregulated as a result (Frankel et al., 2005). Other transcription factors known to be regulated by Ral include NF- $\kappa$ B, FOXO, ATF2, STAT3, and c-JUN. (Berg et al., 2013; Chien et al., 2006; Goi et al., 2000; Ruiter et al., 2000).

## **1.6 Ral Posttranslational Modifications**

Both Ral isoforms carry out distinct cellular functions yet do so by engaging with the same set of regulators and effectors. This is due to both isoforms sharing 100% sequence homology of their G domain. RalA and RalB are able to maintain distinct cellular roles due to their C terminal hypervariable region, which shares only 50% sequence identity (Figure 1.1). The hypervariable region contains a variety of posttranslational modifications (PTMs) that facilitate Ral localization, activity, effector binding and ultimately cellular function. It is hypothesized that PTM dependent changes in Ral localization facilitate their distinct biological

functions. The following section will review the current understanding of the various PTMs on Ral.

### **1.6.1 CAAX Motif**

Like most members of the Ras family, Ral terminates with a CAAX motif (C = cysteine, A = aliphatic amino acid, X = any amino acid) that is prenylated and essential for Ral-membrane interactions (Kinsella et al., 1991). Both Ral proteins are geranylgeranylated, a process in which the enzyme Geranylgeranyltransferase-I (GGTaseI) covalently attaches a geranylgeranyl moiety to the cysteine residue of the CAAX motif (Falsetti et al., 2007; Finegold et al., 1991; Kinsella et al., 1991). Once geranylgeranylated, further processing by Ras converting enzyme 1 (RCE1) cleaves off the AAX residues (Gentry et al., 2015). Lastly, the remaining terminal cysteine residue undergoes methylation via isoprenylcysteine carboxyl methyltransferase (ICMT) (Gentry et al., 2015). These modifications are vital for proper Ral cellular localization and can also influence Ral activity. Pharmacological inhibition of GGTaseI in Cos7 cells prevents Ral localization to the plasma membrane and instead leads to diffuse cytoplasmic and perinuclear localization (Falsetti et al., 2007). Similarly, RalA targeting to the plasma membrane requires RCE1 processing whereas ICMT is dispensable for plasma membrane localization in MEFs (Gentry et al., 2015; Michaelson et al., 2005). Instead, RalA localization to endosomes is dependent on ICMT (Gentry et al., 2015). RCE1 and ICMT are both required for proper RalB localization to the plasma membrane in MEFs. Furthermore, GTP-bound RalA and RalB were both found to be elevated in MEFs lacking RCE1 (Gentry et al., 2015). Interestingly, lack of ICMT has no effect on the activation status of Ral but leads to an increase in total RalB protein levels (Gentry et al., 2015). As will be discussed later, there was great interest by Ral biologists in exploring CAAX motif PTMs as potential cancer therapeutic targets given how important these modifications are to proper localization of Ral and other Ras family members.

In addition to classical CAAX motif processing, Ral proteins can alternatively undergo postprenylation palmitoylation, a process that can occur in proteins that terminate with a CCAX motif (Nishimura and Linder, 2013). In this alternative processing, post GGTaseI-modified proteins undergo palmitoylation on the second cysteine residue (occupying the A<sub>1</sub> position of the CA<sub>1</sub>A<sub>2</sub>X motif) instead of RCE1 mediated cleavage of -AAX (Nishimura and Linder, 2013). It remains unclear what regulates whether Ral protein undergoes alternative palmitoylation instead of classical prenylation. Likewise, it is not known what percentage of cellular Ral undergoes alternative palmitoylation, though it is likely to be a small fraction. However, it was shown that RalA undergoes increased palmitoylation in MEFs lacking RCE1, suggest that there may be competition between both pathways (Nishimura and Linder, 2013). Interestingly, genetically preventing palmitoylation by creating a C204S mutant at the A<sub>1</sub> position in RalB reduces its localization to the plasma membrane but has no effect on RalA localization (Gentry et al., 2015). More studies are needed to fully understand the functionality of alternative palmitoylation of Ral.

### **1.6.2 Phosphorylation**

Both Ral isoforms are known to be phosphorylated by different protein kinases at multiple serine residues. Phosphorylation of Ral leads to changes in their localization, effector binding preferences and is suggested to influence their activity. RalA was first discovered to be phosphorylated on S194 by Aurora-A Kinase (AAK) in a small pool expression screen for AAK substrates (Wu et al., 2005). AAK phosphorylation of RalA S194 was shown to increase RalA activity, enhance RalA interaction with RalBP1 and shift both RalA and RalBP1 localization from the plasma membrane to internal membranes, such as the mitochondria (Kashatus et al., 2011; Lim et al., 2010). In addition to AAK, Protein Kinase A is able to phosphorylate RalA at a yet to be identified residue (Wang et al., 2010a). The tumor

suppressor PP2A A $\beta$  was found to interact with and dephosphorylate RalA at S183 and S194 (Sablina et al., 2007). It is not currently known which enzyme(s) phosphorylate RalA S183.

RalB is phosphorylated on S192 and S198 by protein kinase C $\alpha$  (PKC $\alpha$ ). Phosphorylation of S198 but not S192 leads to increased RalB activity and translocation of RalB from the plasma membrane to internal membranes, including the endosomal pathway (Martin et al., 2012; Wang et al., 2010a). Furthermore, phospho-mimetic S198D RalB preferentially binds to RalBP1 whereas phospho-deficient S198A preferentially binds to Sec5 (Martin et al., 2012).

In addition to these validated phosphorylation sites, Ral proteins contain additional prospective phosphorylation sites which have been identified in high-throughput phosphoproteomic analysis (Palacios-Moreno et al., 2015; Sharma et al., 2014). Further investigation into more phosphorylation sites as well as identification of other kinases and phosphatases that regulate Ral protein will give critical insight into their cellular functions.

### **1.6.3 Ubiquitination**

Ubiquitination is a key PTM that is involved in protein degradation, protein localization, protein activation and protein-protein interaction. Both Ral isoforms can undergo nondegradative monoubiquitination that lead to changes in their cellular localization (Neyraud et al., 2012). Ubiquitinated RalA shifts its localization from endomembranes to enrichment at the plasma membrane whereas RalB relocates from endomembranes into internal punctate-like structures (Neyraud et al., 2012). Specific RalA amino acid residues that are ubiquitinated have yet to be identified and characterized; however, it appears likely that multiple residues can undergo monoubiquitination. While ubiquitin ligases and related enzymes involved in ubiquitination of Ral have not been identified, the deubiquitinase USP33 was found to interact with both RalA and RalB (Simicek et al., 2013). However, only RalB appears to be a direct

target of USP33. Depletion of USP33 leads to increased RalB ubiquitination whereas ubiquitination levels of RalA are unaffected (Simicek et al., 2013). Simicek and coauthors discovered that the ubiquitination status of RalB at Lys47 dictates its preference in binding to either Sec5 or Exo84 (Simicek et al., 2013). Ubiquitinated Lys47 facilitates RalB interaction with Sec5 while inhibiting interaction with Exo84 (Simicek et al., 2013). This ubiquitinated RalB-Sec5 complex functions in innate immune signaling. In nutrient stress conditions, RalB Lys47 is deubiquitinated by USP33, which preferentially allows for the formation of a RalB-Exo84 complex and subsequently facilitates autophagy initiation (Simicek et al., 2013). This discovery gives insight on how multiple levels of regulation fine-tune the various and distinct cellular functions of RalB. There is exciting potential for future studies to uncover the molecular process and players involved in the ubiquitination of Ral. These discoveries will enhance the current understanding of how Ral proteins localize to various cellular compartments, interact with their effectors and ultimately carry out their cellular functions.

### **1.7 Ral Cellular Functions**

RalA carries out many of its cellular functions by regulating the localization of its effectors and interacting partners to specific cellular compartments. This is facilitated by its ability to localize to multiple different organelles in response to upstream signals and different cellular conditions. During mitosis, RalA is phosphorylated and activated by Aurora-A kinase, causing RalA to preferentially bind to RalBP1 (Kashatus et al., 2011; Lim et al., 2010). This phosphorylation induces RalA to relocate to the mitochondria and recruit RalBP1 and the mitochondrial fission GTPase DRP1 to the outer mitochondrial membrane to mediate mitochondrial fission (Kashatus et al., 2011). In metastatic prostate tumor cells, Ral controls the localization of the exocyst complex to protrusive cell extensions (Spiczka and Yeaman, 2008).

Recently, it was found that both isoforms of Ral and PLD1 coordinate the biogenesis and secretion of extracellular vesicles in mammary tumor cells (Ghoroghi et al., 2021). Ghoroghi and coauthors reported a subset of RalA and RalB localize to and maintain homeostasis of multivesicular bodies (MVBs), the site of exosome formation, in 4T1 cells (Ghoroghi et al., 2021). The Ral isoforms carry out this role through PLD1, which also localizes to MVBs in a Ral-dependent manner (Ghoroghi et al., 2021). Importantly, the authors showed that depletion of either Ral or PLD1 led to significantly fewer MVBs and EV secretion (Ghoroghi et al., 2021).

Both Ral proteins play coordinated and non-overlapping roles in cytokinesis, a two-step process consisting of the generation of cleavage furrow followed by abscission (Cascone et al., 2008; Chen et al., 2006). RalA concentrates at the cleavage furrow during early cytokinesis and its depletion leads to cytokinetic regression and binucleate cells (Cascone et al., 2008; Chen et al., 2006). RalB acts downstream, concentrating at the midbody and its depletion results in abscission failure (Cascone et al., 2008). Both functions of RalA and RalB are carried out through the exocyst complex. RalA cooperates with Sec5 to recruit other components of the exocyst, Sec6 and Sec10, to the cleavage furrow (Cascone et al., 2008). Likewise, RalB is necessary for Sec6 localization to the midbody (Cascone et al., 2008). RalA's role in mediating cytokinesis was also examined in early *Drosophila* embryo development (Holly et al., 2015).

It is clear that Ral proteins engage with multiple effectors and interacting partners to participate in various of cellular processes. These functions require tight temporal and spatial regulation and place Ral as a central mediator. As more functions of Ral are discovered, new questions about how Ral is regulated, how it traffics in the cell, and how it selectively engages with its interacting partners will need to be addressed.

## **1.8 Lipid Droplet Background**

Lipid Droplets (LD) are organelles found in most eukaryotic cells that specialize in the storage of neutral lipids. The spherical structure of LDs consists of a neutral lipid core, comprised of mainly triacylglycerides (TAG) and sterol esters (SE), surrounded by a monolayer of phospholipids and associated proteins (Ohsaki et al). Localized to the surface of LDs are a variety of LD associated proteins that carry out different aspects of LD biology. LD are primarily localized to the cytoplasm, but can also be found in the nucleus (Ohsaki et al., 2016). Once thought to be simple inert storage compartments, LDs are now recognized as being dynamic organelles. LDs are diverse in number, composition, and can undergo changes in size (Thiam and Beller). Additionally, LDs communicate with almost all other organelles in the cell via membrane contact sites. LD are involved in a variety of cellular processes including lipid storage, buffering from lipotoxicity, lipid metabolism, intracellular signaling, and protein storage (Fujimoto et al, Listenberger et al, Li et al). Subsequently they have been linked to a number of human pathologies including obesity and other metabolic disease, cancer, liver disease, and cardiovascular disease (Krahmer et al).

### **1.8.1 LD Biogenesis and Growth**

LD biogenesis occurs at the ER, which is the predominant site of neutral lipid synthesis and where enzymes required for TAGs and SEs are localized (Choudhary et al., 2015, 2018; Jacquier et al., 2011; Kassan et al., 2013). These enzymes include members of the Kennedy pathway for TAG synthesis diacylglycerol acyltransferases 1 and 2 (DGAT1 and DGAT2) which convert diacylglycerols (DAG) into TAGs. Additionally, it contains Acyl-CoA cholesterol acyltransferases 1 and 2 (ACAT1 and ACAT2) that convert cholesterol into cholesteryl esters. The current model of LD biogenesis begins with neutral lipid synthesis in the ER bilayer, which is culminated by the aforementioned enzymes (Olzmann and Carvalho, 2019; Walther et al., 2017). Once synthesized, these neutral lipids are deposited and stored in the ER bilayer. As

these neutral lipids accumulate, they begin to assert force against the ER bilayer, forming an oil lens (Figure 1.3). Oil lens structures ranging from 30 to 60 nm in diameter have been detected by EM (Choudhary et al., 2015). Oil lens formation occurs at ER tubules and disruption of ER structure results in altered LD morphology (Falk et al., 2014; Jacquier et al., 2011; Kassan et al., 2013; Klemm et al., 2013). Many fundamental principles of emulsion biophysics apply to oil lens formation. Neutral lipid demixing from other phospholipids and proteins is energetically favorable (Thiam and Forêt, 2016). The transition into an oil lens formation occurs when ER bilayer TAG concentration reach 5-10 mol% (Duelund et al., 2013). However, the process of oil lens formation is not fully understood and many questions remain including whether proteins are involved in this process. Other questions remaining about oil lens formation include how the sites of oil lens on the ER are determined and how ER structure may influence lens formation.

Once a sufficient amount of neutral lipids have conglomerated, the oil lenses bud out of the ER to become nascent LDs (Figure 1.3). Interestingly, the vast majority of LDs bud towards the cytosol, suggesting that this process is tightly regulated. ER and LD surface tension driven by changes in phospholipid composition and protein binding plays an important role in regulating LD budding into the cytoplasm (Chorlay and Thiam, 2018; Chorlay et al., 2019; Choudhary et al., 2018; M'barek et al., 2017). Chorlay and coauthors demonstrated that LD budding directionality is influenced by asymmetry in ER bilayer membrane coverage. Using an artificial LD model, the authors demonstrated that LDs emerge from an artificial bilayer that has higher coverage of phospholipids and proteins (Chorlay et al., 2019). Further, they demonstrated that asymmetrically loading one leaflet with excess phospholipids drove LD budding towards the leaflet that contained more phospholipids (Chorlay et al., 2019). In addition to phospholipid number, the composition of phospholipids on a leaflet can also influence LD budding. Introduction of conical shaped phospholipids such as DAG and PA, which introduce negative membrane curvature prevent LD budding where was phospholipids

with positive intrinsic curvature favor budding (Choudhary et al., 2018; M'barek et al., 2017). Nonetheless, a number of studies have identified DAG and PA as positive regulators for LD growth (Adeyo et al., 2011; Grippa et al., 2015; Skinner et al., 2009; Wolinski et al., 2015). More work is needed to complete our understanding of how phospholipid number and composition influence LD budding.

A number of proteins have been identified to facilitate the LD budding process, some of which may do so by altering the local phospholipid composition. The ER fat storage-inducing transmembrane 2 (FIT2) protein is hypothesized to aid in nascent LD budding as depletion of FIT2 in cells prevents LDs from emerging from the ER (Choudhary et al., 2015; Gross et al., 2011; Kadereit et al., 2008). Furthermore, FIT2 is enriched at sites of LD biogenesis (Chen et al., 2021; Choudhary et al., 2018). The precise mechanism by which FIT2 facilitates LD budding is currently unknown but a subject of intense interest in the field of LD biology. Early studies reported that FIT2 is able to bind to DAGs and TAGs, which led to the hypothesis that FIT2 promotes LD budding by sequestering these neutral lipids in the oil lens (Choudhary et al., 2018; Gross et al., 2011). Recently, it was discovered that FIT2 has lipid phosphatase activity towards PA and lysophosphatidic acid (LPA) (Becuwe et al., 2020). In the same study, FIT2 deficient cells were found to have abnormal ER morphology. These new findings suggesting that FIT2 may promote LD budding by altering ER leaflet composition (Becuwe et al., 2020). Strengthening this hypothesis is the recent finding that FIT2 interacts with the ER tubule forming proteins Rtn4 and REEP5 to promote LD budding (Chen et al., 2021).

Seipin, an ER transmembrane protein found at the LD-ER interface is another protein necessary for LD budding (Fei et al., 2008; Salo et al., 2016; Szymanski et al., 2007; Wang et al., 2016). Seipin deficiency presents an interesting phenotype, the accumulation of multiple, small LDs alongside a few supersized LDs (Fei et al., 2008; Wang et al., 2016). How seipin facilitates LD budding is not completely understood. Seipin is hypothesized to facilitate

the maturation of LDs by enabling lipid transfer into budding LDs (Salo et al., 2016; Wang et al., 2016). Two related studies from the Elina Ikonen lab demonstrated that seipin stabilizes LD-ER contacts and facilitates the transfer of proteins and triacylglycerides into growing LDs from the ER (Salo et al., 2016, 2019). In another study, seipin was found to bind to glycerol-3-phosphate acyltransferase (GPAT), an enzyme that converts glycerol-3-phosphate into lysophosphatidic acid (Pagac et al., 2016). Seipin appears to regulate GPAT activity as seipin deficient cells have elevated GPAT activity and GPAT overexpression in yeast mimics formation of supersized LDs seen in seipin deficient cells (Pagac et al., 2016). Though still far from understood, seipin appears to be a prime protein involved in LD biogenesis and currently under heavy investigation.

Another protein linked to early LD biogenesis is perilipin 3 (PLIN3), a member of the perilipin family of proteins. Perilipins (PLIN1-5) are among the most abundant LD associated proteins and among the first proteins discovered on LDs. Traditionally, PLIN proteins have thought to play a protective role in preventing unregulated lipolysis of LDs. PLIN2 and PLIN3 are found in most types where as PLIN1, PLIN4, and PLIN5 are found in specialized cells. Recent studies suggest that PLIN has additional roles aside from protecting LDs. PLIN3 relocalizes from the cytosol to nascent LDs and aids in stabilizing and promoting LD growth (Bulankina et al., 2009; Gao et al., 2017b; Skinner et al., 2009; Wolins et al., 2005). Loss of PLIN3 prevents LD biogenesis and reduced TAG storage in a variety of cells (Bell et al., 2008; Buers et al., 2009; Bulankina et al., 2009; Gao et al., 2017b; Nose et al., 2013). PLIN2 and PLIN3 are among the first proteins detected on nascent LDs during oleic acid stimulation. The yeast orthologue to mammalian PLIN3, Pln1/Pet10, binds to nascent LDs and interacts with both seipin and FIT2 on the ER membrane (Gao et al., 2017b). Pln1/Pet10 is involved in LD budding, as depletion of Pln1/Pet10 leads to delayed budding (Gao et al., 2017b). The precise mechanism by which PLIN3 aids in LD budding and growth is currently unclear.

After budding from the ER, LDs can be divided into two subpopulations, initial LDs (iLDs) that remain small (400-800 nm in diameter) and expanding LDs (eLDs) that continue to increase in size after budding (Walther et al., 2017; Wilfling et al., 2013). eLDs have been hypothesized to grow in size in a few ways. Firstly, some LDs in mammalian cells and all LDs in yeast maintain a connection to the ER through membrane bridges after budding and recent findings suggest that Arf1/COPI facilitates this connection (Wilfling et al., 2014). These lipid bridges can promote LD growth by allowing lipid transfer from the ER to LDs (Jacquier et al., 2011). Furthermore, a number of enzymes involved in triacylglyceride (TAGs) synthesis (Gpat4, Dgat2, Agpat3) and PC synthesis (Cct1) relocalize from the ER to LDs upon oleic acid stimulation where they catalyze TAG formation and monolayer expansion on site (Krahmer et al., 2011; Kuerschner et al., 2008; Wilfling et al., 2013). These enzymes are also thought to relocalize to eLDs from the ER through membrane bridges onto LDs.

Another mechanism of growth is the fusion or coalescence of LDs, which occurs as a result of altered monolayer phospholipid composition (Murphy et al, Guo et al). Deficiency in the levels of PC or a boost in phosphatidic acid (PA) can cause LD fusion (Krahmer et al, Fei et al). The cell death-inducing DFFA-like effector (CIDE) family of proteins (CIDEA, CIDEB, CIDE C) facilitate LD fusion by localizing to contact sites between two LDs and aiding in the transfer of neutral lipids (Barneda et al., 2015; Gong et al., 2011). CIDE proteins act as molecular tethers by forming dimers with CIDE proteins on adjacent LDs (Gong et al., 2011; Jambunathan et al., 2011). CIDE deficiency leads to the formation of multiple, small LDs in adipocytes, a cell type known for its unilocular LD (Nishino et al., 2008; Toh et al., 2008). On the other hand, ectopic CIDE expression leads to the formation of large LDs (Liu et al., 2009; Puri et al., 2007). Interestingly, CIDEA contains an amphipathic helix that can bind to PA and CIDEA mutants that are unable to bind to PA fail to fuse (Barneda et al., 2015). These recent studies have shed light on LD fusion but many questions remain including identification of other proteins in this process.

### 1.8.2 LD breakdown

LD breakdown is an essential cellular process for generating energy, providing building blocks for membranes, and lipid signaling. During nutrient starvation and instances of high metabolic energy demands, such as exercise, cells utilize the stored lipids in LDs for energy. Degradation of LDs occurs by two mechanisms, lipolysis and lipophagy (Figure 1.4). Discovered half a century ago, lipolysis was considered to be the primary mechanism by which LDs were degraded (Vaughan and Steinberg, 1963; Vaughan et al., 1964). In 2009, a novel study by Singh et al. identified autophagy mediated degradation of LDs in hepatocytes during nutrient deprivation and generated enthusiasm for this new way of recycling LDs (Singh et al., 2009).

Lipolysis is a biochemical process that enzymatically releases fatty acids (FAs) off of the glycerol backbone of TAGs through the sequential actions of LD associated lipases. Lipolysis occurs at the LD surface by three major lipases: adipose triglyceride lipase (ATGL), hormone sensitive lipase (HSL), and monoacylglycerol lipase (MGL). TAG hydrolysis is initiated by ATGL, which catalyzes TAGs into diacylglycerol (DAG) and FA (Jenkins et al., 2004; Villena et al., 2004; Zimmermann et al., 2004). ATGL activity is specific for TAG and is poorly able to hydrolyze DAGs, monoglyceride (MAG) and other lipids, and thus HSL and MGL are required for complete lipolysis (Eichmann et al., 2012; Zimmermann et al., 2004). In the next step, HSL hydrolyzes DAG into MAG and FA (Fredrikson et al., 1981). Unlike ATGL, HSL has enzymatic activity for other lipid ester bonds, including TAGs, MAGs and cholesteryl esters (Lafontan and Langin, 2009). Interestingly, however, HSL does not appear to be able to compensate for loss of ATGL (Haemmerle et al., 2006). In the last step of lipolysis, MGL cleaves MAG into FA and glycerol (Vaughan et al., 1964). Through their actions, these lipases all play an important role in maintaining energy homeostasis. Mice deficient in ATGL have TAG accumulation in both adipose and non-adipose tissue, increased glucose tolerance and

increased insulin sensitivity (Haemmerle et al., 2006). Similarly, mice lacking HSL have increased DAG levels in their adipose tissue (Haemmerle et al., 2002). Finally, mice lacking MGL have elevated MAG levels in numerous tissues (Taschler et al., 2011). Lipases are not normally found on LDs under basal conditions. However, during lipolytic conditions, they translocate to the LD surface. ATGL activity and localization is regulated by multiple proteins and kinases (Ahmadian et al., 2011; Lass et al., 2006; Pagnon et al., 2012; Schweiger et al., 2012; Xie et al., 2014; Yang et al., 2010). Similarly, HSL activity and localization is regulated through phosphorylation at numerous serine residues by PKA, AMPK, and ERK (Egan et al., 1992; Greenberg et al., 2001; Watt and Steinberg, 2008). The relative importance of ATGL, HSL and MAGL in lipolysis is cell and tissue type specific. Aside from the three lipases, a number of other proteins exhibit triglyceride lipase activity (Steinberg et al., 2007).

Lipophagy is a selective form of autophagy in which autophagosomes engulf and deliver LDs to lysosomes for degradation. Lipophagy is thought to employ the same mechanism as macroautophagy, although it is not currently known how LDs are specifically targeted by autophagosomes. Organelle-specific membrane receptors that engage with autophagic machinery have been identified for most organelles except for LDs (Anding and Baehrecke, 2017). Recent studies suggest that members of the Rab family of small GTPases may function to recruit autophagic machinery to LDs. Upon  $\beta$ -adrenergic stimulation and nutrient starvation, which promote lipolysis, Rab7 colocalizes with LDs, autophagosomes and lysosomes (Lizaso et al., 2013; Schroeder et al., 2015). Rab7 knockdown leads to an accumulation of LDs (Schroeder et al., 2015). Strikingly, Rab7 is activated on LDs during nutrient starvation, and facilitates the recruitment of autophagosomes, multivesicular bodies and lysosomes to the LD for lipolysis (Schroeder et al., 2015). Other Rab proteins suggested to be involved in lipolysis include Rab10 and Rab32, both of which also colocalize with LDs and endolysosomal membranes (Li et al., 2016; Wang et al., 2012). Similar to Rab7, loss of Rab10 leads to an accumulation of LDs in hepatocytes (Li et al., 2016). Once LD containing

autophagosomes fuse with lysosomes, LD TAGs and CEs are degraded by lysosomal acid lipase (LAL) (Du et al., 2001; Dubland and Francis, 2015).

Although they are often described and thought of as independent processes, there is evidence of crosstalk between lipolysis and lipophagy. LC3-II has been reported to bind to ATGL on LDs in adipocytes and was shown to be necessary for ATGL translocation to LD (Martinez-Lopez et al., 2016). A separate study by Kaushik and Cuervo demonstrated that chaperone-mediated autophagy (CMA) degrades the LD associated proteins PLIN2 and PLIN3 during nutrient starvation prior to lipolysis (Kaushik and Cuervo, 2015). The degradation of these proteins enhances ATGL localization onto LDs and presumably facilitates lipolysis (Kaushik and Cuervo, 2015). Under nutrient starvation conditions, autophagy and lipolysis work in tandem (Nguyen et al., 2017; Rambold et al., 2015). Autophagy is activated in response to starvation and is utilized to recycle cellular membranes for energy (Rambold et al., 2015). The recycled lipid building blocks are then stored in LD, leading to an accumulation of LDs (Nguyen et al., 2017; Rambold et al., 2015). These lipids are then released by lipases for transport into the mitochondria for ATP generation (Rambold et al., 2015). Consistent with their crosstalk, both lipolysis and lipophagy are regulated by major cellular metabolic signaling pathways including mTOR and AMPK.

Recently, a new form of LD catabolism was described in hepatocytes in which lysosomes directly interacted with and extracted lipid content out of LDs (Schulze et al., 2020). Astoundingly, this interaction did not require an autophagosomal membrane intermediate and provided evidence for a mechanism of direct transfer of proteins and lipids from LDs to lysosomes for breakdown (Schulze et al., 2020).

### **1.9 Lipid droplet contact sites with other organelles**

Bulk material exchange via intracellular vesicle transport is thought to be incompatible with LDs due to their unique architecture. (single monolayer compared to bilayer membrane

of all other organelles, neutral lipid core compared to aqueous lumen). Nonetheless, LDs participate in communication with other organelles by forming membrane contact sites (MCS) (Bohnert, 2020; Hugenroth and Bohnert, 2019; Schuldiner and Bohnert, 2017). LDs can form MCS with various organelles including the ER, mitochondria, endosomes, lysosomes, peroxisomes, and even other LDs (Bohnert, 2020; Drizyte-Miller et al., 2020; Hugenroth and Bohnert, 2019; Schuldiner and Bohnert, 2017).

As with other MCS, LD-organelle contact sites are thought to be maintained by molecular tethers, effectors, and regulators. The most well studied LD contact site is with the ER and is, perhaps, a nearly unique type of cellular contact site. The ER is the site of LD biogenesis but plays an important role in regulating LDs throughout its lifecycle by maintaining close connections. LDs in yeast are believed to never fully separate from the ER but instead maintain distinct organelle identities from the ER through connection with membrane lipid bridges. Lipid bridges are a unique type of membrane contact that differs from the traditional definition of MCS due to the creation of a membrane fusion intermediate. However, fusion of the LD monolayer with an ER bilayer creates hemifusion intermediates, which naturally separate their organelle identities. Unlike yeast cells, eukaryotes have LDs that are completely separated from the ER and electron microscope studies have revealed that they maintain a diversity of LD-ER contact sites including the traditional MCS and lipid bridges. Recent studies have identified a number of proteins that are enriched at LD-ER MCS and that are thought to act as tethers (Hugenroth and Bohnert, 2019). The VPS13 family of proteins (VPS13A-D) localize to multiple MCS in the cell, including ER-LD contacts (Kumar et al., 2018). Kumar and coauthors demonstrated that VPS13A and VPS13C act as tethers for ER-LD contact (Kumar et al., 2018). VPS13 proteins contain a FFAT motif, which binds to the ER resident anchor, VAP (Murphy and Levine, 2016). Given that the ER is the site of LD biogenesis, many proteins found at the LD-ER interface have multifunctional roles in both promoting LD biogenesis as well as maintaining MCS. In addition to its LD biogenesis functions discussed earlier, seipin

is involved in maintaining LD-ER MCS (Pagac et al., 2016; Salo et al., 2016, 2019; Szymanski et al., 2007; Walther et al., 2017; Wang et al., 2016). Yeast *mdm1* and its human homologue *Snx14* have a similar dual functional role in LD biogenesis and LD-ER tethering (Datta et al., 2019; Hariri et al., 2019). *Rab18* has also been shown to tether ER and LDs via Snare and Nrz interactions and facilitate LD growth (Li et al., 2019; Ozeki et al., 2005; Xu et al., 2018).

Our understanding of LD-lysosomal tethering has derived mainly from studies in yeast cells. LD biogenesis in yeast occurs at contact sites between the ER, the vacuole/lysosome, and nascent LDs. This site is termed the nucleus-vacuole junction (NVJ) and tethering is mediated by *mdm1*. *Mdm1* binds to LDs through its PXA domain and to the vacuole via its PX domain (Hariri et al., 2019; Henne et al., 2015). During nutrient stress in yeast, LD biogenesis is increased and occurs at the NVJ in a *mdm1*-dependent manner (Hariri et al., 2017, 2019). Another yeast protein involved in LD biogenesis at the NVJ is *LDO45*, which is able to bind to seipin and may function as a LD-vacuole tether (Eisenberg-Bord et al., 2018). LD-lysosomal tethering is less understood in mammalian cells; however, many have reported LD-lysosomal MCS (Drizyte-Miller et al., 2020).

Perhaps the most interesting LD-organelle contact site is that with mitochondria, the site of  $\beta$ -oxidation. Fittingly, LD-mitochondria MCS have been reported in various cell types with high energetic demands, such as skeletal muscle and brown adipose tissue (Boutant et al., 2017; Shaw et al., 2008; Tarnopolsky et al., 2007). LD-mitochondria MCS increase in abundance during stress conditions, such as nutrient starvation and exercise, presumably to facilitate the utilization of fatty acids as energy (Nguyen et al., 2017; Rambold et al., 2015; Tarnopolsky et al., 2007). While close apposition of LDs and mitochondria are apparent, few proteins have been identified as molecular tethers thus far. The mitochondrial outer membrane protein Mitoguardian 2 (*MIGA2*) was recently reported to function as a LD-mitochondria tether (Freyre et al., 2019). Freyre and coauthors identified an amphipathic segment in *MIGA2* that is able to bind to LDs. Fascinatingly, overexpression of *MIGA2* can

generate LD-mitochondria contacts in Cos-7 cells, a cell type that typically has few LD-mitochondria MCS (Freyre et al., 2019). MIGA2 was also found to mediate mitochondria-ER contacts, as it contains a FFAT motif that binds to the ER anchor VAP (Freyre et al., 2019). Another protein implicated as a LD-mitochondria tether is the SNARE protein SNAP23. Depletion of SNAP23 leads to decreased LD-mitochondria contact and impaired  $\beta$ -oxidation (Jägerström et al., 2009). LD localized Perilipin 1 (PLIN1) and mitochondria localized mitofusin 2 (MFN2) have been hypothesized to act as LD-mitochondria tethers in brown adipose tissue (Boutant et al., 2017). Another perilipin, PLIN5 is found localized at LD-mitochondria MCS and is necessary for maintaining proper mitochondria function and structure (Benador et al., 2018; Gallardo-Montejano et al., 2021; Wang et al., 2011).

The field of LD contacts with other organelles is just beginning to develop. While it is now clear that LDs communicate and interact with most cellular organelles, there remains important gaps in understanding how these interactions are mediated on a molecular basis. Further identification of molecular tethers and their regulation will provide better understanding of this process.

### **1.10 Lipid Droplets and RalA**

A proteomic analysis aimed at identifying LD-associated proteins revealed that both RalA and RalB are found on LD in Chinese hamster ovary K2 cells (Liu et al., 2004). Liu and coauthors detected significant levels of the Ral GTPases by both mass spectrometry and western blot analysis (Liu et al., 2004). RalA was more recently identified to be part of the LD interactome in a Apex2 proximity labeling study done in osteosarcoma U2OS cells (Bersuker et al., 2018). Aside from these two studies identifying RalA to be present on LDs, it is currently unknown if RalA has any functional roles related to LDs biology. The exocyst complex has also been shown to partially colocalize with LDs (Inoue et al., 2015). Given this association, it

is possible that RalA and the exocyst may collaborate to regulate LD trafficking, fusion, or other signaling events.

### **1.11 Lipid Droplets and PLD1**

Unlike RalA, PLD1 has been identified to regulate LDs in a number of studies. Nakamura et al. discovered the presence of PLD1, but not PLD2, on oleic-acid induced LDs in NIH3T3 and CHO cells (Nakamura et al., 2005). Interestingly, the authors in this study also demonstrated that the overexpression with exogenous PLD1, but not PLD2, enhanced oleic acid stimulated LD growth in CHO cells and this effect was mediated by Arf-1 dependent PLD1 activation on LDs (Nakamura et al., 2005). Likewise, Andersson et al. independently reported that PLD1, but not PLD2, overexpression led to a dramatic increase in oleic acid induced LD formation compared to vector control in NIH3T3 cells (Andersson et al., 2006). Furthermore, this increase was dependent on the catalytic activity of PLD1 (Andersson et al., 2006). In a prior study, this group also identified that PA was necessary for the assembly of LDs in a microsome cell-free system (Marchesan et al., 2003). Additionally, Andersson and coauthors demonstrated that knockdown of PLD1 reduced oleic acid induced LD formation compared to controls (Andersson et al., 2006). In Huh-7 cells, both PLD isoforms appear to be required for LD formation (Rohwedder et al., 2014). PLD1 was shown to partially colocalize with LDs and pharmacological inhibition of either PLD1 or PLD2 prevented oleic acid induced LD formation (Rohwedder et al., 2014). Taken together, these findings demonstrate that PLD1 is involved in regulating LDs and is likely doing so by generating PA.

Aside from being a precursor for glycerolipids, PA is a bioactive molecule involved in lipid signaling, intracellular trafficking, and protein recruitment (Athenstaedt and Daum, 1999; Ganesan et al., 2015; Jenkins and Frohman, 2005; Kooijman et al., 2003; Tanguy et al., 2019). PA structure consists on a glycerol backbone that has fatty acyl chain attached to the sn-1 and sn-2 position via ester linkages. The glycerol sn-3 position is attached to a phosphate

group. Due to its small headgroup, PA has a cone shape structure and introduces negative curvature when added into membranes (Kooijman et al., 2003) This altered local architecture is thought to affect the fusion and fission of cellular membranes (Jenkins and Frohman, 2005; Kooijman et al., 2003; Tanguy et al., 2019). PA has been identified as a key phospholipid in LD biology. While the precise mechanism of how PA influences LDs is not fully understood, recent discoveries suggest that PA is involved in controlling the size of LDs and may do so by facilitating the fusion of existing LDs. Fei and coauthors utilized a genome-wide screen to study LD size and identified 10 yeast mutants that generated supersized LDs (Fei et al., 2011). Each of these 10 mutants not only had elevated cellular PA levels but also displayed increased LD fusion events (Fei et al., 2011). The authors further demonstrated the potential for PA to induce LD fusion by generating artificial LDs with different ratios of PA and other phospholipids and found that introducing small amounts of PA led to a significant increase of artificial LD size (Fei et al., 2011). Among the identified mutations was for the gene that encodes FLD1, the homologue of mammalian seipin (Fei et al., 2011). In a later study, Seipin was shown to regulate LD expansion by maintaining PA levels through its regulation of ER-residing GPAT (Pagac et al., 2016). Seipin maintained GPAT activity homeostasis as Seipin-deficient cells had elevated GPAT activity, elevated cellular PA, and supersized LDs (Pagac et al., 2016). The CIDE family proteins have been identified as critical regulators of LD fusion and are found to cluster at LD-LD contact sites (Gao et al., 2017a). One member of the family, CIDEA, is able to bind to PA and does so at the LD monolayer to facilitate LD fusion in yeast (Barneda et al., 2015). Importantly, a CIDEA mutant that is unable to bind to PA failed to facilitate LD fusion in this same study (Barneda et al., 2015). PA can be generated by numerous enzymes in lipid pathways and thus may play a role independent of PLD1.

In addition to its influence on membrane structure, PA is able to recruit proteins to specific compartments of the cell. PA is reported to recruit proteins to the PM (Faugaret et al., 2011; Lopez-Andreo et al., 2003), endolysosomal system (Frias et al., 2020; Rizzo et al.,

2000; Zhao et al., 2012), and secretory vesicles (Faugaret et al., 2011; Manifava et al., 2001; Tanguy et al., 2020). Consistent with this role, PA may influence LD size is by recruitment of LD associated proteins to the LD surface. One such protein hypothesized to be recruited by PA is PLIN3. Experiments utilizing model phospholipid monolayers showed that monolayers with anionic negative curvature (such as with PA or PE) increase PLIN3 interaction and insertion into the monolayer (Mirheydari et al., 2016). Given that PA has been implicated in multiple steps along the LD biogenesis pathway, recruitment of proteins may be one of its pleiotropic roles in promoting LD growth. How PA is able to recruit proteins is not understood. More than 50 proteins have been discovered to interact with PA yet there does not appear to be a clearly defined PA binding domain. There are likely multiple factors involved. Kassas and coauthors report that PA binding proteins possess some level of specificity for the fatty acyl chain length on PA (Kassas et al., 2017). The immediate phospholipid composition around PA also appears to dictate protein binding (Kassas et al., 2017). Others have proposed that the protein binding pocket for PA likely has a positive charge to facilitate binding to negatively charged PA (Potocký et al., 2014; Tanguy et al., 2018). In addition to being negatively charged, PA has a small head group compared to PC. This small head group may promote protein binding as a means to cover any gaps in the membrane, thereby protecting the hydrophobic interior of the bilayer from the hydrophobic aqueous cytosol.

### **1.12 Lipid droplets and the cellular stress response**

LDs are dynamic and cells are constantly undergoing LD biogenesis, growth, and degradation in response to cellular demands and environmental cues. Recent studies have identified LDs as essential participants of the cellular stress response. LDs are vital in preventing lipotoxicity through their ability to sequester and buffer excess lipids. Appropriate release of these stored lipids can be modulated between finely tuned through lipolysis vs bulk supply via lipophagy to meet the requirements of the cell. The ability to control the release of

content is one of the LDs most important functions and is directly influential in the LDs ability to maintain energy homeostasis, protect membrane and organelle composition, manage ER stress, and produce lipid signals. LDs accomplish these roles through communication with other cellular organelles including the mitochondria, lysosomes, and ER. Characteristic of many stress responses is abundance of excess of lipids and accumulation of LDs. The origin of these lipids can be either exogenous, such as lipids taken up from the surrounding environment, or endogenous, such as through autophagy. Regardless of the source, the response is to sequester these excess lipids into LDs. Different forms of stress that lead to LD accumulation include excess lipids, oxidative stress, pathogen infection and nutrient stress (Figure 1.5).

#### **1.12.1 Oxidative stress**

Lipid accumulation in cells exposed to oxidative stress and hypoxic conditions have been reported for over half a century (Adebonojo et al., 1961; Gordon et al., 1977). More recently, studies have begun to uncover the mechanism of hypoxia induce LD accumulation, which is primarily mediated by hypoxia-inducible factors (HIFs). Mylonis and coauthors reported that human cells exposed to hypoxic conditions accumulate TAGs and LDs through HIF-1 mediated upregulation of lipin1 (Mylonis et al., 2012). In another study, Bensaad et al. subjecting U87 glioblastoma cells to hypoxic conditions which resulted in LD accumulation (Bensaad et al., 2014). This increase in cellular LDs was driven by increased uptake of extracellular lipids mediated by HIF-1 $\alpha$  upregulation of Fatty Acid Bindings Proteins 3 and 7, proteins that function in fatty acid uptake (Bensaad et al., 2014). Importantly, this accumulation protected cells against reactive oxygen species and promoted tumor cell survival (Bensaad et al., 2014). Hypoxia-inducible protein 2 (HIG2), another protein upregulated by HIF-1 during hypoxia, is found localized on LDs and its induction leads to LD accumulation in various cells (Gimm et al., 2010; Maier et al., 2017). HIG2 likely facilitates LD accumulation by inhibition of

lipolysis, including inhibiting ATGL (Zhang et al., 2017). As can be seen from these studies above, cells utilize numerous pathways downstream of HIF-1 to elicit an accumulation of LDs during hypoxic conditions. Failure to accumulate LDs leads to cell death, including tumor cells likely through a combination of lipotoxicity and lack of available energy stores.

### **1.12.2 Pathogen infection**

One fascinating and emerging role of LDs is their relationship with invading pathogens. LDs are involved in the coordinated immune response and participate in the generation of important inflammation mediators. At the same time, they are targets for invading viruses and bacteria that seek the LDs resources for their own needs. The hepatitis C virus (HCV) utilizes the LD as a factory for the generation of nascent virions. The HCV core protein localizes to the LD membrane, where it recruits viral proteins and replication complexes and this localization is essential for viral reproduction (Boulant et al., 2007; Miyanari et al., 2007; Moradpour et al., 1996). Aside from HCV, other viruses have been documented to be found on LDs including components of GB virus B, Dengue virus, and rotaviruses (Cheung et al., 2010; Hope et al., 2002; Samsa et al., 2009). Fascinatingly, many viral infections lead to the accumulation of LDs through different mechanisms. Infection by HCV core protein leads to LD accumulation by decreasing lipid turnover. (Harris et al., 2011; Miyanari et al., 2007). Hepatitis B virus and adenovirus 36 infection increase LD abundance by upregulation lipogenesis pathways (Na et al., 2009; Wang et al., 2010c). Likewise, infection by bacteria such as *M. tuberculosis*, *M. leprae*, *C. trachomatis* can lead to biogenesis of LDs and LD accumulation in immune and other cell types (Daniel et al., 2011; Kumar et al., 2006; Mattos et al., 2010; Melo et al., 2006; Saka and Valdivia, 2012). Fittingly, as a defense against infections, some reports suggest that cells have employed antiviral tools for LDs to fight back against certain infections. Viperin, a protein encoded by an interferon-stimulated gene localizes to LDs (Hinson and Cresswell, 2009). The immunity-related GTPases Irgm3 and

Irgb6 have also been shown to localize to LDs in IFN-stimulated cells (Bougnères et al., 2009; Saka and Valdivia, 2012).

### **1.12.3 Nutrient stress**

Befitting their role as nutrient reservoirs, LDs provide cells with energy in the form of fatty acids during nutrient-poor conditions. As discussed earlier, LDs increase proximity and contact with mitochondria upon nutrient stress conditions. This allows for a direct flow of fatty acids out of LDs and into the mitochondria, the site of  $\beta$ -oxidation. Initially surprising, LDs and TAGs accumulate in cells upon nutrient starvation. This has been observed in yeast, drosophila, as well as a number of cell lines including MEFs and HeLa (Bjedov et al., 2010; Hariri et al., 2019; Nguyen et al., 2017; Rambold et al., 2015). The fact that cells upregulate an anabolic process in packaging and growing LDs during a time when energetic supply is low indicate that this process of LD accumulation is vital for the cellular response to nutrient stress. The prevailing hypothesis of why cells accumulate LDs during nutrient starvation is ultimately to prevent lipotoxicity (Nguyen et al., 2017). Nutrient stress triggers autophagy, a process that recycles cellular components and frees up building blocks for utilization in times of need (Rambold et al., 2015). Fatty acids are among the components made available in abundance through autophagic recycling of cellular membranes. These fatty acids are eventually utilized by the mitochondria for  $\beta$ -oxidation but are toxic to the cell if left in the cytoplasm (Nguyen et al., 2017). As a mechanism to avoid lipotoxicity, these newly liberated fatty acids are first esterified into TAGs and stored into LDs until they are ready to be used (Nguyen et al., 2017; Rambold et al., 2015). Given that this process depends upon coordination between multiple organelles, it likely requires and is regulated by multiple proteins. A number of questions remain about this process including how autophagy generated fatty acids make their way to LDs, which LD biogenesis machinery is involved

facilitating this LD accumulation and which proteins mediate LD-mitochondria contact during nutrient starvation.

### **1.13 Goals and Significance**

This project began with the intention of understanding RalA's function in response to nutrient starvation. As discussed in detail above, Ral is capable of responding to different cellular conditions and eliciting an appropriate cellular response. Ral proteins act as intermediaries that receive upstream signals and relay them to downstream targets. We initially began by exploring a RalA function related to mitochondrial elongation. Mitochondria are dynamic organelles that undergo cycles of fusion and fission. Among the mediators of mitochondrial dynamics is RalA, which promotes mitochondrial fission during mitosis (Kashatus et al., 2011). Mitochondria undergo fusion mediated elongation during nutrient starvation and while the identity of the fusion machinery is known, which protein mediates this process is not. Given that RalA already has a known function in mitochondrial dynamics and that its paralog RalB is actively involved in autophagy initiation during nutrient starvation, it was hypothesized that RalA may be the mediator for starvation-induced mitochondrial elongation. Subsequently, studies were performed in WT and RalA KO MEFs to determine if RalA was required for mitochondrial elongation in response to nutrient depletion. While RalA appeared to not regulate starvation-induced mitochondrial elongation, it was noticed that cells lacking RalA had significantly fewer LDs during nutrient starvation. At the time of this observation, there was no reported study in the literature ascribing a role for RalA in LD regulation. Given this significant and reproducible phenotype, we became intrigued by how RalA could be regulating LDs and began our work in understanding this process.

The primary goal of this thesis was to identify how RalA is facilitating LD accumulation in response to nutrient starvation. We sought to understand the molecular regulation of RalA during nutrient stress, the interacting partner of RalA that facilitated this function, and the

molecular machinery that was utilized in LD growth during nutrient starvation. Completion of this thesis work has identified a novel function for RalA. Additionally, it has filled gaps in knowledge of the process of starvation-induced LD accumulation. However, this work has also generated future areas of work that need investigation as will be discussed in chapter 3.

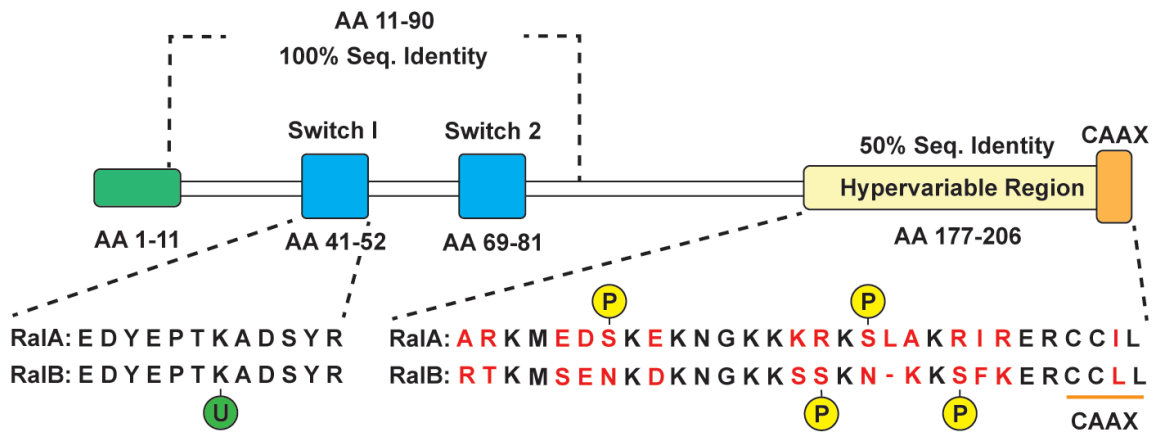


### Figure 1.1 Ral protein structure

Schematic highlighting important Ral domains. The first 11 amino acids are hypothesized to be important for PLD1 interaction and are not found on Ras. RalA and RalB share 100% sequence identity in their switch I and switch II regions, which are important for binding to upstream regulators and downstream effectors. The C-terminal hypervariable region contains various phosphorylation sites and is only 50% identical between RalA and RalB. Both Ral GTPases contain a CAAX motif that anchors them to membranes.

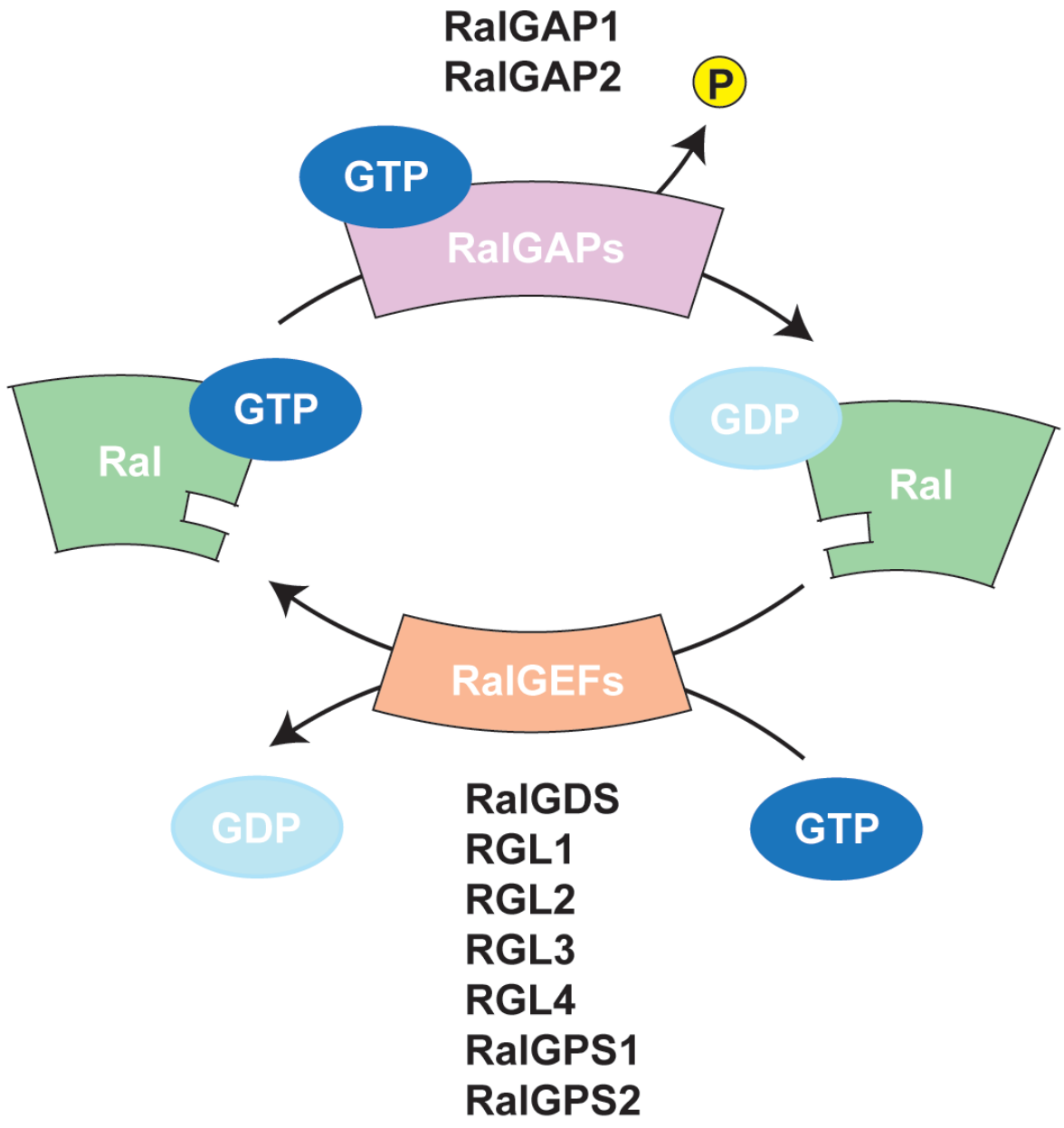


**Figure 1.2 Ral GTP Cycling and Regulators**

Ral proteins cycle between an active GTP and inactive GDP bound state. RalGEF and RalGAPs help facilitate this cycling.

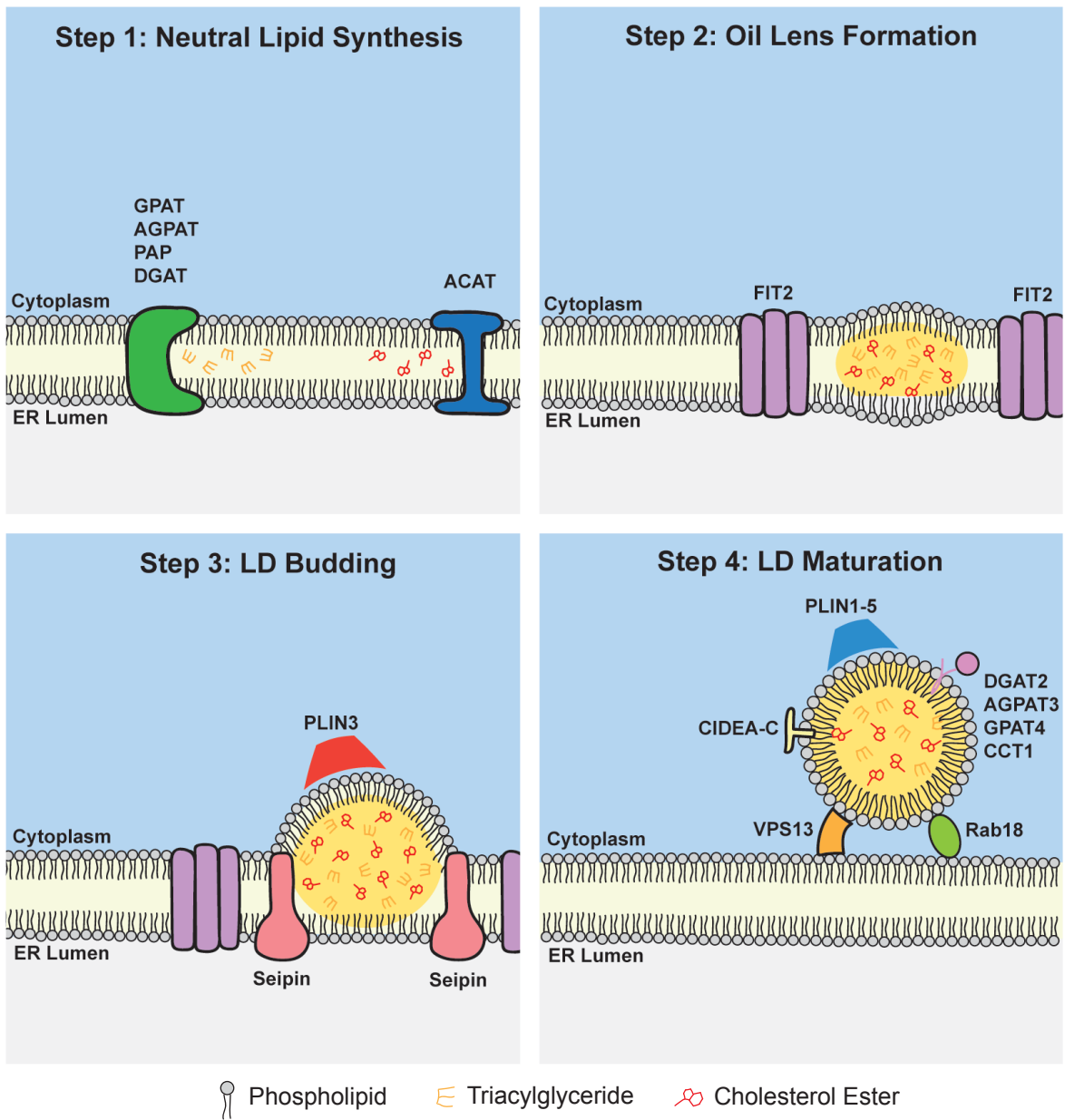


**Figure 1.3 Lipid Droplet Biogenesis**

The current model places LD biogenesis at the ER membrane, where TAG and sterol ester (SE) enzymes reside. Generated TAG and SE are deposited into the ER bilayer and form an oil lens once they reach a minimal threshold. FIT2 is hypothesized to aid in oil lens formation by restricting TAGs to the oil lens. LDs continue to grow as more neutral lipids flow into the oil lens, which is thought to be mediated by seipin. PLIN3 is recruited to nascent LDs and aids in LD growth. After budding, LDs can maintain association with the ER via MCS through VPS13, Rab18, FIT2 and seipin. Mature LDs have numerous LD associated proteins.

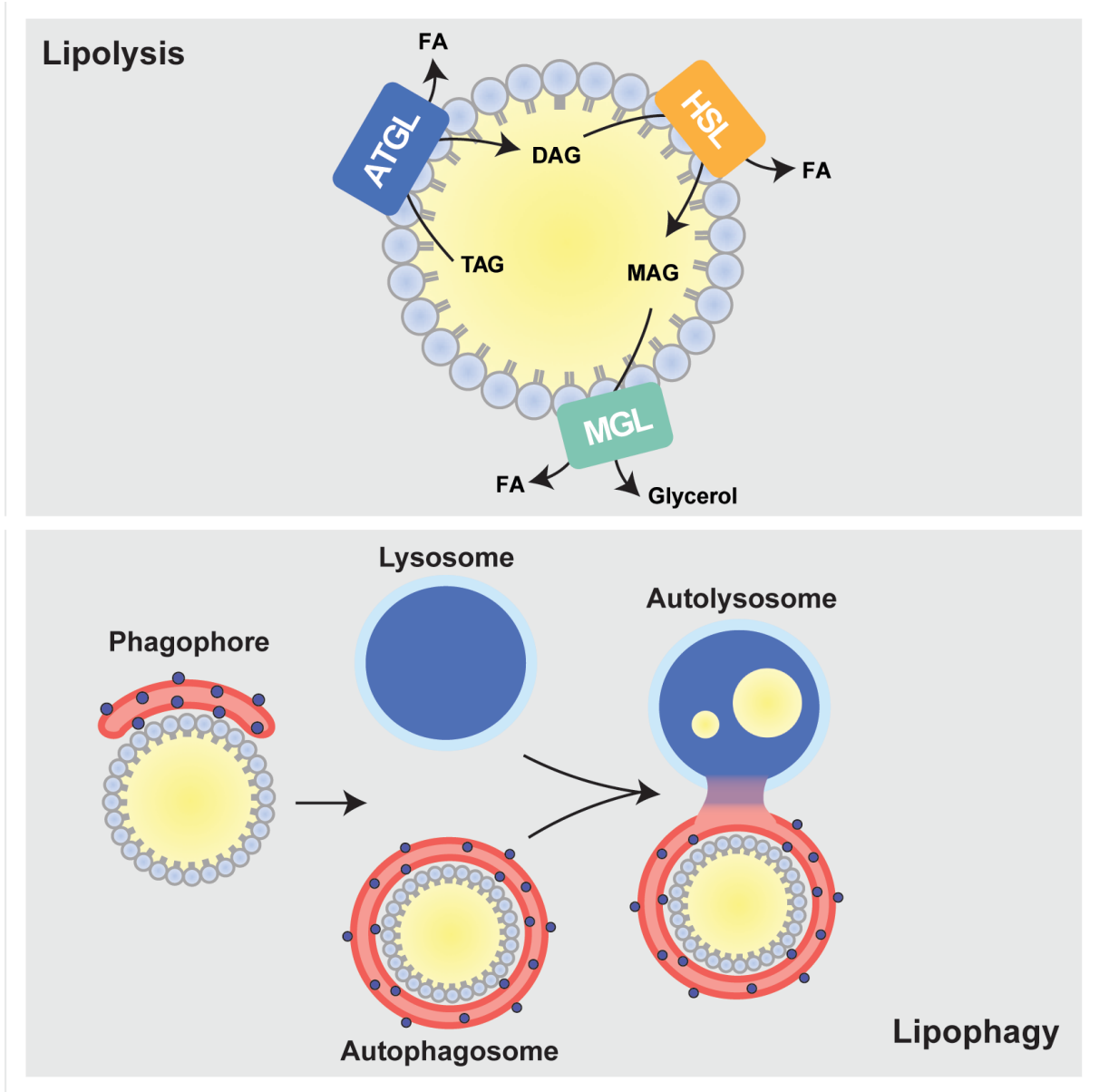


**Figure 1.4 Lipid Droplet Breakdown**

The two primary forms of LD breakdown are lipolysis (upper panel) and lipophagy (lower panel). Lipolysis breaks down LDs through the sequential actions of LD associated lipases, ATGL, HSL, and MGL. Lipolysis allows for a highly regulated release of LD content and is depicted above by release of FA. Lipophagy is the bulk degradation of LDs through engulfment by autophagosomes that fuse with lysosomes to breakdown LDs and release fatty acids (depicted by yellow circles).

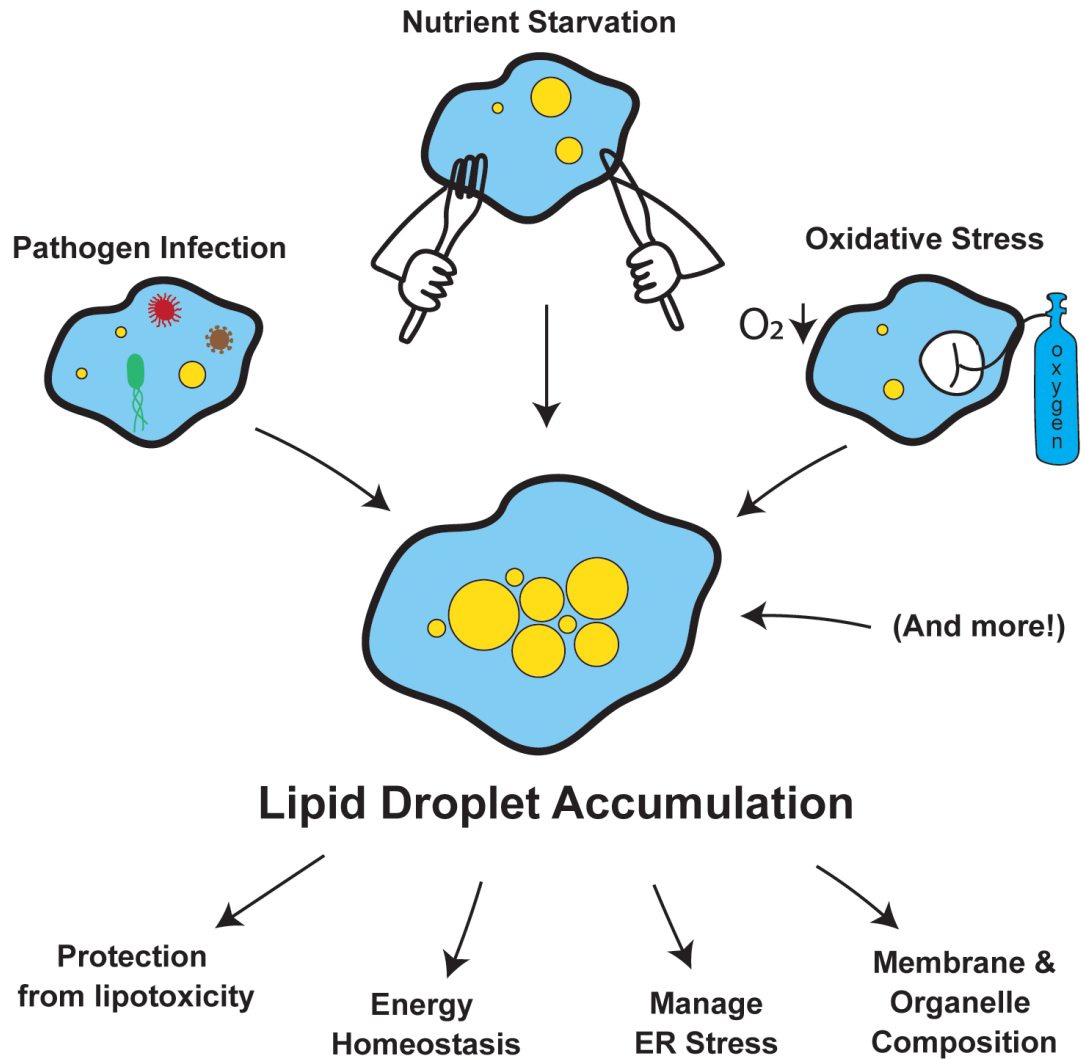


**Figure 1.5 Lipid Droplets accumulate during Cellular Stress**

Numerous cellular stress conditions converge on LDs, which generate an adaptive cellular response. A common feature of cellular stress is the accumulation of LDs. This accumulation of lipids into LDs prevents lipotoxicity, providing the cell with a reservoir for energy generation or for building new membranes or organelles.

## **Chapter 2: RalA and PLD1 promote lipid droplet growth in response to nutrient withdrawal**

This chapter is a modified version of the manuscript following manuscript:

**Hussain SS**, Tran T, Ware TB, Luse MA, Prevost CT, Ferguson AN, Kashatus JA, Hsu K, Kashatus D. RalA and PLD1 Promote Lipid Droplet Growth in Response to Nutrient Withdrawal. *Cell Reports*. Accepted Publication (June 2021).

### **2.1 Introduction**

Cells maintain homeostasis during nutrient scarcity with a coordinated effort between multiple organelles. Activation of nutrient sensing pathways initiates autophagy, a lysosomal-dependent process that recycles cellular components (Kroemer et al., 2010). Among the building blocks generated through autophagy are free fatty acids. These fatty acids are toxic if left in the cytosol and are quickly shuttled into lipid droplets (LDs), organelles that specialize in the storage of neutral lipids (Listenberger et al., 2003; Nguyen et al., 2017; Rambold et al., 2015). This leads to a dramatic accumulation of cellular LDs (Nguyen et al., 2017; Rambold et al., 2015). Concurrently, nutrient scarcity shifts the mitochondrial networks towards an elongated morphology and induces closer spatial proximity between mitochondria and LDs (Nguyen et al., 2017; Rambold et al., 2011). These changes are required for efficient flux of fatty acids into the mitochondria, the location of  $\beta$ -oxidation and ATP production. The ultimate consequence of these dynamic changes is to facilitate a shift in the cell's reliance from glucose to fatty acids for energy production.

The highly similar RalA and RalB proteins are members of the Ras family of small GTPases (Chardin and Tavitian, 1986). Ral proteins carry out their cellular functions by engaging with an overlapping set of effector proteins and are involved in a number of shared

processes including vesicular trafficking, membrane dynamics, and cell migration (Gentry et al., 2014; Yan and Theodorescu, 2018). Ral proteins mediate the response to a variety of cellular conditions and extracellular stimuli. RalA is activated upon amino acid and glucose stimulation and is necessary for mTORC1 signaling during nutrient replete conditions (Maehama et al., 2008). RalA is also necessary for insulin stimulated GLUT4 translocation to the plasma membrane and glucose uptake in adipocytes (Chen et al., 2007; Skorobogatko et al., 2018). RalB triggers innate immunity signaling through Sec5-TBK1 in response to infection (Simicek et al., 2013). Interestingly, RalB was identified to mediate the cellular response to nutrient scarcity by initiating autophagosome formation (Bodemann et al., 2011; Simicek et al., 2013). This role was specific to RalB and there is currently no identified role for RalA in the cellular starvation response. Thus, we investigated whether RalA was involved in dynamic processes during nutrient starvation.

Here we report that RalA is essential for nutrient starvation-induced lipid droplet accumulation. Acting downstream of autophagy, RalA recruits phospholipase D1 (PLD1), an enzyme that produces phosphatidic acid (PA) to the lysosome, which forms close contacts with LDs and the endoplasmic reticulum (ER), the site of LD biogenesis. The localized production of PA then supports the recruitment of the LD-associated protein perilipin 3 (PLIN3) and the subsequent expansion of the LD pool.

## **2.2 Results**

### **2.2.1 RalA is required for starvation-induced lipid droplet accumulation**

To determine if RalA plays a role in starvation-induced LD formation, we cultured wild-type (WT) and RalA knockout (KO) MEFs (Figure 2.1A) in HBSS for 4 hours and compared the levels of LDs. Compared with complete DMEM growth media, HBSS has lower levels of glucose (25mM vs 5.5mM) and lacks amino acids and serum. This commonly used *in vitro*

model for nutrient stress exposes cells to near-physiological concentrations of glucose and concentrations of amino acids comparable to those that have been measured in certain tumor microenvironments (Kamphorst et al., 2015; Sullivan et al., 2019). Consistent with previous reports (Rambold et al., 2015), WT MEFs exhibit a significant increase in cellular LDs over the course of nutrient starvation (Figure 2.1B and 2.1C). Surprisingly, RalA KO MEFs fail to accumulate LDs to the same extent as WT MEFs and have significantly fewer LDs by 4 hours of HBSS starvation (Figure 2.1B and 2.1C). Similar results are observed in RalA knockdown HeLa cells (Figure 2.1D-2.1F). Importantly, LD accumulation during nutrient starvation is rescued in RalA KO MEFs that stably express exogenous RalA at levels comparable to WT MEFs (Figure 2.2A-2.2C). These data indicate that RalA is necessary for starvation-induced LD accumulation.

In both MEFs and HeLas, the LD content in unstarved cells is comparable between WT and RalA-depleted cells (Figure 2.1C and 2.1F), suggesting that cells lacking RalA are still able to form LDs under nutrient-replete conditions. Because LD formation can also be induced by supplementation with exogenous fatty acids (Listenberger et al., 2003; Vries et al., 1997), we stimulated MEFs and HeLa cells with oleic acid for 4 hours and monitored LD levels. Interestingly, MEFs and HeLa cells lacking RalA accumulate LDs at levels comparable to WT cells, indicating that RalA is not necessary for oleic acid stimulated LD formation (Figure 2.3). From this data we conclude that RalA regulation of LD accumulation is not universal, but is limited to specific conditions, including nutrient starvation.

### **2.2.2 Triacylglyceride levels increase in a RalA dependent manner during nutrient starvation**

A primary function of LDs is storage of neutral lipids such as triacylglycerides (TG) and cholesteryl esters (CE). Considering the substantial difference in LD levels in cells lacking RalA compared to control cells, we sought to understand if these changes could be detected

at the level of different lipid species. Therefore, we performed liquid chromatography-mass spectrometry (LC-MS) to measure the lipid composition of WT and RalA KO MEFs during nutrient starvation. WT MEFs exhibit a significant increase in the total amount of TGs measured compared with a minor increase in RalA KO MEFs. (Figure 2.4A). This effect is also observed at the level of individual TG species with specific fatty acid tails (Figure 2.4B). The levels of other lipid classes measured are not significantly altered over the course of nutrient starvation nor are they RalA dependent (Figure 2.4A and 2.5). Together, these results are consistent with LD imaging data and with the requirement for RalA in starvation-induced LD growth.

### **2.2.3 RalA acts downstream of autophagy in starvation-induced LD accumulation**

Starvation-induced LD formation requires autophagy as a source of free fatty acids (Rambold et al., 2015). Because the closely related GTPase RalB has previously been shown to regulate starvation-induced autophagy induction, we next sought to determine whether the role of RalA was at the level of autophagy (Bodemann et al., 2011). To do this, we repeated the HBSS starvation experiments in the presence of the pharmacological inhibitor chloroquine. Inhibition of autophagy prevented an increase in LD accumulation in WT MEFs but did not lead to further defects in RalA KO MEFs (Figure 2.6A and 2.6C). Similar results were obtained when using another autophagy inhibitor, Bafilomycin A1 (Figure 2.6B and 2.6D). As a complement to pharmacological inhibition of autophagy, we genetically blocked autophagy initiation by knocking down ATG5, a key protein required for autophagosome biogenesis (Mizushima et al., 2001), in WT and RalA KO MEFs (Figure 2.6E and 2.6F). Similar to chloroquine treatment, knockdown of ATG5 prevented LD accumulation during HBSS starvation in WT MEFs and had no effect on LD composition in RalA KO MEFs (Figure 2.6G and 2.6H). These results indicate that autophagy is necessary for RalA-dependent LD

accumulation and consistent with RalA and autophagy functioning in the same pathway during nutrient starvation.

We next sought to determine whether RalA acts upstream or downstream of autophagy. We began by assessing whether the nutrient sensing pathway upstream of autophagy is intact. mTORC1 signaling negatively regulates autophagy and is inhibited during nutrient starvation to allow for autophagy initiation (Jung et al., 2009; Noda and Ohsumi, 1998). We hypothesized that RalA deficient cells may be unable to accumulate LDs during nutrient starvation due to dysregulation of mTORC1 signaling. We monitored phosphorylation of the mTORC1 target 4E-BP1 during HBSS starvation and observed a decrease in phosphorylated 4E-BP1 starting at 1h of HBSS starvation in both WT and RalA KO MEFs (Figure 2.7A). This result indicates that mTORC1 signaling is inhibited by starvation independently of RalA and that the defect in LD induction in RalA deficient cells is not due to a failure in nutrient sensing.

Next, we sought to determine whether loss of RalA prevents cells from efficiently undergoing autophagy. We measured autophagic flux in WT and RalA KO MEFs using an mCherry-GFP-LC3 reporter (Pankiv et al., 2007). mCherry is insensitive to lysosomal pH and its fluorescence does not degrade upon autophagosomal fusion to lysosomes. GFP, however, is sensitive to lysosomal pH and its fluorescence degrades once fusion has occurred. We starved WT and RalA KO MEFs that stably express mCherry-GFP-LC3 and measured the rate of autophagosomal fusion with lysosomes (indicated by decrease in GFP punctae) over 8 hours of starvation. We observed no impairment in the rate of autophagy in RalA KO MEFs compared with WT MEFs during starvation (Figure 2.7B-2.7D). Similar results were obtained when comparing LC3 lipidation by western blot (Figure 2.7E). Collectively, these data suggest that autophagy is intact in RalA deficient cells and that RalA acts downstream of autophagy to promote the accumulation of LDs in low nutrient conditions.

#### **2.2.4 PLIN3 recruitment to LDs during nutrient starvation is dependent on RalA**

We reasoned that there are two potential ways loss of RalA could result in impaired LD accumulation if autophagy is unaffected. RalA could either promote the growth of LDs or prevent LD breakdown. LDs are broken down by two distinct mechanisms, lipolysis and lipophagy (Singh et al., 2009; Zechner et al., 2017; Zimmermann et al., 2004). Lipolysis involves the enzymatic release of FAs stored in LDs by the sequential action of cytoplasmic lipases. Lipophagy is a selective form of autophagy that targets the bulk degradation of LDs and involves autophagosomal engulfment of partial or whole LDs that eventually fuse with the lysosome. Unlike lipophagy, lipolysis allows for a regulated release of FAs from LDs and fine-tuned usage of FAs for energy production based on the energetic needs of the cells. Different nutrient deprivation conditions (serum starved, glucose starved, amino acid starved, etc) trigger specific cellular responses for LD breakdown (Zechner et al., 2017). In the case of HBSS starvation, cells primarily utilize lipolysis, but not lipophagy, for FA release from LDs (Rambold et al., 2015). These FAs released by lipolysis are trafficked into the mitochondria, which form close contact sites with LDs (Nguyen et al., 2017; Rambold et al., 2015).

To determine whether RalA-dependent LD accumulation is due to negative regulation of lipolysis, we compared the rates of FA transfer from LDs to the mitochondria in starved WT and RalA KO MEFs. We performed a pulse-chase assay to visualize FA movement in relation to LDs and mitochondria using BODIPY 558/568 (Red C12), a fluorescent fatty acid analog that has been validated to reliably track FA trafficking (Rambold et al., 2015; Wang et al., 2010b). We pulsed Red C12 into WT and RalA KO MEFs for 16 hours, removed media containing Red C12 and chased for 24 hours in HBSS (Figure 2.8A). At 0 hours, Red C12 is highly colocalized with LDs (Figure 2.8B and 2.8D). By 24 hours, Red C12 is no longer colocalized with LDs in a significant number of cells and has relocated to mitochondria (Figure 2.8B and 2.8D). The Red C12 redistribution from LDs to mitochondria is detected as early as 4 hours following HBSS starvation (Figure 2.8B and 2.8D). Importantly, the rate of

Red C12 movement out of LDs and into mitochondria is comparable between WT and RalA KO MEFs (Figure 2.8C and 2.8E), suggesting that FA release from LDs is not altered by loss of RalA. Collectively, these data are consistent with a model in which RalA is acting downstream of autophagy but upstream of FA mobilization in starvation-induced LD accumulation.

The previous experiments suggest that RalA may be directly impacting LD growth during nutrient starvation. To gain further insight into this possibility, we examined Perilipin protein localization following starvation. Perilipins (1-5) are the most characterized LD-associated proteins and have important functions related to LD stabilization and growth (Itabe et al., 2017). We focused on Perilipin 2 (PLIN2) and Perilipin 3 (PLIN3) because they are expressed in most cell types (Brasaemle et al., 1997; Robenek et al., 2005; Sztalryd et al., 2006; Wolins et al., 2001). Further, PLIN3 translocates to LDs during growth stimulating conditions and is thought to aid in LD formation (Bulankina et al., 2009; Nose et al., 2013; Wolins et al., 2001, 2005). In both WT and RalA KO MEFs, PLIN2 forms ring-like structures around LDs under both basal and starved conditions (Figure 2.9A and 2.9B). PLIN3, on the other hand, exhibits a dramatic shift in localization upon starvation, from a dispersed cytoplasmic staining to focused punctae overlapping with LDs (Figure 2.9C and 2.9D). Notably, PLIN3 does not relocalize to LDs in RalA KO MEFs (Figure 2.9C and 2.9D). This effect is not due to differences in the amount of PLIN3 protein levels during nutrient starvation between WT and RalA KO MEFs (Figure 2.9E). These results indicate that RalA is required for starvation-induced recruitment of PLIN3 to LDs and point to a potential mechanism by which RalA is promoting LD growth.

Loss of PLIN3 protein expression has been reported to reduce LD and triglyceride content in a variety of cells (Bell et al., 2008; Buers et al., 2009; Bulankina et al., 2009; Gu et al., 2010; Nose et al., 2013). The requirement of RalA for both PLIN3 recruitment and LD accumulation following nutrient starvation led us to ask whether loss of PLIN3 is sufficient to

impair LD accumulation during nutrient stress. We knocked down PLIN3 in both WT and RalA KO MEFs and subjected these cells to HBSS starvation (Figure 2.10A). Consistent with our hypothesis, knockdown of PLIN3 significantly impaired LD accumulation in WT MEFs during nutrient starvation compared to scramble control (Figure 2.10B and 2.10C). In contrast, PLIN3 knockdown had no additional effect on LDs in RalA KO MEFs, consistent with a model in which RalA and PLIN3 regulate LD expansion as part of the same pathway. Taken together, these data support a model in which RalA promotes LD growth during nutrient starvation by influencing PLIN3 recruitment to LDs.

### **2.2.5 PLD1 is required for RalA dependent starvation-induced LD accumulation**

We next aimed to understand the molecular mechanisms through which RalA responds to nutrient stress to induce PLIN3 recruitment and LD accumulation. RalA carries out its various cellular functions by engaging downstream effectors and other non-effector interacting proteins (Cantor et al., 1995; Gentry et al., 2014; Moskalenko et al., 2003; Ohta et al., 1999; Vitale et al., 2005). RalA cycles between GTP-bound and GDP-bound states and nucleotide binding dictates RalA effector interactions (Gentry et al., 2014). Under nutrient replete conditions, intracellular levels of GTP are several fold higher than GDP. The GTP/GDP ratio is highly sensitive to nutrient fluctuations and decreases upon nutrient starvation (Rudoni et al., 2001). Given this, we hypothesized that RalA is acting in a nucleotide-dependent fashion to promote starvation-induced LD accumulation. However, we did not detect significant changes in RalA nucleotide bound status during nutrient starvation (Figure 2.11A and 2.11B), in agreement with a previous study looking at RalA activity during nutrient stress (Bodemann et al., 2011). This is in contrast to RalB, which has been reported to shift towards a GTP bound state during nutrient starvation (Bodemann et al., 2011). Although we did not detect changes in total cellular RalA activity, it is possible that only a subset of RalA in specific cellular compartments is acting to promote LD accumulation during nutrient starvation.

Indeed, a recent study showed that Ra1B activity is increased specifically at autophagosomes compared to other cellular compartments upon starvation (Singh et al., 2019). Thus, we stably expressed either a GTPase deficient Ra1A Q72L (GTP-bound) or the dominant negative Ra1A S28N mutant (GDP-bound) in Ra1A KO MEFs (Figure 2.11C). Both mutants rescue LD accumulation in Ra1A KO MEFs to levels similar to WT MEFs (Figure 2.11D and 2.11E). Collectively, these data indicate that Ra1A acts in a nucleotide-independent manner to facilitate starvation-induced LD accumulation. Further strengthening this conclusion is the fact that knocking out Ra1BP1, a well-known Ra1A effector, had no effect on LD accumulation during nutrient starvation (Figure 2.11F-2.11H).

Because Ra1A acts in a nucleotide-independent manner to promote LD accumulation, we turned our attention to downstream Ra1A interacting proteins that bind Ra1A outside of its nucleotide-binding domain. We first investigated phospholipase D (PLD), an enzyme that catalyzes the conversion of phosphatidylcholine into phosphatidic acid (PA) and choline. Mammalian cells encode two forms of PLD: PLD1 and PLD2. Both PLD1 and PA have been linked to LD formation and growth (Andersson et al., 2006; Fei et al., 2011; Marchesan et al., 2003; Pagac et al., 2016). Knockdown of PLD1 in NIH 3T3 cells results in significantly less cellular LD content compared to control cells (Andersson et al., 2006). Interestingly, PLD1 can translocate to LDs (Nakamura et al., 2005). PLD2 has not been shown to localize to LDs or influence LD formation. Based on this, we hypothesized that Ra1A is acting through PLD1 to facilitate LD accumulation during nutrient deprivation. To test this, we treated scramble and Ra1A KD HeLas with FIPI, a potent PLD inhibitor in either DMEM or HBSS for 4 hours (Su et al., 2009). FIPI treatment significantly reduces LD accumulation after 4 hours of starvation in scramble HeLas but has no effect on Ra1A KD HeLas (Figure 2.12C and 2.12D). Similar results were obtained in MEFs (Figure 2.12A and 2.12B). This suggests that PLD1 and/or PLD2 and Ra1A function in the same pathway to facilitate LD growth. Additionally FIPI inhibits

PLD by binding to the catalytic site, which suggests that the effects of PLD inhibition on LDs are directly related to its enzymatic activity, the production of PA.

To gain further insight into whether PLD1 acts upstream or downstream of RalA, we transiently transfected GFP-PLD1 into shRalA HeLa cells and asked whether overexpression of PLD1 rescues LD accumulation during starvation. We took advantage of the fact that transient transfection efficiently delivers GFP-PLD1 to some but not all HeLa cells and compared LD accumulation in non-transfected cells (cells with no GFP expression) to cells transfected with GFP-PLD1 (cells with GFP expression). Remarkably, overexpression of GFP-PLD1 in shRalA HeLa rescues LD accumulation to levels comparable to control (cells with no GFP expression) (Figure 2.13A and 2.13B). The ability of cells to overcome the loss of RalA with the addition of PLD1 suggests that PLD1 acts downstream of RalA. Next, to further characterize the role of PLD1 activity in LD accumulation, we utilized a catalytically inactive PLD1 that has a lysine to arginine point mutation at amino acid 898 (K898R) (Sung, 1997). Interestingly, transfection of the catalytically inactive GFP-PLD1 (K898R) fails to rescue LD accumulation during starvation in shRalA HeLa cells (Figure 2.13C and 2.13D). This complements the results from the FIPI experiments and further implicates PLD1 activity, the production of PA, in LD accumulation.

As RalA is required for both PLIN3 recruitment and LD accumulation, we next sought to determine whether PLD1 and PA similarly impact PLIN3 recruitment to LDs during nutrient stress. PA is a bioactive molecule involved in lipid biogenesis, signaling, and protein recruitment. Due to its cone shape structure, PA introduces negative curvature on membranes that can facilitate membrane protein association. A study utilizing model artificial phospholipid monolayers showed increased PLIN3 interaction and insertion into monolayers enriched with PA (Mirheydari et al., 2016). Based on this, we hypothesized that PLD1-dependent PA production is necessary for proper PLIN3 recruitment to budding or fully formed LDs and subsequent growth of LDs during nutrient starvation. To test this, we measured PLIN3

localization upon inhibition of PLD1 activity using FIPI during HBSS starvation. Similar to the previous experiment, PLIN3 relocalized to LDs upon HBSS starvation in control WT MEFs treated with DMSO (Figure 2.13E and 2.13F). However, PLIN3 failed to relocalize to LDs in MEFs treated with FIPI (Figure 2.13E and 2.13F). This result is consistent with the hypothesis that PLIN3 recruitment during HBSS starvation is dependent on PA production.

### **2.2.6 RalA recruits PLD1 to lysosomes during nutrient stress**

RalA and PLD1 are both membrane-associated proteins. RalA is anchored to membranes by geranylgeranylation of its C-terminal CAAX motif (Kinsella et al., 1991). PLD1 is associated with membranes by palmitoylation (Han et al., 2002). RalA localization has been characterized as primarily at the plasma membrane, but relocalizes to various internal membranes, including the endosomal system, lysosomes and mitochondria, under different cellular conditions (Chen et al., 2006; Corrotte et al., 2010; Kashatus et al., 2011; Neyraud et al., 2012; Shipitsin and Feig, 2004). Like RalA, PLD1 is found in a diversity of organelles including the plasma membrane, golgi apparatus, nucleus, endoplasmic reticulum, endosomes, and lysosomes (Brown et al., 1998; Corrotte et al., 2010; Du et al., 2003; Freyberg et al., 2001; Toda et al., 1999). Additionally, both PLD1 and RalA have previously been shown to localize to LDs (Bersuker et al., 2018; Liu et al., 2004; Nakamura et al., 2005). To better understand the localization of RalA and PLD1 during HBSS starvation, we monitored the localization of fluorescently tagged RalA and PLD1. Interestingly, RalA and PLD1 colocalize under nutrient-replete conditions and the degree of colocalization is not significantly altered upon starvation (Figure 2.14A). To our surprise, neither RalA nor PLD1 are detected at LDs during nutrient starvation (Figure 2.14B). However, we observe significant redistribution of both proteins to internal membranes upon starvation. Given that autophagy is induced during nutrient stress, we next sought to determine if RalA relocalizes to autophagosomes or other compartments within the endolysosomal system. We observed

minimal RaIA association with autophagosomes (labeled with YFP-LC3) or early endosomes (labeled with GFP-EEA1) (Figure 2.14C). However, RaIA clearly localizes to late endosomal/lysosomal vesicles labeled with GFP-Rab7 under both fed and starved conditions (Figure 2.14C). Additionally, RaIA forms distinct ring-like structures around Limp2-positive lysosomes under starved, but not fed, conditions (Figure 2.14C-2.14D). Consistent with RaIA and PLD1 functioning together during nutrient stress, we also observed that a subset of GFP-PLD1 becomes enriched at lysosomes during starved, but not fed, conditions (Figure 2.14E-2.14F). Furthermore, the redistribution of PLD1 to the lysosome is dependent on RaIA (Figure 2.14E-2.14F). Collectively, these data support a model in which RaIA recruits PLD1 to lysosomes upon nutrient starvation.

The localization of RaIA and PLD1 to lysosomes but not LDs during HBSS starvation raises the question of how lysosomal RaIA and PLD1 can influence LD accumulation and PLIN3 recruitment. We envision two plausible ways, both involving organelle contacts. First, there may be direct contacts between lysosomes and LDs, which has been reported in mammalian and yeast cells (Drizyte-Miller et al., 2020; Hariri et al., 2019; Kaushik and Cuervo, 2015; Wang et al., 2014; Zutphen et al., 2014). Contact between lysosomes and LDs could allow for PLD1 dependent PA generation at the lysosome and subsequent PA transfer to LDs to promote recruitment of PLIN3. Recent studies have highlighted stable LD-lysosomal contact sites involved in LD breakdown as well as lipid and protein transfer (Kaushik and Cuervo, 2015; Schroeder et al., 2015; Schulze et al., 2020). Second, both lysosomes and LDs may be connected by a third organelle, the ER. The ER is the site of LD biogenesis and can make membrane contacts with both lysosomes and LDs (Henne et al., 2015; Jacquier et al., 2011; Pan et al., 2000; Schuldiner and Bohnert, 2017; Szymanski et al., 2007; Wilfling et al., 2013). Lysosomal PA may traffic to the ER through ER-lysosome contacts, where it can promote LD biogenesis through the recruitment of PLIN3 to the site of LD budding or to newly formed LDs. Consistent with both of these models, high-resolution airyscan confocal analysis

of ER (calnexin), Lysosomes (Limp2) and LDs (Bodipy 493/503) reveals direct Lysosome-LD contacts following HBSS starvation, as well as multiple ER-Lysosome and ER-LD contacts (Figure 2.15B). Notably, we still observe these contacts in RalA KO MEFs, suggesting that the defect in LD growth is due to loss of PLD1 recruitment, rather than a loss of contact between Lysosomes, ER and LDs. Importantly, we also observe spatial proximity between these three organelles by electron microscopy (Figure 2.15A). These findings are in agreement with a recent study in yeast showing that ER-vacuole contact sites become sites for LD biogenesis during nutrient stress (Hariri et al., 2017). Given the close proximity of the ER to the lysosomes and LDs, we hypothesized that PLIN3 redistribution during HBSS starvation in WT MEFs occurs at sites of LD biogenesis on the ER. PLIN3 has previously been shown to be recruited to nascent LDs emerging from the ER (Kassan et al., 2013; Skinner et al., 2009). Consistent with this, high resolution confocal microscopy reveals PLIN3 ring-like structures forming adjacent to and budding from the ER in WT MEFs upon HBSS starvation (Figure 2.15C). Combined, these results suggest that specific organelle contacts between lysosomes, ER and LDs are critical for RalA induced LD accumulation.

### **2.2.7 Enrichment and depletion of PA at lysosomes impacts LD accumulation and PLIN3 redistribution**

The model that PLD1-derived PA generated at the lysosome traffics to LDs to support PLIN3 recruitment and LD expansion predicts that independently increasing PA levels at either Lysosomes or LDs should rescue starvation-induced LD growth in the absence of RalA. To test this prediction, we initially targeted PLD1 directly to LDs by fusing it in frame with the C-terminus of PLIN2 (GFP-PLIN2-PLD1) and stably introducing it into WT and RalA KO MEFs (Figure 2.16A). While both GFP-PLIN2-PLD1 and the control GFP-PLIN2 localize to LDs (Figure 2.16B), only GFP-PLIN2-PLD1 expression is able to rescue HBSS-induced LD growth in RalA KO cells (Figure 2.16C-2.16E). Importantly, GFP-PLIN2-PLD1 expression also

rescues recruitment of PLIN3 to LDs in RalA KO MEFs, indicating that increasing the levels of PA at LDs is sufficient to promote PLIN3 recruitment and LD growth during nutrient stress (Figure 2.16F). Next, to test whether recruitment of PLD1 to lysosomes independently of RalA is sufficient to rescue the loss of PLIN3 recruitment and LD growth we fused PLD1 to the C terminus of TMEM192, a lysosomal transmembrane protein with both N and C-termini facing the cytosol, and confirmed lysosomal localization in both HeLa and MEFs (Figure 2.17A and 2.17B). Expression of lysosome-targeted PLD1 (mCherry-TMEM192-PLD1), but not the mCherry-TMEM192 control, rescues both LD growth and PLIN3 recruitment in RalA KO MEFs (Figure 2.17C, 2.17E and 2.17G). These data demonstrate that the function of RalA in starvation induced LD growth can be replaced with a lysosome-targeted PLD1 and thus further predict that decreasing the levels of PA at the lysosome independent of RalA or PLD1 manipulation should recapitulate the effects of RalA or PLD1 inhibition. To test this, we fused the PA phosphatase LIPIN1 to the C-Terminus of TMEM192 (mCherry-TMEM192-LIPIN1) and stably expressed it in WT and RalA KO MEFs (Figure 2.17B). Consistent with our model, expression of mCherry-TMEM192-LIPIN1, but not the control mCherry-TMEM192, impairs both LD accumulation and PLIN3 recruitment in WT MEFs during HBSS starvation (Figure 2.17C, 2.17D and 2.17F).

Collectively, the data from these experiments demonstrate that manipulation of PA at the lysosome is sufficient to impact both LD growth and PLIN3 recruitment during starvation and is consistent with the model that RalA and PLD1 relocalize to lysosomes during nutrient stress induced autophagy where PLD1 converts PC to PA. This PA then traffics to the ER where it supports LD growth through the recruitment of PLIN3 to budding or newly formed LDs (Figure 2.18).

## 2.3 Discussion

How cells respond to fluctuations in nutrient availability has implications for both normal and pathological physiology. LDs have emerged as important metabolic hubs and recent studies have highlighted the important role that LDs play during nutrient starvation. Starvation-induced autophagy triggers a rapid increase in the amount of cellular LDs (Rambold et al., 2015). These LDs act to provide a readily available pool of fatty acids for energy and also function to buffer the lipotoxic effects of fatty acids (Listenberger et al., 2003; Nguyen et al., 2017). Here, we describe a pathway through which the small GTPase RalA and the enzyme PLD1 regulate fatty acid storage during the cellular starvation response. Our data indicate that RalA acts downstream of autophagy to directly facilitate LD growth under nutrient stress through the recruitment of PLD1 to lysosomes and the localized production of PA. Though how this PA is transported to sites of LD biogenesis remains to be determined, we demonstrate that lysosomal generated PA facilitates recruitment of PLIN3 and subsequent LD expansion.

The finding that RalA functions in LD growth through recruitment of PLD1 to lysosomes is consistent with its established role in recruiting proteins to distinct cellular compartments, allowing them to carry out spatially-regulated biological functions. During mitosis, RalA recruits RalBP1 to mitochondria to promote mitochondrial fission (Kashatus et al., 2011). Similarly, RalA recruits Filamin to the cell surface to induce filopodia formation (Ohta et al., 1999). We show here that PLD1 relocalizes to lysosomes over the course of nutrient starvation in WT cells, but not those lacking RalA. While RalA has been shown to precipitate PLD1 activity in a nucleotide-independent manner (Jiang et al., 1995), whether lysosomal recruitment of PLD1 by RalA is through direct binding remains unclear. Intriguingly, we observe only a subpopulation of PLD1 relocalized to lysosomes. Both RalA and PLD1 are membrane bound and share overlapping localizations under various cellular conditions. A subpopulation of both RalA and PLD1 are localized at endosomes and only this endosomal

pool may be relocating to lysosomes. Consistent with this possibility, we detect a large population of RalA on late endosomes. Additionally, other studies have shown that PLD1 partially relocates from the endosomal compartment to LC3 puncta and the lysosome in HeLa cells during nutrient deprivation and the evidence suggests that PLD1 is targeted to these compartments by endosomal membranes (Dall'Armi et al., 2010). PLD1 is thought to localize to endosomes through the PX and PH domains found on its N-terminus (Hodgkin et al., 2000; Stahelin et al., 2004). In another study, PLD1 translocates to lysosomes in HEK293 cells in a Vsp34 dependent manner (Yoon et al., 2011). Vsp34 is a Class III PI 3-Kinase required for autophagy. Interestingly, it was found that PLD1 translocates to lysosomes in amino acid stimulated conditions (Yoon et al., 2011). It is likely that PLD1 movement in the cell is regulated by multiple distinct proteins and cellular conditions, adding spatial and temporal control of its cellular functions.

An interesting question from this study is understanding how RalA and PLD1 cooperate to facilitate LD accumulation under nutrient deprivation. We demonstrate that PLD1 rescues starvation-induced LD accumulation in RalA deficient cells and this ability requires its enzymatic activity. The enzymatic product of PLD1, phosphatidic acid (PA) is a multifunctional lipid involved in intracellular trafficking, lipid signaling, protein recruitment, and biophysical membrane remodeling (Athenstaedt and Daum, 1999; Tanguy et al., 2019). Increasing evidence has emerged of PA's involvement in LD formation and growth. Elevated PA levels in yeast cells lead to LD coalescence and subsequent formation of "supersized" LDs (Fei et al., 2011). Additionally, PA and PLD1 were shown to be required for LD formation in a microsome based, cell-free system (Marchesan et al., 2003). Given its unique anionic, conical shape, PA has been proposed to be involved in other LD formation processes, including LD formation on the ER membrane and scission of LDs from the ER (Skinner et al., 2009). Importantly, others have reported that PLD1 activity increases during HBSS starvation (Dall'Armi et al., 2010). While an increase in PLD1 activity might be predicted to increase

cellular PA levels, we did not observe significant changes to total PA levels in MEFs following starvation. Since PA is a precursor to downstream metabolites such as diacylglyceride (DAG), it may be quickly converted upon synthesis during nutrient starvation, explaining the lack in detectable changes. Alternatively, increased PA at the lysosome may be offset by loss of PA production from other sites. Furthermore, a number of PLD1 interacting proteins such as Arf, PKC, and the Rho family of GTPases increase PLD1 activity upon binding (Brown et al., 1993; Kuribara et al., 1995; Singer et al., 1996). Although RalA interacts with PLD1, this interaction has no effect on PLD1 activity (Luo et al., 1998). We speculate that the RalA-PLD1 axis is facilitating LD accumulation without enhancing its ability to generate PA. Instead, it is the localized production of PA at lysosomes that leads to LD accumulation. This is consistent with the lysosome releasing PC, a substrate for PLD1, from recycled membranes. Remarkably, by forcing PLD1 to localize to the lysosome in MEFs lacking RalA, we were able to rescue LD accumulation during HBSS starvation as well as PLIN3 relocalization to LDs. This result also confirmed that the RalA-PLD1 interaction is not necessary for PLD1-dependent PA production. However, this does not rule out other proteins being involved in this process, such as the PLD1 activating proteins mentioned above.

While the precise mechanisms of PLD1 activity and PA involvement remain to be fully elucidated, gaining a better understanding of the cellular distribution of PA during nutrient starvation would prove useful. PA could potentially be used for TAG production and packaged into LDs, for insertion into the ER bilayer to facilitate LD formation and budding, or for insertion into the LD monolayer to facilitate protein recruitment, among other possibilities. Our data is consistent with PLD1-produced PA being utilized in any of these ways. PLIN3 rapidly localizes to growing LDs upon fatty acid stimulated conditions (Bulankina et al., 2009; Kassar et al., 2013; Nose et al., 2013). PA and DAG have both been proposed to recruit PLIN3, both onto LD monolayers and onto LD formation sites on the ER (Mirheydari et al., 2016; Skinner et al.,

2009). Upon nutrient starvation, we observe a remarkable RalA-dependent relocalization of PLIN3 from the cytosol to LDs. These data support the model in which RalA function during LD formation is to promote PLIN3 recruitment through compartmentalization of PA production. PA being produced at the lysosome instead of the ER raises the question of how it is transferred between these organelles. Close inspection by EM and high-resolution confocal microscopy shows clear examples of LDs, lysosomes, and ER in close proximity to one another. These observations suggest that PA transfer is through membrane contact sites (MCS) and not vesicular trafficking. It is unlikely that PA is entering the ER by passive diffusion. A more likely scenario is that a lipid transfer protein (LTP) shuttles PA from the lysosome to the ER. Interest in ER-endolysosomal MCS has grown in recent years. Increasing studies demonstrate a variety of LTPs are enriched at ER-endolysosomal MCS (Alpy et al., 2013; Höglinger et al., 2019; Kvam and Goldfarb, 2004; Lim et al., 2019; Ouimet et al., 2016; Rocha et al., 2009). While a specific PA LTP at the ER has yet to be reported, PA LTPs have been identified in other organelles, such as the mitochondria (Connerth et al., 2012). The cellular coordination in forming spatial localization of organelles during HBSS starvation is unclear, though RalA does not appear to be involved in this process as we observe the ER, LD and lysosomes in close proximity regardless of RalA expression.

Several additional questions are raised by these findings. First, how does RalA sense starvation and what molecular changes occur to allow RalA to perform this function? While the current evidence does not support a role for RalA nucleotide binding in this regulation, RalA contains a number of post-translational modification sites that may be playing a role (Neyraud et al., 2012; Sablina et al., 2007; Wu et al., 2005). Phosphorylation at serine 194 relocalizes RalA from the plasma membrane to internal membranes such as the mitochondria (Kashatus et al., 2011). Additionally, phosphorylation of RalB at serine 198 relocalizes RalB from the plasma membrane to the perinuclear region (Martin et al., 2012). Furthermore, non-degradative mono-ubiquitination on lysine residues can impact RalA and RalB localization

(Neyraud et al., 2012). We speculate Ra1A phosphorylation and/or ubiquitination following nutrient starvation drives its movement to lysosomes. We recently reported that Ra1A accumulates at depolarized mitochondria in a clathrin-mediated endocytosis dependent manner (Pollock et al., 2019). It is possible that Ra1A relocalization to lysosomes during nutrient stress is also reliant on the endocytic pathway. A key function of the endocytic pathway is internalization of nutrients found outside the cell. Imported nutrients are sorted into the early endosome, an organelle that sorts cargo into multiple cellular destinations. A subset of early endosomes mature into late endosomes, which eventually fuse with and digest their cargo in the lysosome. Consistent with this idea and in agreement with other reported studies, we detect Ra1A on late endosomes under fed conditions and on lysosomes in both fed and starved conditions. This data points to a mechanism by which Ra1A can localize to lysosomes, but further exploration of the upstream of signaling and Ra1A trafficking in the cell is needed to fully understand the Ra1A response to nutrient starvation.

In summary, we have identified a novel function for Ra1A and PLD1 in facilitating LD accumulation under nutrient stress. It is critical for cells to be able to regulate the amount of energy stored as triacylglycerides (TAG). Exceeding physiological capacity of TAG storage is linked to a number of diseases including obesity, diabetes, and cancer. Several studies have emerged in recent years describing altered LD content in different types of malignancies and metabolic disorders. Additionally, dysfunction of LD-related processes like lipolysis and lipophagy lead to physiological conditions such as neutral lipid storage disease, fatty liver disease, and atherosclerosis. As our knowledge of LD biology expands, new avenues to treat and prevent these diseases will arise. Further characterization of the mechanism by which Ra1A and PLD1 regulate LDs will contribute to these efforts.

## **2.4 Materials and Methods**

### **2.4.1 Chemicals**

The following chemicals were used at the indicated concentrations: 100  $\mu$ M Chloroquine (MP Biomedicals), 200 nM Bafilomycin A1 (Sigma-Aldrich), 750 nM FIPI (Calbiochem), 1  $\mu$ g/ml BODIPY 493/503 (Invitrogen) 1  $\mu$ M BODIPY 558/568 C12 (Invitrogen), 1:250 LipidTOX Deep Red (Invitrogen). All inhibitor concentrations were used at sub-lethal doses.

### **2.4.2 Cell Culture**

HeLa cells were obtained from ATCC. Mouse Embryonic Fibroblasts (MEFs) were obtained from Christopher Marshall (Peschard et al., 2012). Sex of HeLa cells is female. Sex of MEF cells used in this study has not been determined. Cells were kept at 37°C with 5% CO<sub>2</sub>. Both HeLa and MEFs were maintained in Dulbecco's Modified Eagle Medium (DMEM - Gibco) supplemented with 10% Fetal Bovine Serum (FBS – Gibco) and 1% Penicillin-Streptomycin (Gibco). For all nutrient starvation studies performed, cells were replenished with fresh DMEM 1 hour prior to starvation in Hank's Balanced Salt Solution (HBSS – Gibco) supplemented with 800  $\mu$ M MgCl<sub>2</sub> and 1.8 mM CaCl<sub>2</sub>. HeLa cells, and all of the stable genetic variants of those HeLa cells, are periodically authenticated using short tandem repeat (STR) profiling. MEF cell lines are regularly authenticated through PCR and immunoblot to confirm expression or deletion of genes.

### **2.4.3 Western Blotting**

Cells were lysed in RIPA buffer containing protease inhibitors. Protein concentration was determined by Bio-Rad Protein Assay (Bio-Rad). Equivalent protein was loaded and resolved by SDS-PAGE. Gels were transferred onto PVDF membranes (Millipore) and

immunoblotted using the following antibodies: anti-Ra1A (BD Transduction Laboratories), anti-GAPDH (Cell Signaling Technology - CST), anti- $\beta$ -Actin (CST), anti- $\beta$ -Tubulin (CST), anti-4E-BP1 (CST), anti-phospho-4E-BP1 (Thr37/46 – CST), anti-LC3B (CST), anti-Perilipin 3/Tip47 (Santa Cruz), anti-Ra1BP1 (Santa Cruz), anti-Vinculin (CST). Goat  $\alpha$ -rabbit and goat  $\alpha$ -mouse HRP secondary antibodies (Jackson ImmunoResearch Laboratories, Inc) were used for detection. Western blot images were taken on a ChemiDoc (Bio-Rad) using chemiluminescence detection with WesternBright ECL (Advansta). Where applicable, band pixel intensities were quantified using ImageJ.

#### **2.4.4 Immunofluorescence**

Cells were seeded at 30% confluency onto glass coverslips (Fisher Scientific). After 48 hours, cells were treated with HBSS/Oleic Acid/inhibitors as described elsewhere in methods. After treatment, cells were fixed with 3% formaldehyde in PBS for 10 min, washed 3x in PBS and permeabilized in microscopy buffer for 10 min. Microscopy buffer contains 0.1% Saponin (Sigma-Aldrich), 1% BSA (Fisher Scientific) in 1x PBS. Cells were then blocked in either 5% normal goat or 5% normal donkey serum (Cell Signaling Technology) in microscopy buffer for 20 mins. After blocking, cells were incubated for 1 hr in one of the following antibodies diluted in microscopy buffer: anti-Perilipin2/ADRP (Santa Cruz), anti-Perilipin 3-Tip47 (Santa Cruz), anti-Limp2 (Gift from John D. Castle – University of Virginia), anti-Calnexin (Gift from John D. Castle). Cells were then washed 3x in PBS and incubated in one of the following secondaries diluted in microscopy buffer for 30 mins: Alexa Fluor 488 (Invitrogen), Alexa Fluor 568 (Invitrogen) Alexa Fluor 647 (Invitrogen). Lastly, cells were washed 3x in PBS and mounted in DAPI solution (Cell Signaling Technology) to visualize nuclei. Images were taken on Zeiss LSM 700, 710, and 880 confocal microscopes (UVA Advanced Microscopy Facility). Airyscan images were taken using Zeiss LSM 880 (UVA Advanced Microscopy Facility).

For lipid droplet imaging, cells were seeded and fixed in formaldehyde as described above. Next, cells were incubated in 1 mg/ml BODIPY 493/503 (Invitrogen), 1:200 LipidTOX Deep Red (Invitrogen), or 100  $\mu$ M Monodansylpentane (Abcepta) in PBS for 30 min. In immunofluorescence studies with co-staining of LDs, 1 mg/ml BODIPY 493/503 was added to the secondary antibody step. After staining, cells are washed 3x in PBS before mounting onto slides.

#### **2.4.5 Image Analysis**

Zeiss Zen, ImageJ and Fiji software were used to process and analyze images captured by confocal microscopy. ImageJ was used to process electron micrographs. LD quantitation was done on Image/Fiji. Uniform threshold function was applied to LD images and used to generate a mask on LDs. Analyze particles function was used to generate total area of LDs. Fiji coloc2 function was used to generate Pearson's correlation coefficient's for colocalization studies. Image J was used to quantitate mCherry and GFP LC3B punctae and ratios.

#### **2.4.6 Transfection and Constructs**

For transient transfections, cells were seeded at 30% confluency onto glass coverslips (VWR). After 24 hours, cells were transfected with the indicated constructs using FuGENE 6 (Promega). 500 ng of the following fluorescent constructs were used per coverslip: pEGFP-RalA, mCherry-RalA, pEGFP-PLD1, pEGFP-PLD1 (K898R), pEx-YFP-LC3, pEGFP-Rab7, pEGFP-EEA1. pEGFP-PLD1 and mutant pEGFP-PLD1 (K898R) were gifts from the Michael A. Frohman lab (Stony Brook University). pEGFP-Rab7 was a gift from the James E.

Casanova lab (UVA). 24-48 hours post-transfection, cells were fixed in 3% formaldehyde in PBS for 5 mins, washed in PBS and mounted on glass slides.

All stable cell lines were generated using Calcium-phosphate transfection using the retroviral packaging vector, pCL-10A1 (Novus Biologicals) followed by antibiotic selection. The following constructs were used to generate stable cell lines: pBabe puro mCherry-EGFP-LC3B, pWZL blasti mito-YFP, pbabe puro myc-RalA, pbabe puro myc-RalA S28N, pbabe puro myc-RalA Q72L, pbabe puro GFP-PLIN2, pbabe puro GFP-PLIN2-PLD1, pbabe neo mCherryTmem192, pbabe neo mCherryTMEM192-PLD1, pbabe neo mCherryTMEM192-LIPIN1. Site directed mutagenesis was used generate pbabe puro myc-RalA S28N and pbabe puro myc-RalA Q72L from pbabe puro myc-RalA (WT).

#### **2.4.7 Knockdowns and Knockouts**

For stable knockdown of RalA, short hairpin RNA (shRNA) target sequence (5'-AAGACAGGTTTCTGTAGAAGA-3') was used as reported previously (Lim et al., 2005). For stable knockdown of PLIN3, shRNA target sequence (5'- GAATGAGACATGTGTTTAA -3') was used as reported previously (Gu et al., 2019; Sztalryd et al., 2006). For stable knockdown of ATG5, shRNA target sequence (5'- CCTTGGAACATCACAGTACAT -3') was used as reported previously (Hollomon et al., 2013). All shRNA constructs were made in a pSuperior-Retro vector backbone and stable cell lines expressing constructs were generated as describe above.

Knockout of RalBP1 was done by CRISPR. The guide RNAs (sgRNA) target sequences are listed below. sgRNA sequences were cloned into lentiCRISPR v2 vector (addgene #52961). psPAX2 (Addgene #12260) and pCMV-VSV-G (Addgene #8454) was used to package shRNA constructs and generate lentiviral particles via calcium-phosphate transfection.

sgRalBP1-1 (exon 2): 5'-CACCGTCACTAGGGCTGCTGCTCGG-3'

sgRalBP1-2 (exon 3): 5'-CACCGCAGCTGATGTTGTAAACAG-3'

sgRalBP1-3 (exon 4): 5'-CACCGAAAAGCAGCCTATGACCGAG-3'

#### **2.4.8 Fatty Acid Pulse Chase Assay**

Fluorescent fatty acid pulse chase experiments were performed as described previously with slight modifications (Rambold et al., 2015). MEFs were seeded at 30% confluency onto glass coverslips. After 48 hours, cells were incubated in DMEM containing 1 $\mu$ M BODIPY 558/568 C12 (Red C12 – Invitrogen) overnight. Cells were washed in DMEM to remove Red C12 and incubated in DMEM for 1 hour. Cells were then chased in HBSS for the indicated time points. At each time point, cells were washed and fixed in 3% formaldehyde before mounting onto glass slides in DAPI solution (Cell Signaling Technology). For LD co-staining experiments, cells were incubated with 1 mg/ml BODIPY 493/503 (Invitrogen) for 30 mins after fixation to visualize LDs. For mitochondria co-staining experiments, MEFs stably expressing Mito-YFP to visualize the mitochondria were used.

#### **2.4.9 Oleic Acid Stimulation**

Oleic acid was conjugated to fatty acid-free BSA (Fisher Scientific) at an approximately 6:1 molar ratio. Oleic acid was solubilized in 70% EtOH and heated at 70°C for 15 min. Fatty acid-free BSA was dissolved in DMEM at 37°C for 30 min with vortexing. Heated EtOH containing oleic acid was slowly added to BSA in DMEM and mixed thoroughly. Cells were seeded onto coverslips as described above. DMEM was replenished on cells 1 hour prior to oleic acid stimulation. Cells were treated with a final concentration of 200  $\mu$ M oleic acid. LDs were stained and imaged as described above.

#### **2.4.10 Ral GTP Pulldown**

Generation of RalBP1-RBD sepharose beads were done as described previously (Pollock et al., 2019). Briefly, BL21 Escherichia coli cells expressing pGEX-KG-RalBD were induced with Isopropyl  $\beta$ -d-1-thiogalactopyranoside (IPTG) and rocked at 37°C for 3 hours. Bacteria pellets were lysed in PBST containing inhibitors and sonicated. Supernatant containing GST-RalBP1-RBD was collected and rocked overnight with Gluthathione Sepharose 4B (Sigma-Aldrich) beads overnight at 4°C. Beads were washed and resuspended in lysis buffer. To measure RalA GTP status, cells were incubated in HBSS starvation media for 0, 1, 2, and 4 hours. At each endpoint, cells were washed in ice-cold PBS, scraped and pelleted. Cells were lysed in GTP lysis buffer (1% NP-40, 50 mM Tris pH 7.5, 200 mM NaCl, 10 mM MgCl<sub>2</sub>, 1% aprotinin, 1 mM PMSF, 0.5 mM DTT), spun down and supernatant was collected. Protein concentration was determined by Bradford Assay (Bio-Rad). 500  $\mu$ g of protein was incubated with GST-RalBP1-RBD beads for 45 minutes at 4°C. Total RalA and GTP-RalA levels were detected by SDS-PAGE and immunoblotting.

#### **2.4.11 Lipid Extraction**

A modified Folch method (CHCl<sub>3</sub>:MeOH:H<sub>2</sub>O/2:1:2; 0.1N HCl) was used to extract lipids from RalA MEF cell pellets. Antioxidant BHT (butylated hydroxy toluene) was added at 50  $\mu$ g/mL during extraction. CHCl<sub>3</sub> (2 mL), and MeOH (1 mL) were added with 1.5 mL of ddH<sub>2</sub>O containing resuspended MEFs in a two-dram vial. 1N HCl (500  $\mu$ L) was added last to bring the final concentration of acid to 0.1 N. Samples were vortexed, incubated on ice for 20 min, and centrifuged at 2,000 x g for 5 min at 4 °C. The organic layer was transferred and aqueous layer extracted with addition of 1.5 mL of 2:1 CHCl<sub>3</sub>:MeOH solution. The extracted organic layers were combined and dried down under nitrogen stream. Samples were resuspended in 240  $\mu$ L of 1:1 MeOH:isopropanol and stored at -80 °C until further analysis.

#### **2.4.12 LC-MS/MS Analysis of Lipid Extracts**

The lipid samples were analyzed by LC-MS/MS. A Dionex Ultimate 3000 RS UHPLC system was used with an analytical column (Kinetex® 1.7  $\mu\text{m}$  C18 100 Å, Phenomenex, LC column 100 x 2.1 mm) and reverse phase LC solvents (C: ACN:H<sub>2</sub>O/50:50, 10 mM NH<sub>4</sub>HCO<sub>2</sub>, 1% formic acid; D: ACN:IPA:H<sub>2</sub>O/10:88:2, 10 mM NH<sub>4</sub>HCO<sub>2</sub>, 1% formic acid) with the following gradient: Flowrate 0.25 mL/min, 0 min 65% C, 4 min 40% C, 12 min 15% C, 21 min 0% C, 24 min, 0% C, 24.1 min 100% C, 27 min 0% C, 30 min 100% C, 33 min 0% C, 35 min 65% C. The eluted lipids were ionized by electrospray using a HESI-II probe into an Orbitrap Q-Exactive Plus mass spectrometer (Thermo Scientific). Data acquisition was performed using a Top10 data-dependent (ddMS2) global analysis method that consisted of one full MS1 scan (250-1,200 m/z) followed by 10 MS2 scans of the most abundant ions recorded in the MS1 scan. Lipid identifications and peak alignments were performed using LipidSearch™ software (version 4.0) while quantitative analysis of the aligned intensities was exported and analyzed using Prism GraphPad (version 7.03). Positive and negative ion annotations for each sample were combined and aligned within a chromatographic time window to allow greater confidence in lipid identifications using appropriate MS2 product ions and neutral losses from the compiled dataset in LipidSearch™ analysis software.

#### **2.4.13 Lipid Species Identification from LC-MS/MS Analysis**

Data analysis was performed using the LipidSearch™ software package, which used MS1 monoisotopic precursor ions for the in-silico database search followed by the product ions search from MS2 spectra (search parameters: Target database: Q Exactive, SearchType: product, ExpType: LC-MS, Precursor tolerance 5.0 ppm, product tolerance 5.0 ppm, intensity threshold: product ion 1.0%, m-score threshold 2.0). Results from positive and negative ion mode analyses were merged to generate a matched lipid dataset. The searched data were aligned with selected parameters (ExpType: LC-MS, Alignment Method: Median,

Toprank Filter: on, Main node Filter: Main isomer peak, m-Score Threshold: 5.0, ID quality filter: A, B, C, D) and curated with species with high-confidence grade scores “A” and “B” for further analysis.

#### **2.4.14 Electron Microscopy**

Cells were seeded at 40% confluency onto thermanox coverslips (Fisher Scientific). After 48 hours, cells were treated with HBSS as described elsewhere in methods. Preparation of samples for transmission electron microscopy was done by the UVA Advanced Microscopy Facility. After treatment, cells were fixed in 2% paraformaldehyde/2.5% Glutaraldehyde in 1x cacodylate buffer. Fixed samples were washed in 1x cacodylate buffer and then incubated in 2% osmium tetroxide for 1 hour (postfixation). Samples were then dehydrated by incubating in increasing concentrations of EtOH (50%-100%) for 10 min each followed by incubation in 100% propylene oxide for 10 min. Samples were then incubated in 1:1 propylene oxide/epoxy resin overnight, followed by incubation in 1:2 and 1:4 propylene oxide/epoxy resin for approximately 3 hours each. Afterwards, samples were incubated overnight in 100% epoxy resin. After dehydration, samples were embedded in fresh 100% epoxy resin and baked in a 65 degree oven. Following embedding, ultra-thin sections cut at 75 nm were made and placed on mesh copper grids. Samples were post stained for contrast with 0.25% lead citrate and 2% uranyl acetate. Images were taken on JEOL 1230 TEM (UVA Advanced Microscopy Facility).

#### **2.4.15 Quantification and Statistical Analysis**

GraphPad Prism was used for graphical representation and statistical analysis of data. Two-way ANOVA with Tukey's multiple comparison statistical analysis was applied to experiments unless stated otherwise in figure legends. Statistical significance is denoted in figures as \* $p < 0.05$ , \*\* $p < 0.01$ , \*\*\* $p < 0.001$ , and \*\*\*\* $p < 0.0001$ . Biological replicates are

denoted as n values and are listed in the figure legends for each experiment. n values represent the number of times an experiment was performed. Data are presented as mean  $\pm$  SEM.

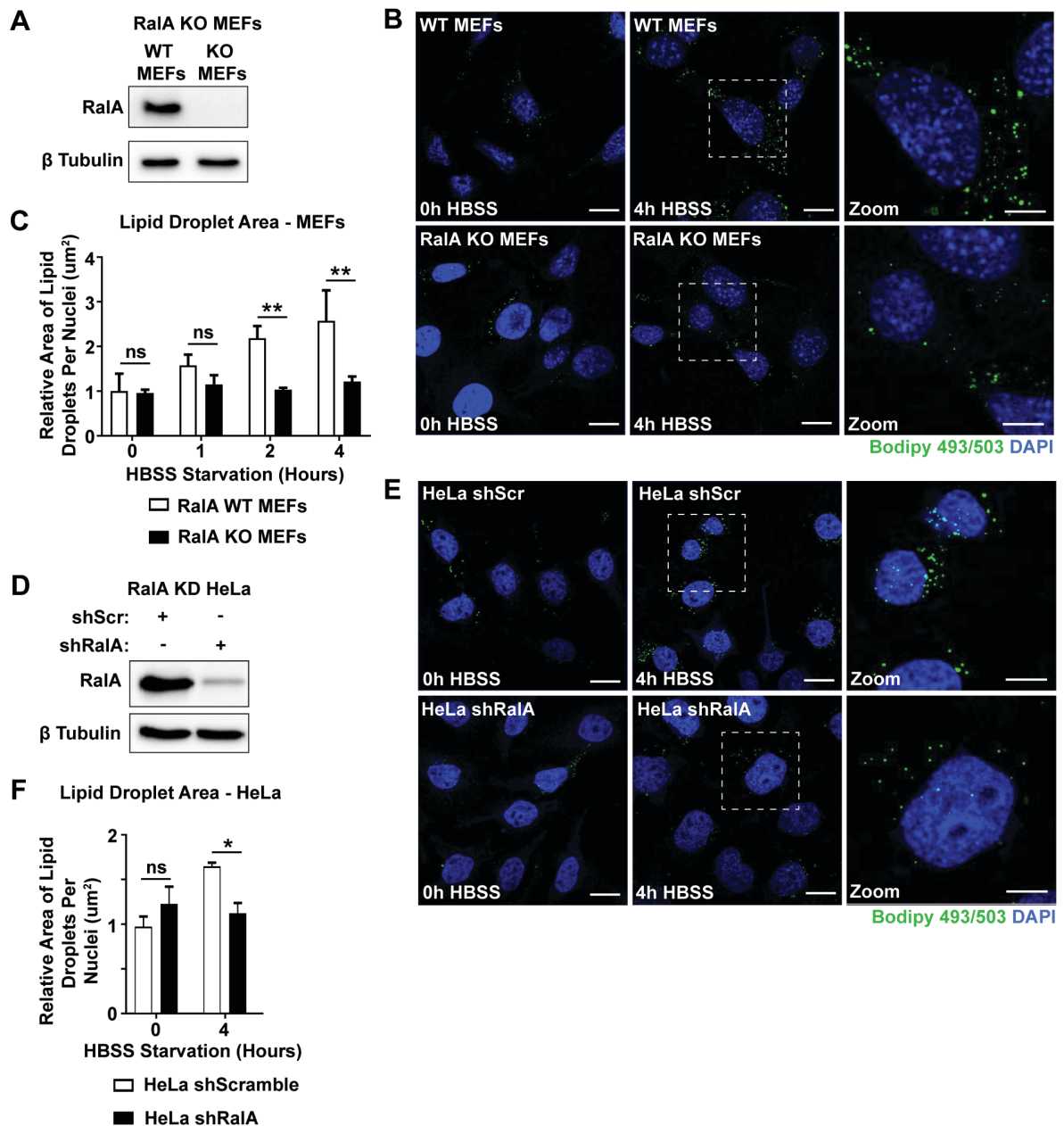


### Figure 2.1 RalA is required for starvation-induced lipid droplet accumulation

(A) Western blot confirming knockout of RalA protein expression in RalA KO MEFs.

(B) Representative images of LDs in WT and RalA KO MEFs starved in HBSS media for 4 hours. LDs (green) were labeled using BODIPY 493/503 and nuclei (blue) were labeled using DAPI. Scale bars are 20  $\mu\text{m}$  in all panels except for zoom. For zoom panels, scale bars are 10  $\mu\text{m}$ .

(C) Quantification of LD area per cell from B. At least 100 cells were analyzed for each time point.  $n=3$ . Two-way ANOVA using Tukey's multiple comparisons test, mean  $\pm$  SEM, \*\* $p < 0.01$ .

(D) Western blot confirming knockdown of Ra1A protein expression in HeLa cells.

(E) Representative images of LDs in scramble control and Ra1A knockdown HeLa cells. Scale bars, 20  $\mu\text{m}$ .

(F) Quantification of LD area per cell from E. At least 100 cells were analyzed for each time point.  $n=3$ . Two-way ANOVA using Tukey's multiple comparisons test, mean  $\pm$  SEM, \* $p \leq 0.05$ .

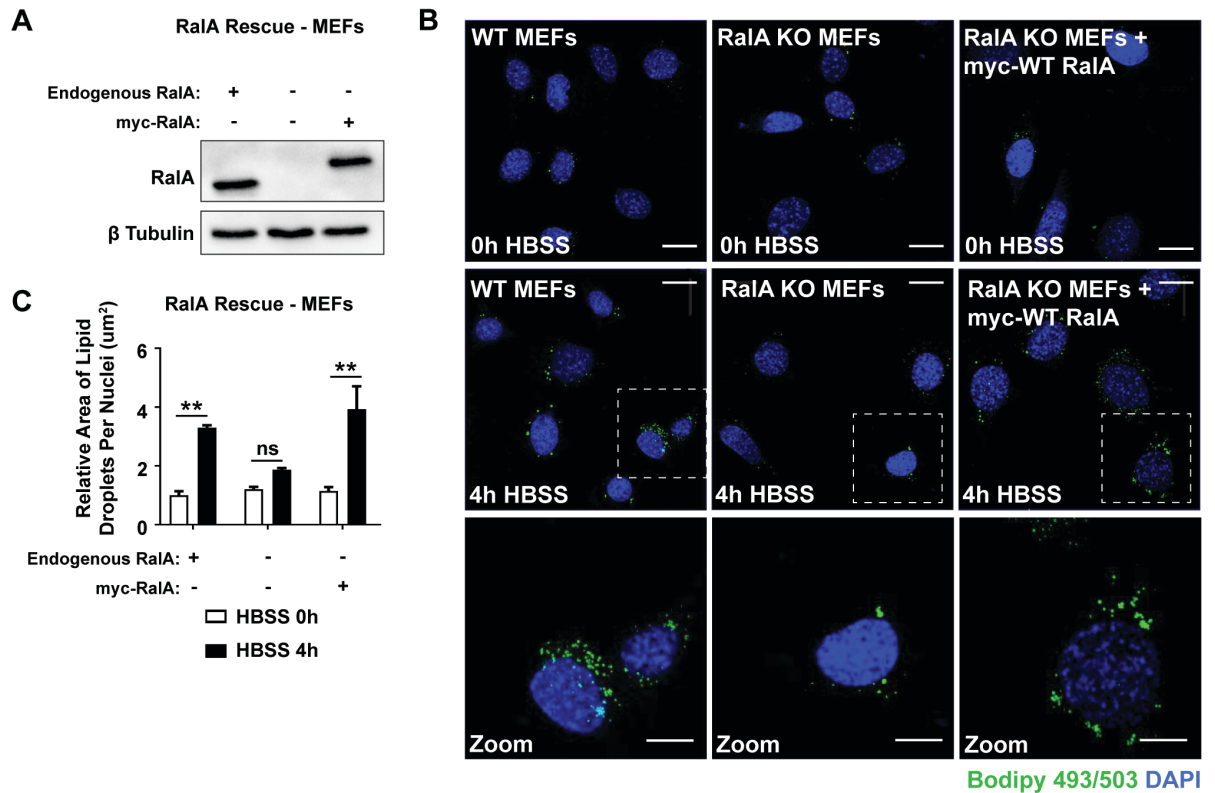


**Figure 2.2 WT RalA is sufficient to rescue LD accumulation in RalA KO MEFs**

(A) Western blot confirming expression of myc-RalA in RalA KO MEFs.

(B) Representative images of LDs in RalA KO MEFs expressing myc-RalA. Scale bars are 20 µm in all panels except for zoom. For zoom panels, scale bars are 10 µm.

(C) Quantification of LD area per cell from B. At least 100 cells were analyzed for each time point. n=3. Two-way ANOVA using Tukey's multiple comparisons test, mean ± SEM, \*\*p ≤ 0.01.

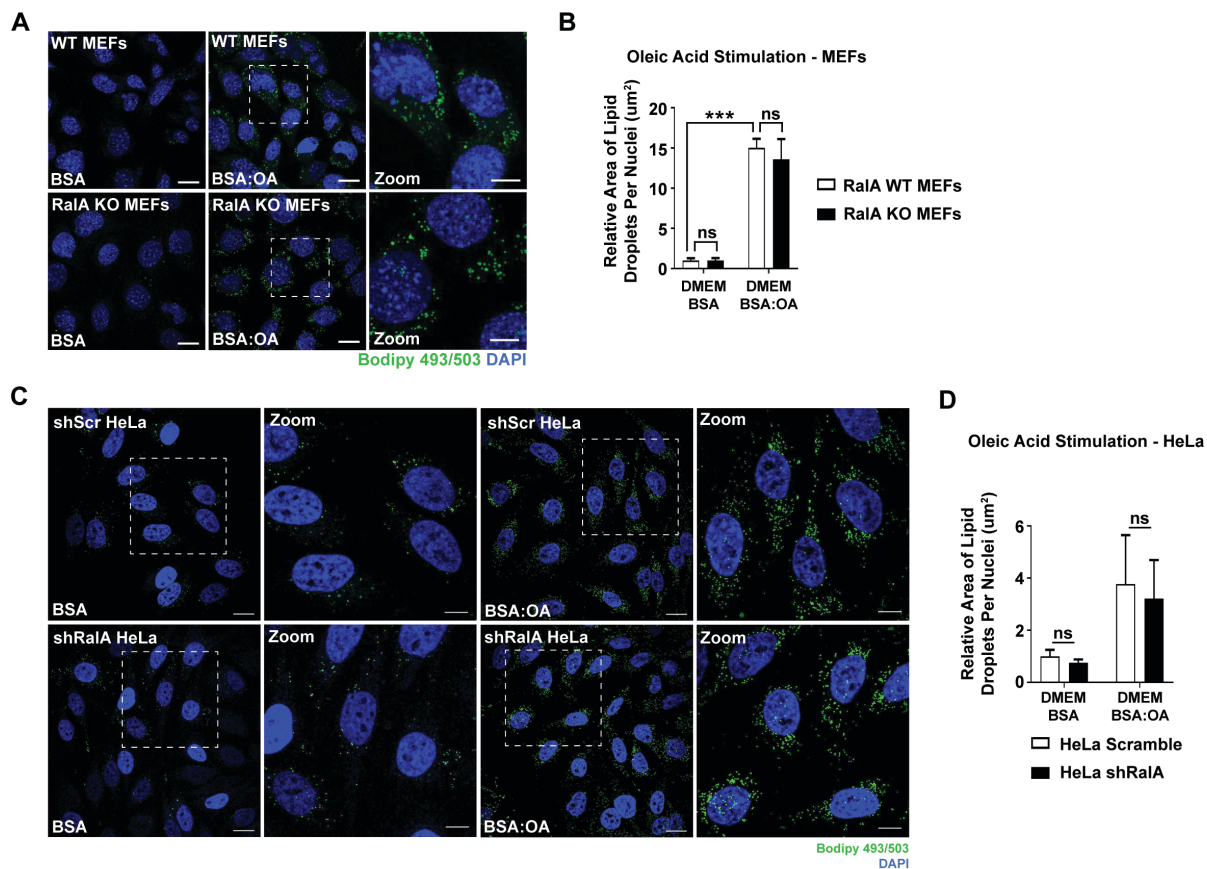


### Figure 2.3 Oleic acid-induced LD accumulation is RaIA-independent

(A) Representative images of LDs in WT and RaIA KO MEFs stimulated with 200 µM Oleic Acid conjugated to BSA in DMEM for 4 hours. Scale bars are 20 µm in all panels except for zoom. For zoom panels, scale bars are 10 µm.

(B) Quantification of LD area per cell from A. At least 100 cells were analyzed for each time point. n=3. Two-way ANOVA using Tukey's multiple comparisons test, mean ± SEM, \*\*\*p < 0.0001.

(C) Representative images of LDs in scramble and RaIA KD HeLa stimulated with 200 µM Oleic Acid conjugated to BSA in DMEM for 4 hours. Scale bars are 20 µm in all panels except for zoom. For zoom panels, scale bars are 10 µm.

(D) Quantification of LD area per cell from C. At least 100 cells were analyzed for each time point. n=3. mean ± SEM.

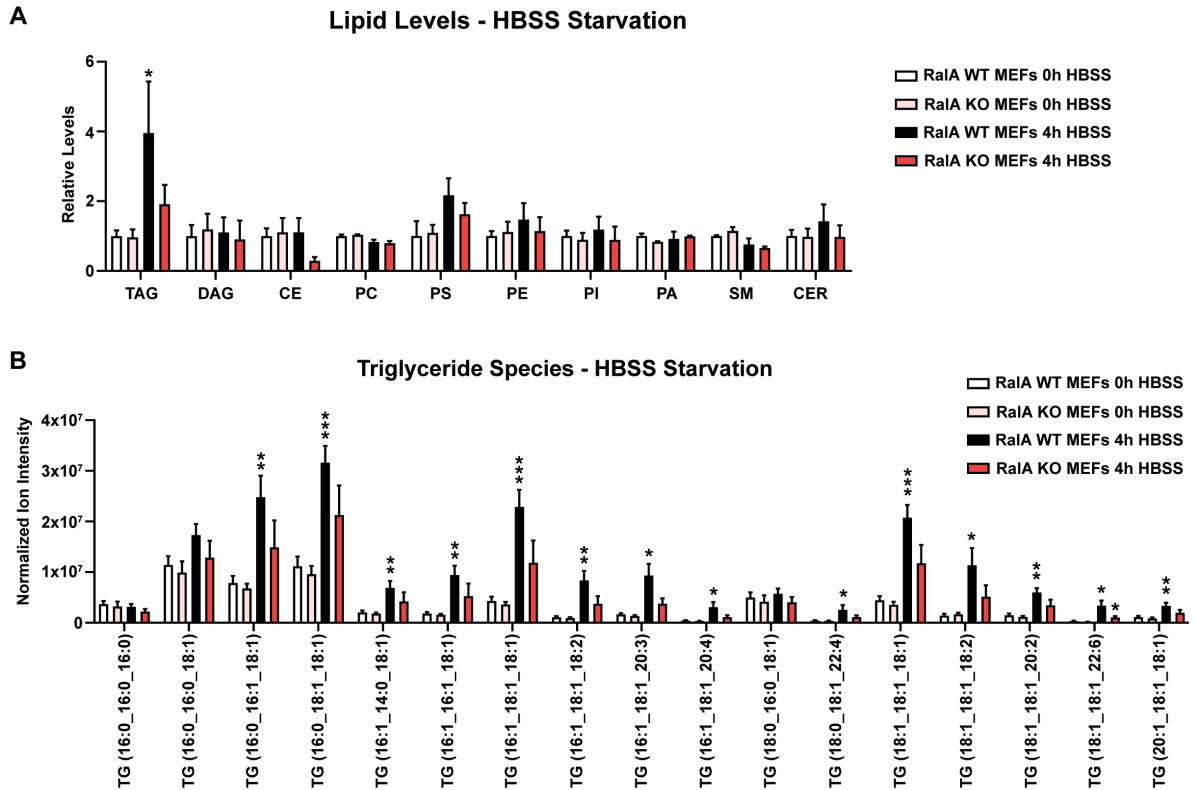


**Figure 2.4 Analysis of lipid composition during nutrient starvation shows significant difference in triacylglyceride levels between WT and RalA KO MEFs.**

MEFs were incubated in either DMEM (0h) or HBSS (4h) for 4 hours, lipids were extracted by modified Folch method and analyzed by LC-MS/MS.

(A) Relative levels of various lipids. Raw values were normalized to cell counts taken prior to lipid extraction.  $n=5$ . Two-way ANOVA using Tukey's multiple comparisons test was done for each set of individual lipid type, mean  $\pm$  SEM,  $*p \leq 0.05$ .

(B) Normalized ion intensity values for most abundant individual triacylglyceride (TG) species detected. The numerical value in the TG nomenclature indicate the fatty acid carbon length : number of unsaturated bonds. Raw values were normalized to cell counts taken prior to lipid extraction. Separate Multiple t-tests were used to compare 0h and 4h WT MEFs and 0h and 4h RalA KO MEFs.  $n=5$ . mean  $\pm$  SEM,  $*p \leq 0.05$ ,  $**p \leq 0.01$ ,  $***p \leq 0.001$ .

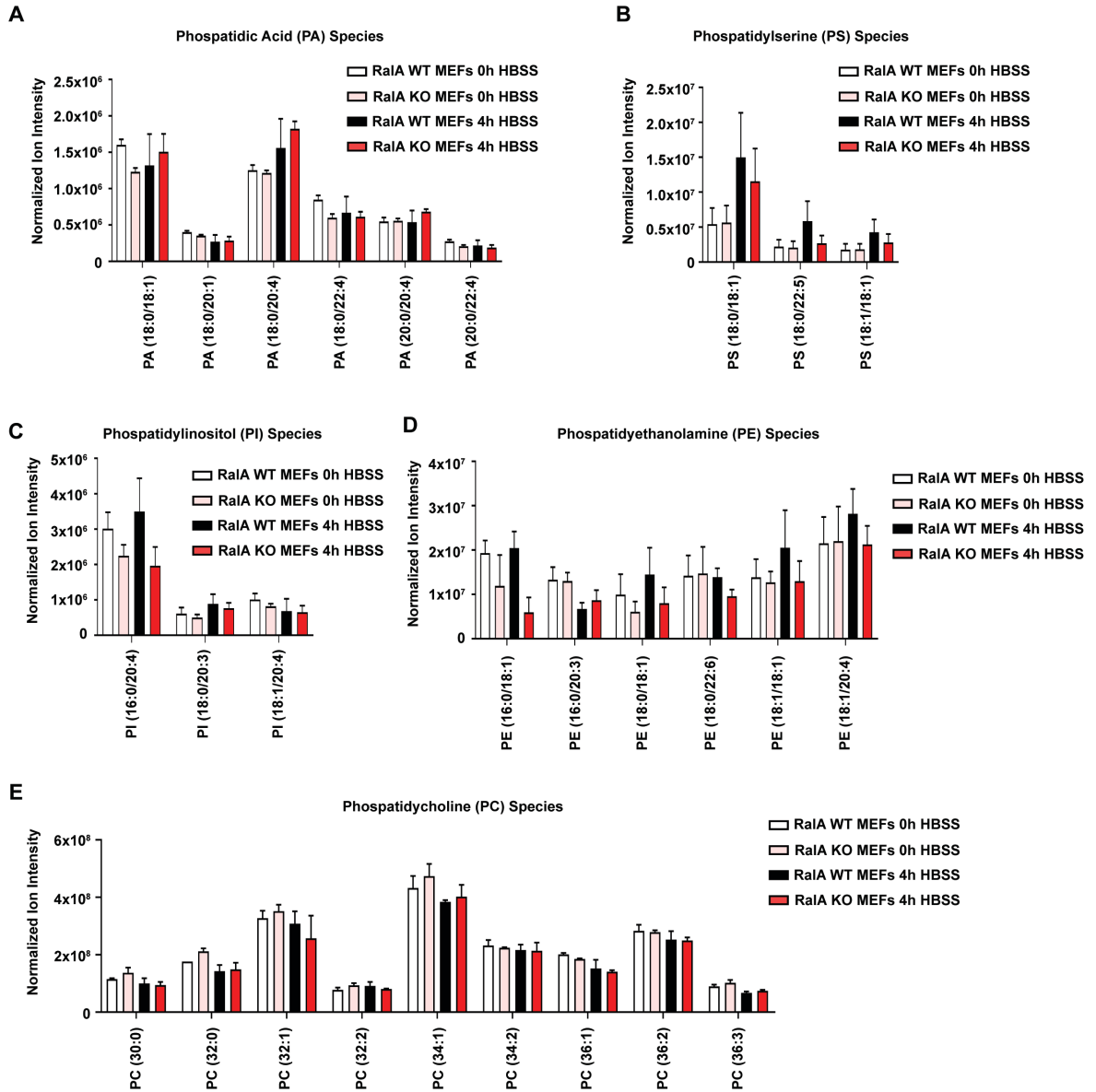


**Figure 2.5 Levels of major phospholipid species are not significantly different between WT and RaIA KO MEFs during nutrient starvation.**

(A-E) Normalized ion intensity values for most abundant individual lipid species detected A) phosphatidic acid, B) phosphatidylserine, C) phosphatidylinositol, D) phosphatidylethanolamine, E) phosphatidylcholine. MEFs were incubated in either DMEM (0h) or HBSS (4h) for 4 hours, lipids were extracted by modified Folch method and analyzed by LC-MS/MS. The numerical value in the lipid nomenclature indicate the fatty acid carbon length : number of unsaturated bonds. Raw values were normalized to cell counts taken prior to lipid extraction. n=2 for A and E, n=5 for B-D. mean  $\pm$  SEM.

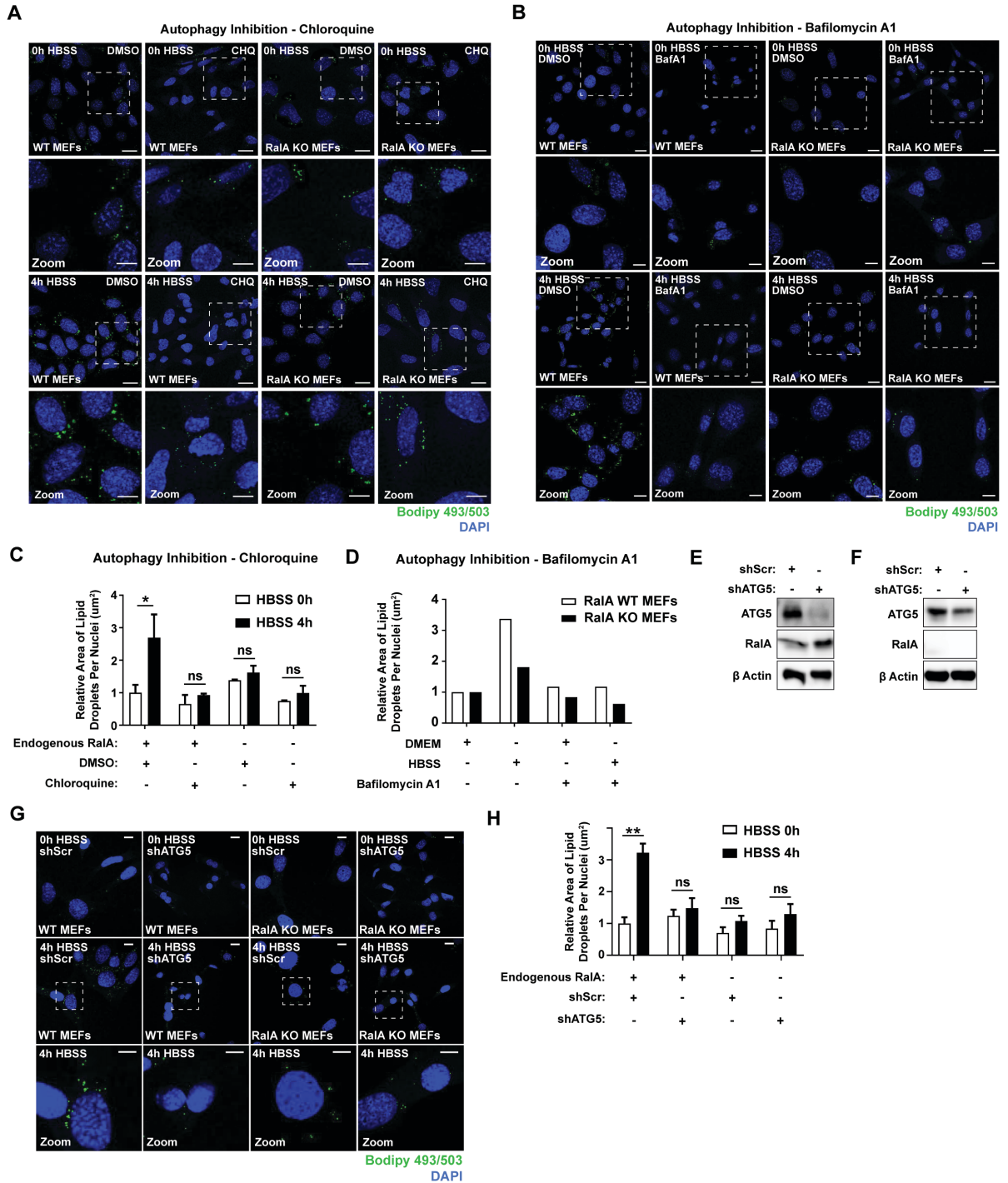


**Figure 2.6 Autophagy is necessary for RalA-dependent LD accumulation**

(A) Representative images of LDs in WT and RalA KO MEFs incubated in DMEM or HBSS media  $\pm$  100  $\mu$ M Chloroquine for 4 hours. LDs (green) were labeled using BODIPY 493/503 and nuclei (blue) were labeled using DAPI. Scale bars are 20  $\mu$ m in all panels except for zoom. For zoom panels, scale bars are 10  $\mu$ m.

- (B) Representative images of LDs in WT and Ra1A KO MEFs incubated in DMEM or HBSS media  $\pm$  200 nM Bafilomycin A1 for 8 hours. LDs (green) were labeled using BODIPY 493/503 and nuclei (blue) were labeled using DAPI. Scale bars are 20  $\mu$ m in all panels except for zoom. For zoom panels, scale bars are 10  $\mu$ m.
- (C) Quantification of LD area per cell from A. At least 100 cells were analyzed for each time point. n=3.
- (D) Quantification of LD area per cell from B. At least 25 cells were analyzed for each time point. n=1.
- (E) Western blot confirming knockdown of ATG5 protein expression in WT MEFs.
- (F) Western blot confirming knockdown of ATG5 protein expression in Ra1A KO MEFs.
- (G) Representative images of LDs (green) in WT and Ra1A KO MEFs expressing either shScramble or shATG5 constructs during HBSS starvation. Detection of LDs was done as described previously. Scale bars are 20  $\mu$ m in all panels except for zoom. For zoom panels, scale bars are 10  $\mu$ m.
- (H) Quantification of LD area per cell from G. At least 100 cells were analyzed for each time point. n=3. Two-way ANOVA using Tukey's multiple comparisons test, mean  $\pm$  SEM, \*\*p  $\leq$  0.01.

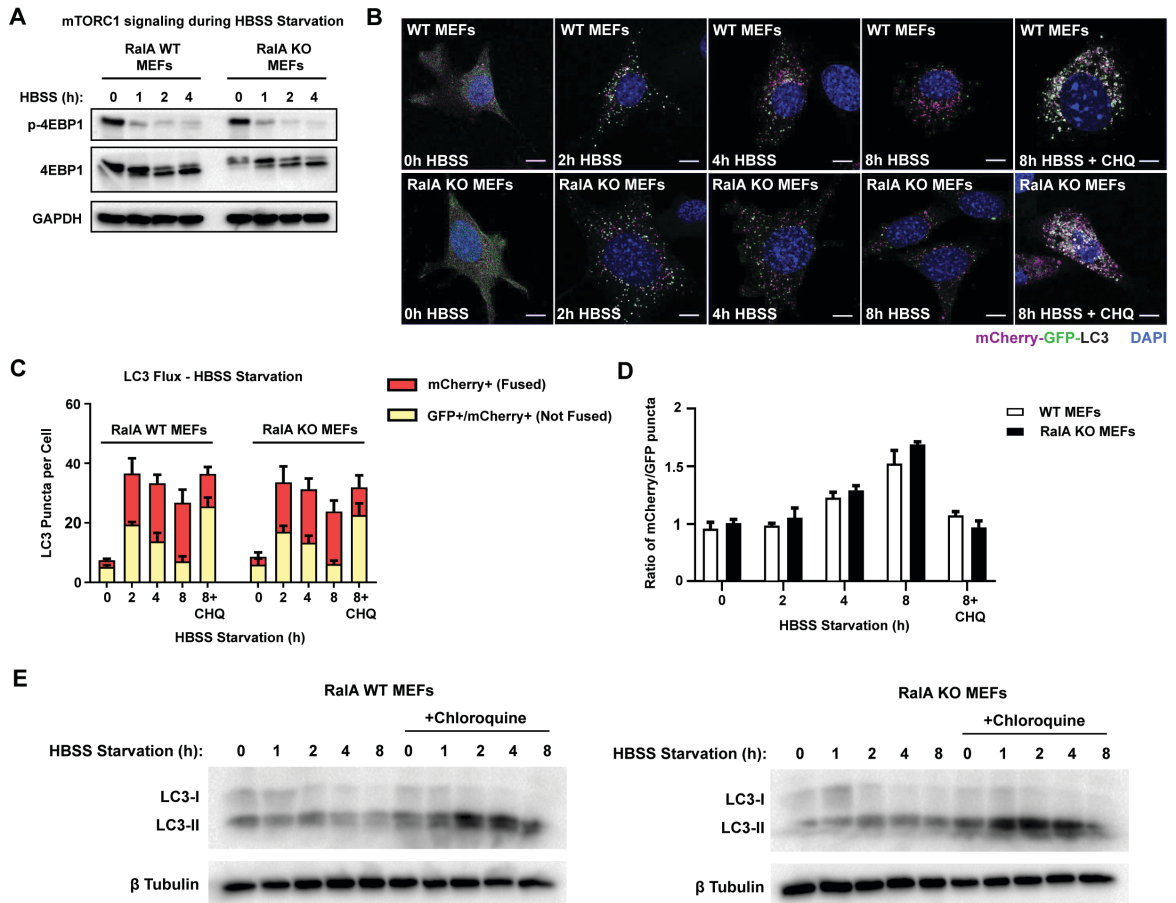


**Figure 2.7 Autophagy is not Impaired in RalA KO MEFs**

(A) Western blot analysis of phospho-4E-BP1 (Thr37/46), total 4E-BP1, and GAPDH protein levels in MEFs starved in HBSS for the indicated timepoints.

(B) Representative images of mCherry-EGFP-LC3B expression in MEFs starved in HBSS ± 100 uM Chloroquine for the indicated timepoints. mCherry only LC3B punctae indicate LC3 marked autophagosomes that have fused with lysosomes. mCherry-EGFP expressing LC3B punctae indicate LC3 autophagosomes that have not fused with lysosomes Scale bars, 20 μm.

(C) Quantification of mCherry-EGFP-LC3B punctae from B. Approximately 35-40 punctae were analyzed per cell and approximately 50 cells were analyzed for each time point. n=3. mean ± SEM.

(D) Ratio of mCherry+/GFP+ puncta calculated from B.

(E) Western blot analysis of LC3 protein levels in MEFs incubated in HBSS media ± 100 μM Chloroquine for the indicated time points.

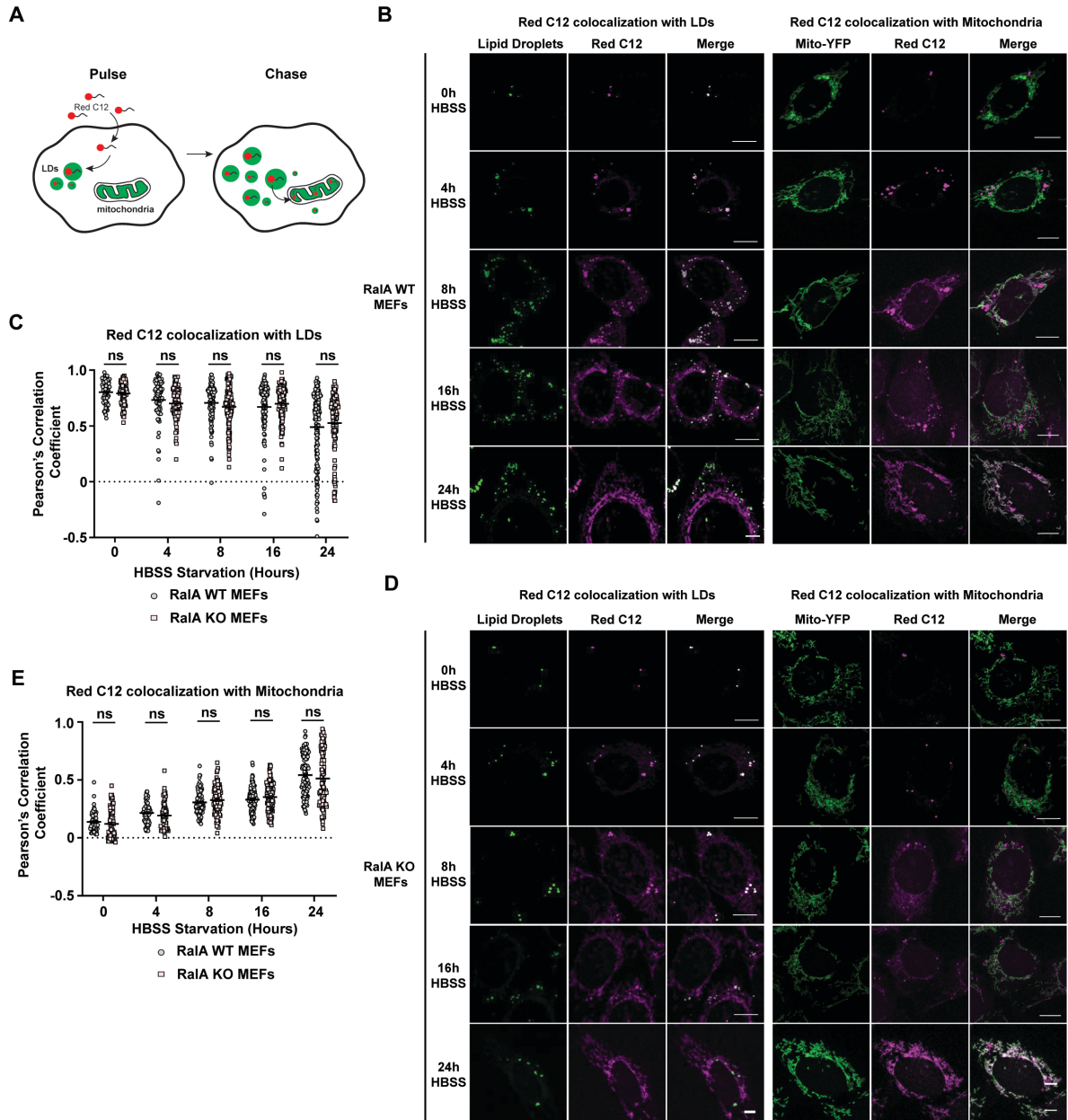


### Figure 2.8 Fatty acid trafficking to the mitochondria is RaiA-independent

(A) Schematic showing fluorescent Red C12 pulse chase experimental set up. MEFs were pulsed with Red C12 in DMEM overnight. Afterwards, cells were chased in HBSS for the indicated timepoints. Figure demonstrates fatty acid trafficking pattern observed.

(B,D) Representative images of Red C12 (magenta) pulse chase experiment in B) WT MEFs and D) RaiA KO MEFs. MEFs were starved in HBSS for the indicated timepoints. LDs (green) were labeled using BODIPY 493/503. MEFs stably expressing mito-YFP were used to visualize the mitochondria (green). Scale Bar, 5  $\mu$ m.

(C,E) Relative colocalization of C) Red C12 and LDs or E) Red C12 and mitochondria performed by Pearson's correlation coefficient. Each point on the graph represents a

Pearson's coefficient value for one cell. At least 75 cells were analyzed for each time point n=3. Two-way ANOVA using Tukey's multiple comparisons test. mean  $\pm$  SEM.

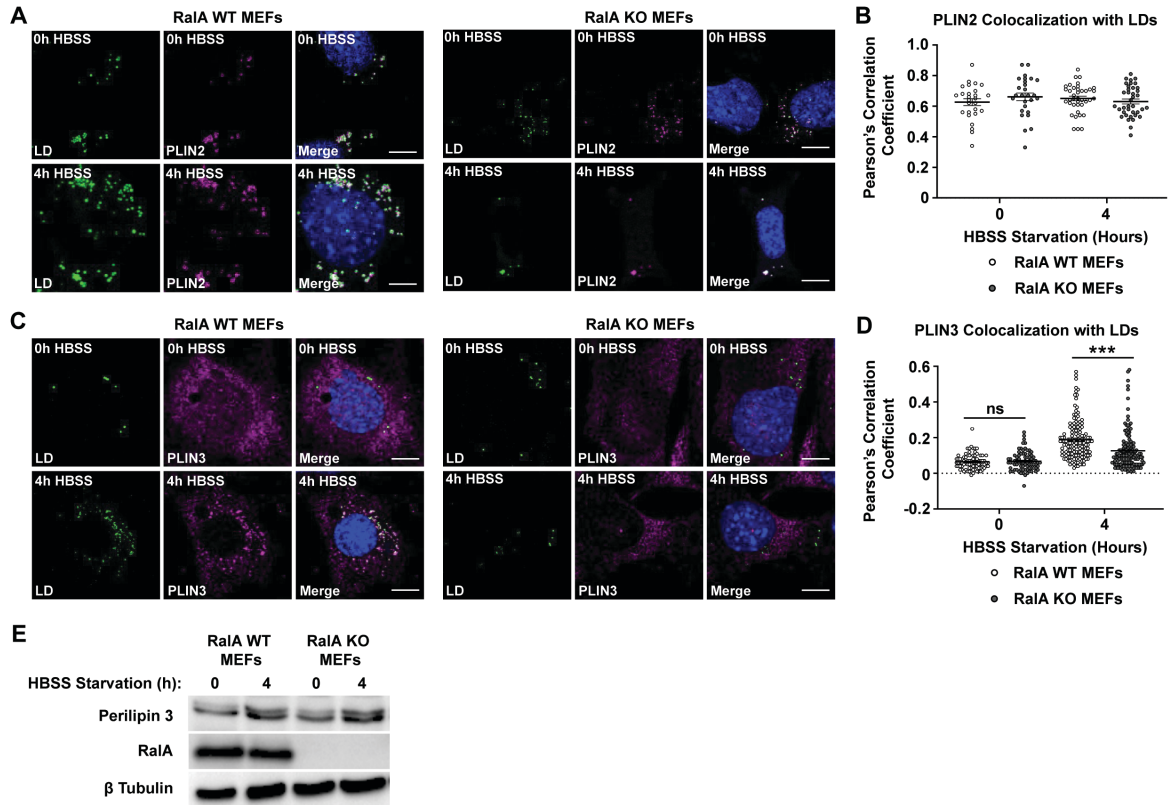


## Figure 2.9 PLIN3 but not PLIN2 recruitment to LDs during nutrient starvation is RalA dependent

(A) Representative images of PLIN2 and LDs in MEFs during 0h and 4h of HBSS starvation. PLIN2 (magenta) antibody was used to visualize localization. LDs (green) were labeled using BODIPY 493/503 and nuclei (blue) were labeled using DAPI. Scale bar, 10  $\mu$ m.

(B) Relative colocalization of PLIN2 and LDs during 0h and 4h of HBSS starvation performed by Pearson's correlation coefficient. Each point on the graph represents a Pearson's coefficient value for one cell. At least 25 cells were analyzed for each time point  $n=2$ . mean  $\pm$  SEM.

(C) Representative images of PLIN3 and LDs in MEFs during 0h and 4h of HBSS starvation. PLIN3 (magenta) antibody was used to visualize localization. LDs (green) were labeled using BODIPY 493/503 and nuclei (blue) were labeled using DAPI. Scale bar, 10  $\mu$ m.

(D) Relative colocalization of PLIN3 and LDs during 0h and 4h of HBSS starvation performed by Pearson's correlation coefficient. Each point on the graph represents a Pearson's coefficient value for one cell. At least 75 cells were analyzed for each time point  $n=3$ . mean  $\pm$  SEM. \*\*\* $p \leq 0.0001$ .

(E) Western blot analysis of PLIN3 protein levels in MEFs incubated in HBSS media for 0 or 4 hours.

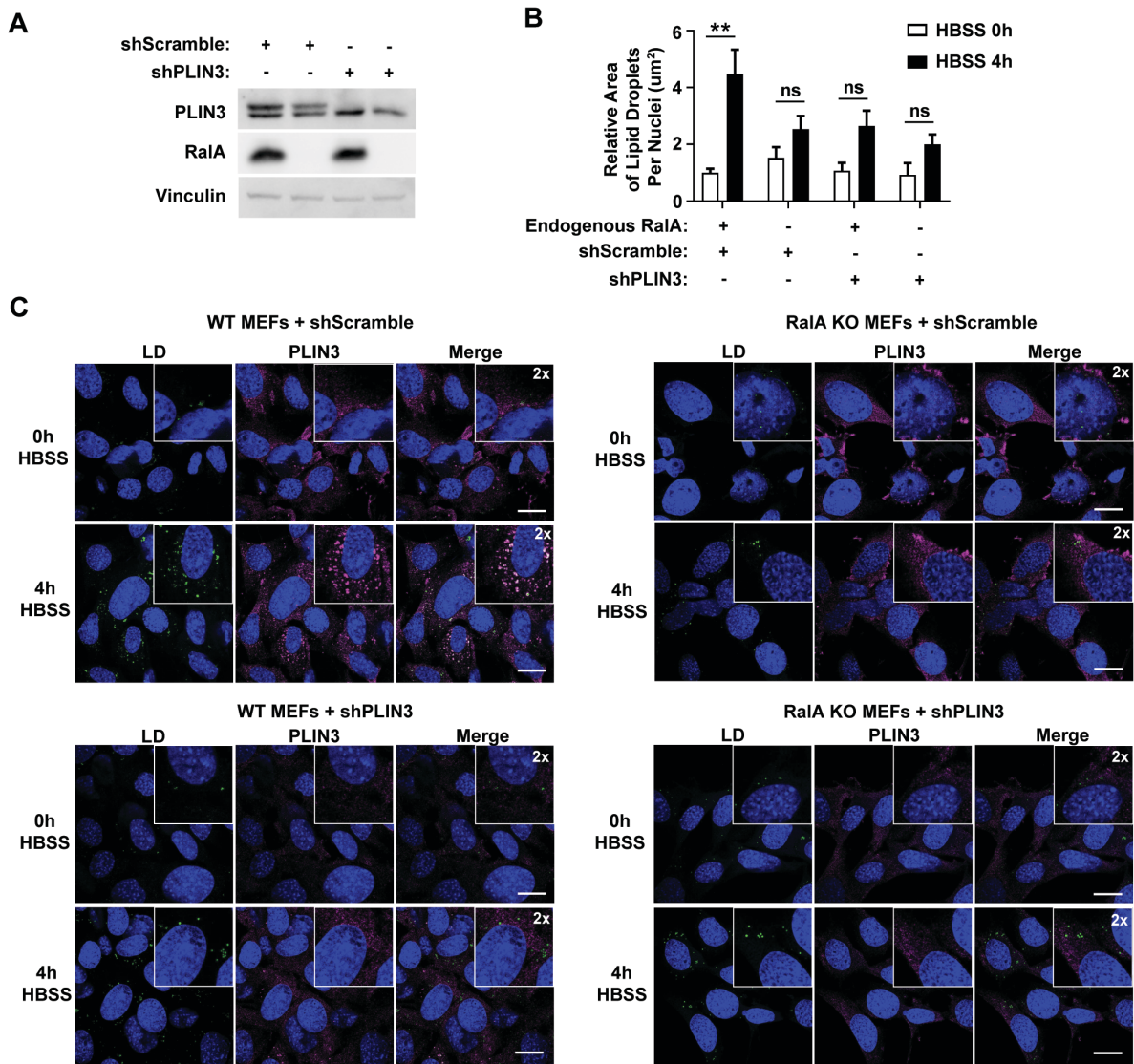


**Figure 2.10 PLIN3 is necessary for LD accumulation during nutrient starvation**

(A) Western blot confirming knockdown of PLIN3 protein expression in MEFs.

(B) Representative images of PLIN3 (magenta) and LDs (green) in WT and Ra1A KO MEFs expressing either shScramble or shPLIN3 constructs during 0h and 4h of HBSS starvation. Detection of PLIN3 and LDs was done as described previously. Scale bar, 20  $\mu$ m. Zoomed inserts are 2x magnification.

(C) Quantification of LD area per cell from B. At least 75 cells were analyzed for each timepoint. n=3. Two-way ANOVA using Tukey's multiple comparison test, mean  $\pm$  SEM, \*\*p $\leq$  0.01.

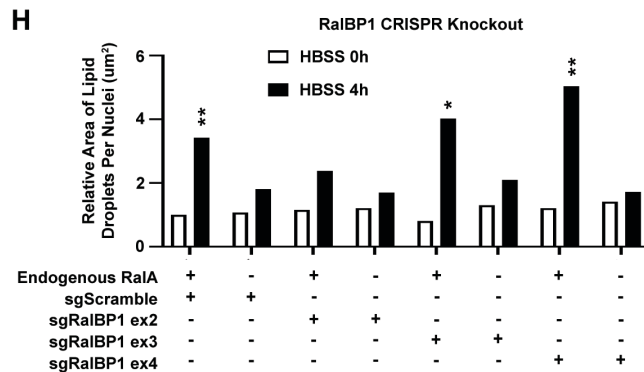
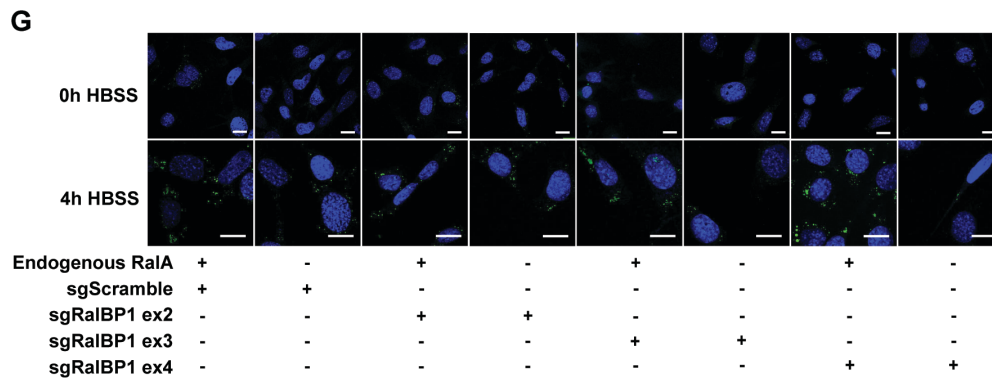
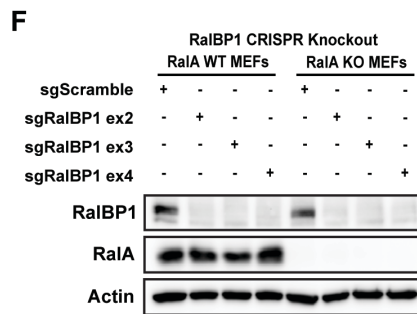
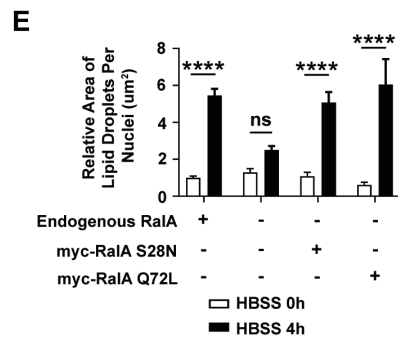
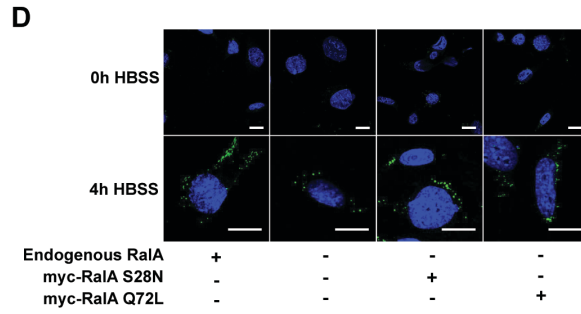
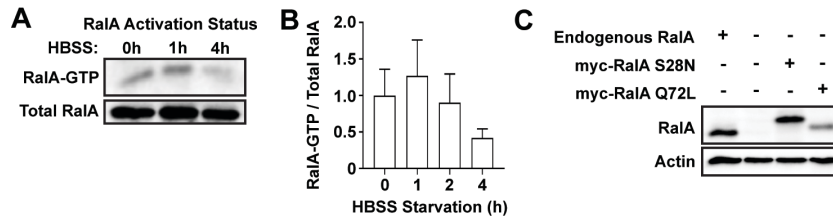


**Figure 2.11 RalA function during HBSS starvation is nucleotide-independent**

(A) Western blot analysis of RalA-GTP pulldown.

(B) Densitometry analysis of A.

(C) Western blot confirming expression of myc-RalA S28N or myc-RalA Q72L mutants in RalA KO MEFs.

(D) Representative images of LDs in RalA KO MEFs expressing myc-RalA S28N or myc-RalA Q72L. Scale bars, 20  $\mu$ m.

(E) Quantification of LD area per cell from D. At least 75 cells were analyzed for each time point. n=3-6. Two-way ANOVA using Tukey's multiple comparisons test, mean  $\pm$  SEM, \*\*\*p  $\leq$  0.0001.

(F) Western blot confirming knockout of RalBP1 protein expression in WT and RalA KO MEFs. Three guide RNAs targeting different exons were used to knockout RalBP1.

(G) Representative images of LDs in WT, RalA KO, RalBP1 KO and RalA/RalBP1 double KO MEFs. Scale bars, 20  $\mu$ m.

(H) Quantification of LD area per cell from G. At least 50 cells were analyzed for each time point. n=1-3. Two-way ANOVA using Tukey's multiple comparisons test, \*p  $\leq$  0.05, \*\*p  $\leq$  0.01.

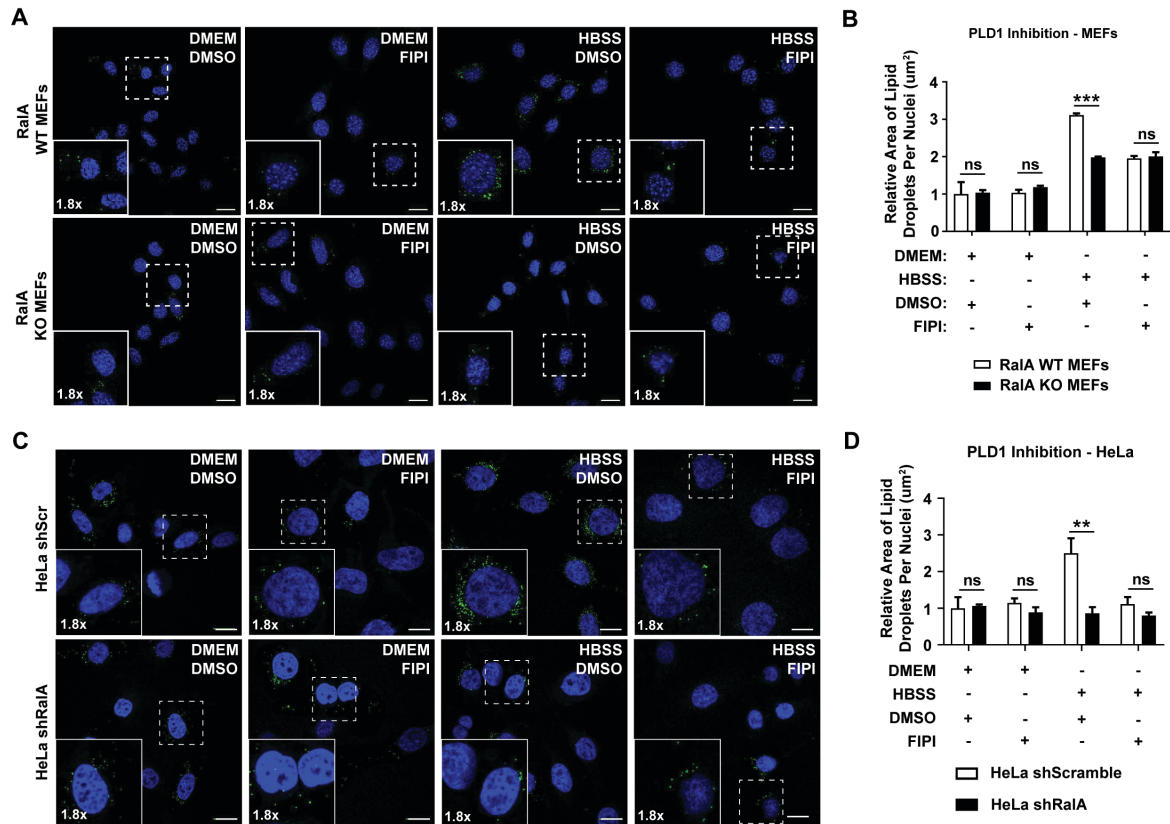


**Figure 2.12 PLD is Required for RaIA-Dependent Starvation Induced LD Accumulation**

(A) Representative images of LDs in WT and RaIA KO MEFs incubated in DMEM or HBSS media  $\pm$  750 nM FIPI for 4 hours. LDs (green) were labeled using BODIPY 493/503 and nuclei (blue) were labeled using DAPI. Scale bars, 20  $\mu$ m. Zoomed inserts are 1.8x magnification.

(B) Quantification of LD area per cell from A. At least 100 cells were analyzed for each time point.  $n=3$ . Two-way ANOVA using Tukey's multiple comparisons test, mean  $\pm$  SEM, \*\*\* $p \leq 0.001$ .

(C) Representative images of LDs in scramble and RaIA KD HeLa cells incubated in DMEM or HBSS media  $\pm$  750 nM FIPI for 4 hours. LDs (green) were labeled using BODIPY 493/503 and nuclei (blue) were labeled using DAPI. Scale bars, 20  $\mu$ m. Zoomed inserts are 1.8x magnification.

(D) Quantification of LD area per cell from C. At least 100 cells were analyzed for each time point.  $n=3$ . Two-way ANOVA using Tukey's multiple comparisons test, mean  $\pm$  SEM, \*\* $p \leq 0.01$ .

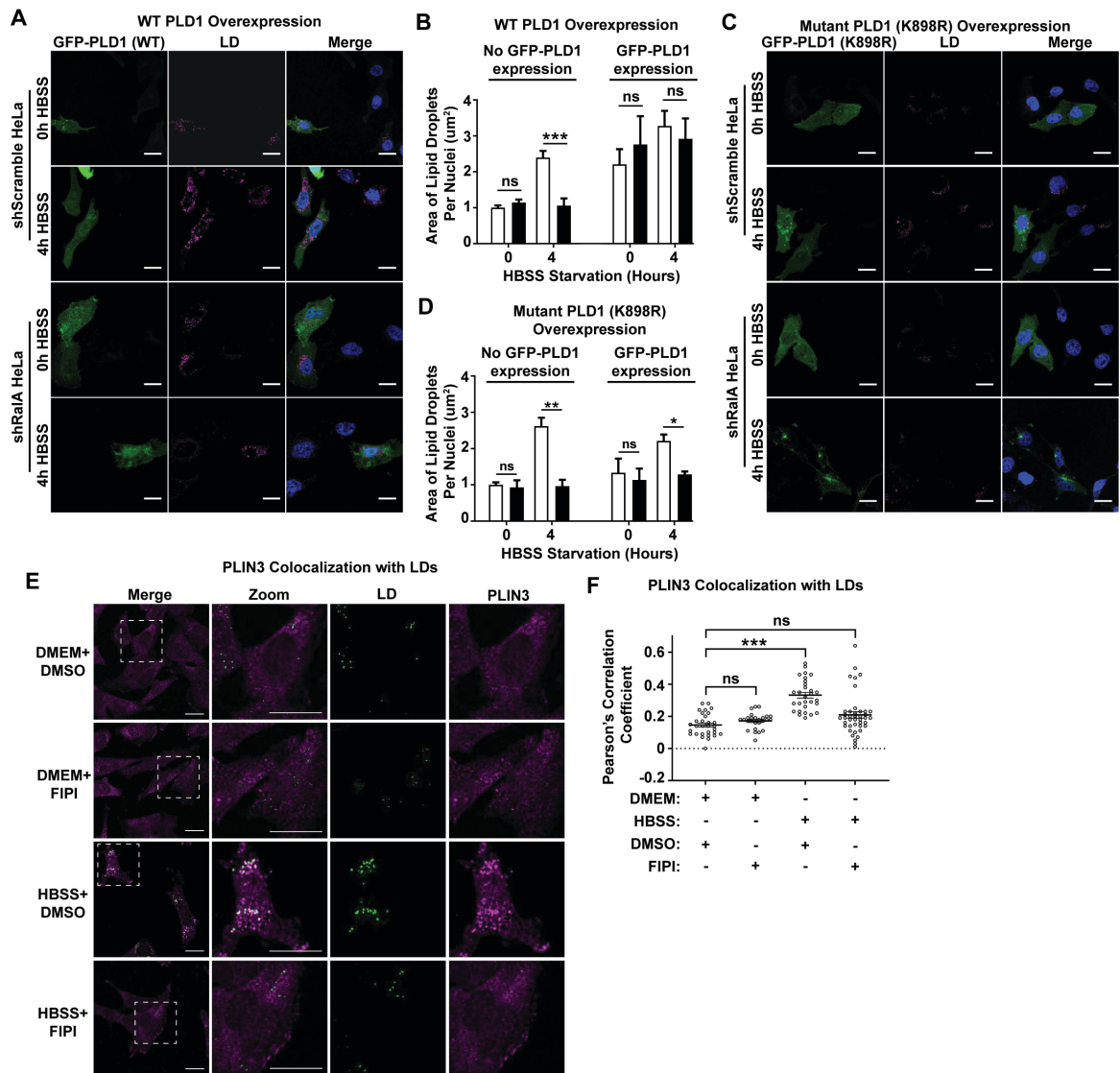


**Figure 2.13 PLD1 rescues LD accumulation in Ra1A KD HeLa**

(A, C). Representative images of LDs in scramble and Ra1A KD HeLa cells expressing (A) GFP-PLD1 or (C) GFP-PLD1 K898R. Cells were starved in HBSS for the indicated timepoints. LDs (magenta) were labeled using LipidTOX Deep Red. Scale bars, 20  $\mu$ m.

(B, D) Quantification of LD area per cell from A and C, respectively. At least 40 cells were analyzed for each time point. White bars are shScramble HeLa. Black bars are shRa1A HeLa. n=3. Two-way ANOVA using Tukey's multiple comparisons test, mean  $\pm$  SEM, \*p  $\leq$  0.05, \*\*p  $\leq$  0.01.

(E) Representative images of PLIN3 and LDs in MEFs in DMEM or HBSS media  $\pm$  750 nM FIPI for 4 hours. Perilipin 3 (magenta) antibody was used to detect localization. LDs (green) were labeled using BODIPY 493/503 and nuclei (blue) were labeled using DAPI. Scale Bar, 20  $\mu$ m.

(F) Relative colocalization of PLIN3 and LDs from E performed by Pearson's correlation coefficient. Each point on the graph represents a Pearson's coefficient value for one cell. At least 30 cells were analyzed for each time point  $n=2$ . mean  $\pm$  SEM. \*\*\* $p \leq 0.001$ .

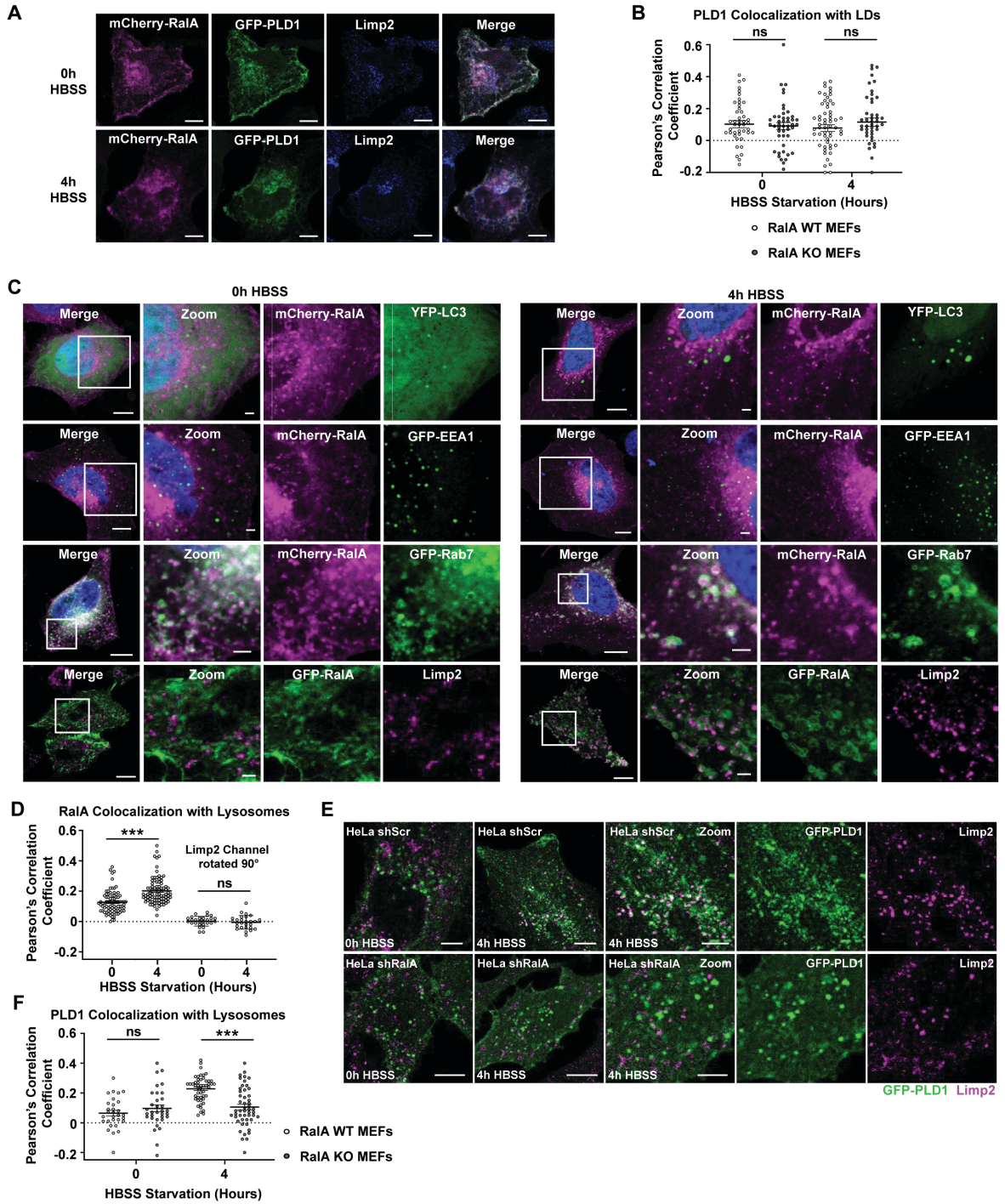


**Figure 2.14 RaIA Recruits PLD1 to Lysosomes during HBSS Starvation**

(A) Representative images of lysosomes, GFP-PLD1 and mCherry-RaIA in scramble and RaIA KD HeLa cells. Lysosomes were labeled using an antibody for the lysosomal membrane protein, Limp2 (magenta). Cells were starved in HBSS for the indicated timepoints. Scale bars, 10  $\mu$ m.

(B) Relative colocalization of GFP-PLD1 and LDs during 0h and 4h of HBSS starvation performed by Pearson's correlation coefficient. Each point on the graph represents a Pearson's coefficient value for one cell. At least 50 cells were analyzed for each time point  $n=3$ . mean  $\pm$  SEM.

(C) Representative images of fluorescently-tagged RalA localization to autophagosomes (YFP-LC3), early endosomes (GFP-EEA1), late endosomes (GFP-Rab7) and lysosomes (Limp2 ab) in HeLa cells. Cells were starved in HBSS for the indicated timepoints. Scale bar, 10  $\mu$ m in merge panels and 2  $\mu$ m in zoom panels.

(D) Quantification of relative colocalization of GFP-RalA and Limp2 from panel C performed by Pearson's correlation coefficient. Each point on the graph represents a Pearson's coefficient value from one cell. At least 50 cells were analyzed for each timepoint.  $n=3$ . Two-way ANOVA using Tukey's multiple comparisons test. mean  $\pm$  SEM. \*\*\* $p \leq 0.001$ .

(E) Representative images of lysosomes (Limp2, magenta) and GFP-PLD1 (green) in scramble and RalA KD HeLa cells. Cells were stained in HBSS for the indicated timepoints. Scale bar, 10  $\mu$ m for merge panels, 5  $\mu$ m for zoom panels.

(F) Quantification of relative colocalization from panel E performed by Pearson's correlation coefficient. Each point on the graph represents a Pearson's coefficient value for one cell. At least 50 cells were analyzed for each timepoint.  $n=3$ . Two-way ANOVA using Tukey's multiple comparisons test. mean  $\pm$  SEM. \*\*\* $p \leq 0.001$ .

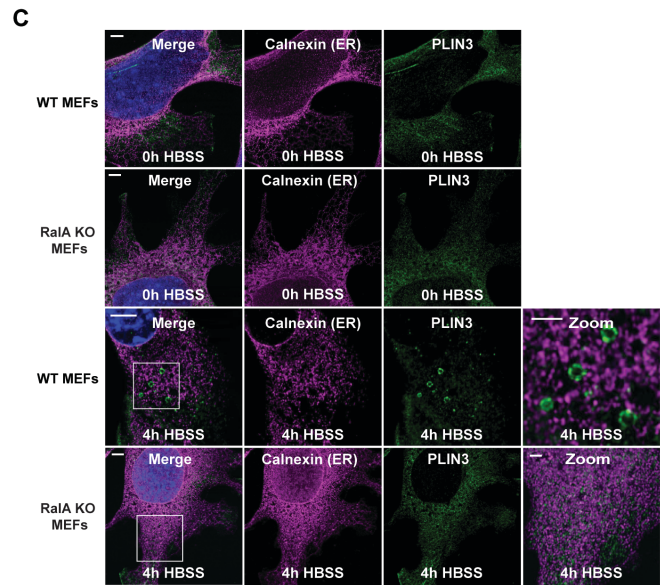
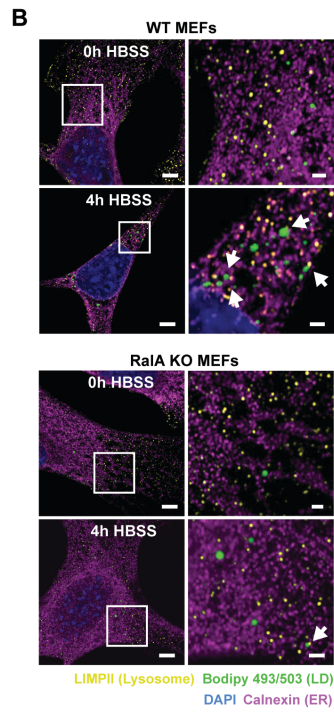
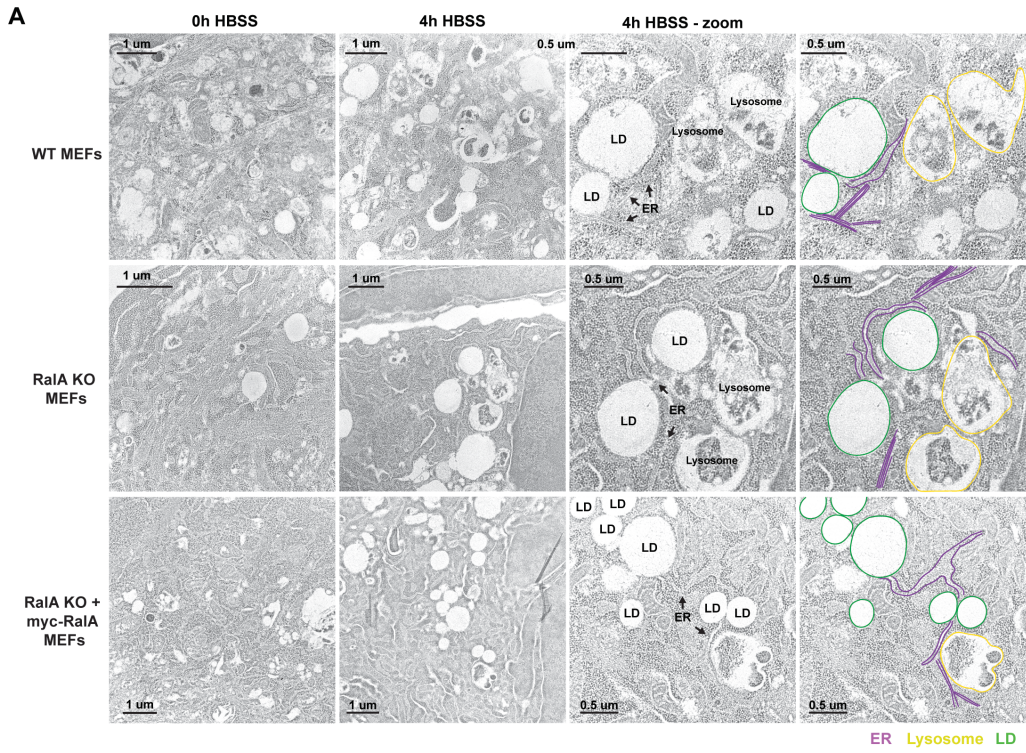


**Figure 2.15 ER, LDs, and Lysosomes come into close proximity during HBSS starvation**

(A) Electron micrographs of WT, Ra1A KO, and Ra1A KO+myc-Ra1A MEFs during 0h and 4h of HBSS starvation. LDs, lysosomes, and the ER are annotated and outlined.

(B) Airyscan images of LDs, lysosomes, and ER localization in WT and Ra1A KO MEFs. LDs (green) were labeled using Bodipy 493/503. Lysosomes (yellow) were detected using an antibody for the lysosomal membrane protein, Limp2. ER (magenta) was detected using an antibody for calnexin. Cells were starved in HBSS for the indicated timepoints. White arrows point to instances of close proximity of organelles to one another. Scale bar, 5  $\mu\text{m}$  for merge images, 2  $\mu\text{m}$  for zoom images.

(C) Airyscan images of PLIN3 (green) and calnexin (magenta) in WT and Ra1A KO MEFs during 0h and 4h of HBSS starvation. Scale Bar, 5  $\mu\text{m}$  for merge images and 2  $\mu\text{m}$  for zoom images.

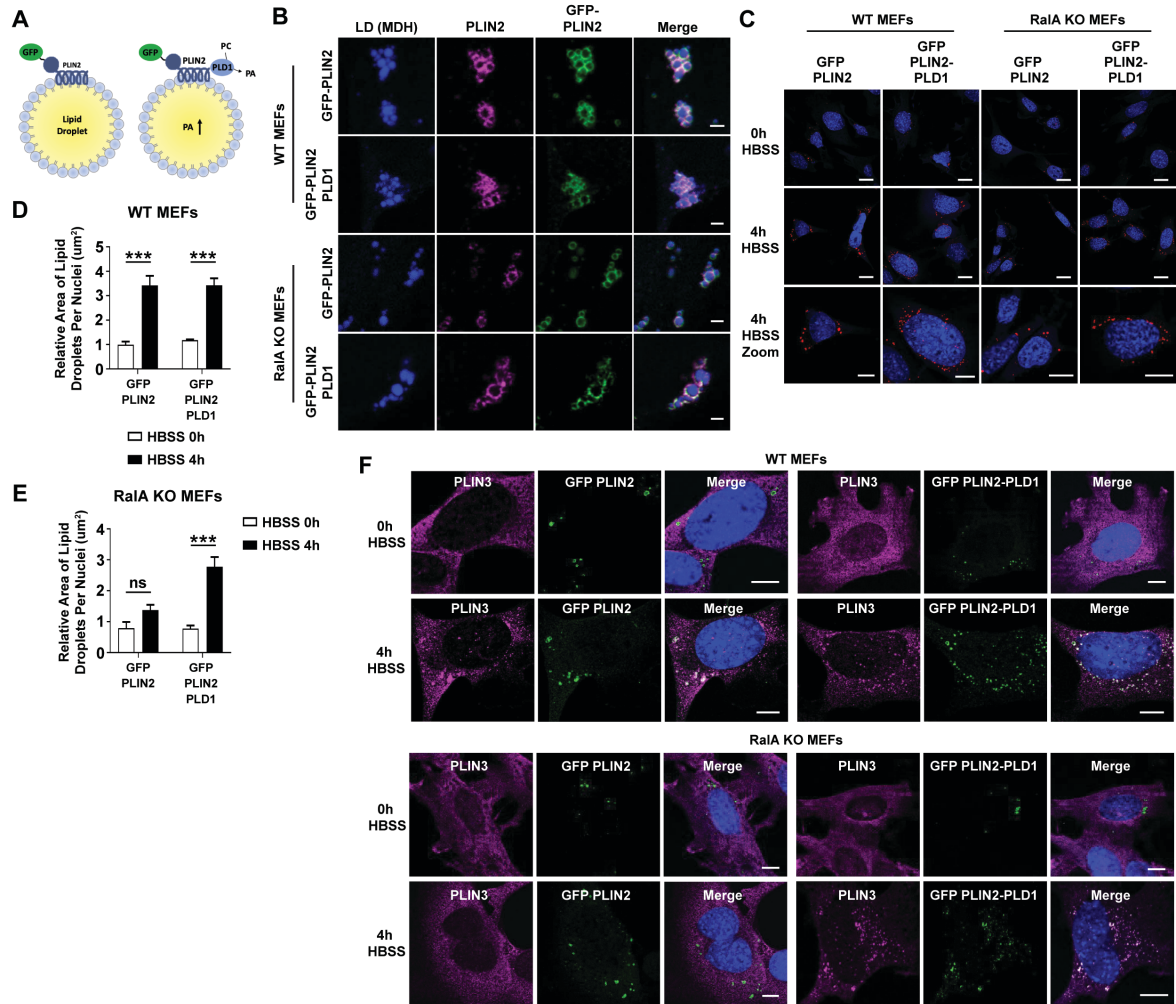


**Figure 2.16 Forced PLD1 localization to LDs rescues LD accumulation and PLIN3 recruitment in Ra1A knock-out MEFs**

(A) Schematic showing LD localized GFP-PLIN2 with PLD1 fused to the C-terminus. (B) Localization of GFP-PLIN2 and GFP-PLIN2-PLD1 on LDs in WT and Ra1A KO MEFs. PLIN2 (magenta) antibody was used to detect both endogenous PLIN2 as well as GFP-PLIN2. MDH (blue) was used to label LDs. Scale bar, 2  $\mu\text{m}$ . (C) Representative images of LDs in WT and Ra1A KO MEFs expressing either GFP-PLIN2 or GFP-PLIN2-PLD1. LDs were labeled using LipidTOX Deep Red. Cells were starved for the indicated timepoints. Scale bar, 10  $\mu\text{m}$  in merge panel, 4  $\mu\text{m}$  in zoom panel. (D-E) Quantification of LD area per cell shown in panel C for D) WT MEFs or E) Ra1A KO MEFs. At least 75 cells were analyzed for each timepoint.  $n=3$ . mean  $\pm$  SEM. (F) Representative images of PLIN3 (magenta) in WT and Ra1A KO MEFs expressing either GFP-PLIN2 or GFP-PLIN2-PLD1. PLIN3 was detected using an antibody. Scale bar, 10  $\mu\text{m}$ .

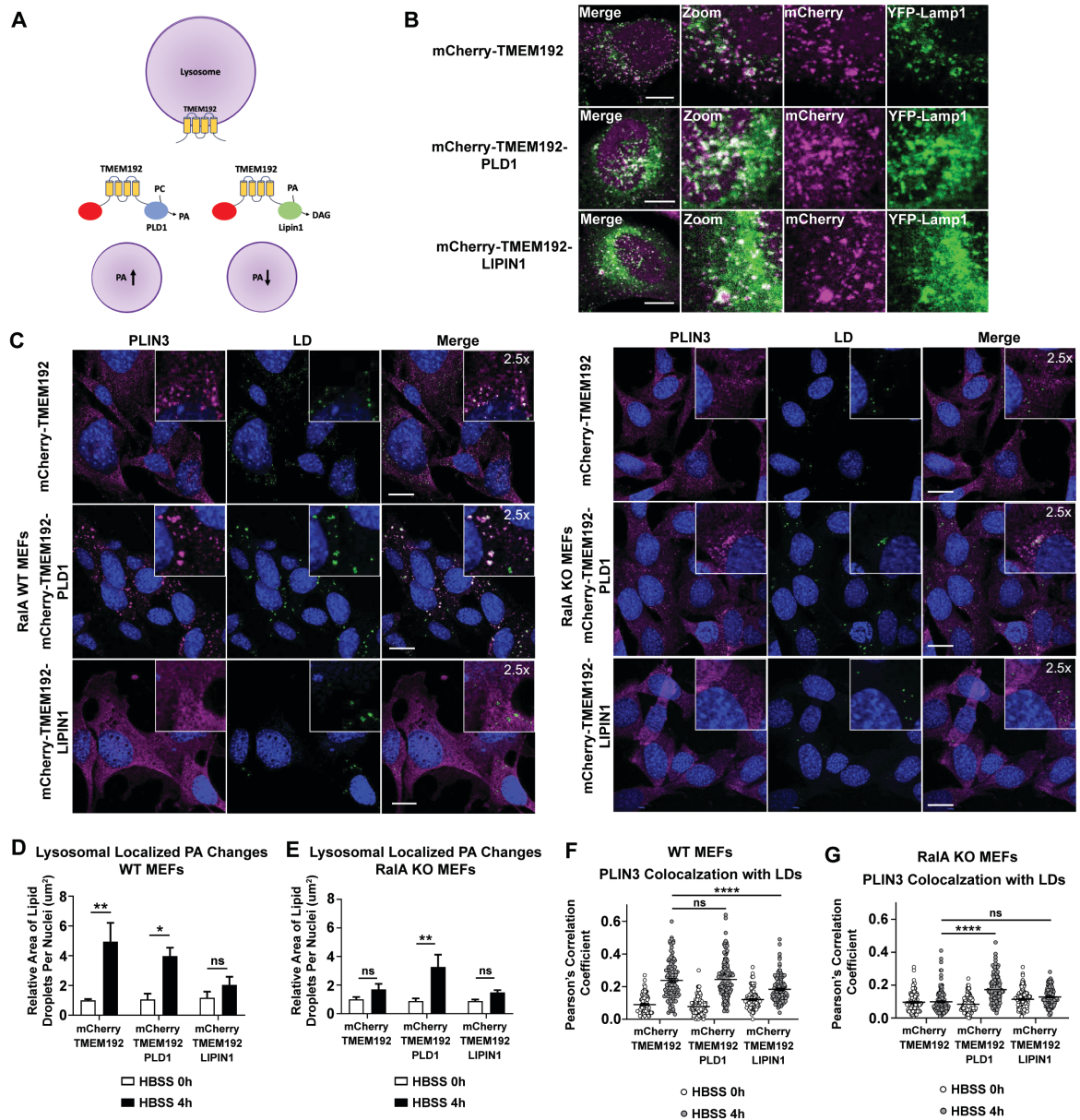


**Figure 2.17 Enrichment and depletion of PA at lysosomes impacts LD accumulation and PLIN3 redistribution**

(A) Schematic showing lysosomal localized mCherryTMEM192 with either PLD1 or LIPIN1 fused to the C-terminus.

(B) Localization of mCherryTMEM192, mCherryTMEM192-PLD1, and mCherry-TMEM192-LIPIN1 to lysosomes (green) detected with antibody against Limp2 in HeLa cells. Scale bar, 10  $\mu\text{m}$ .

(C) Representative images of PLIN3 (magenta) and LDs (green) in WT (left panel) and RalA KO (right panel) MEFs expressing either mCherryTMEM192, mCherryTMEM192-PLD1, or mCherryTMEM192-LIPIN1 during 4h of HBSS starvation. Detection of PLIN3 and LDs was done as described previously. Scale bar, 20  $\mu\text{m}$ . Zoomed inserts are 2.5x magnification.

(D-E) Quantification of LD area per cell in D) WT MEFs and E) RalA KO MEFs expressing the lysosomal targeted fusion proteins. At least 100 cells were analyzed for each timepoint. n=4. Two-way ANOVA using Tukey's multiple comparisons test. mean  $\pm$  SEM. \*p  $\leq$  0.05, \*\*p  $\leq$  0.01.

(F-G) Quantification of relative colocalization between PLIN3 and LDs in F) WT MEFs and G) RalA KO MEFs during 4h of HBSS starvation. Colocalization performed by Pearson's correlation coefficient. Each point on the graph represents a Pearson's coefficient value for one cell. At least 50 cells were analyzed for each timepoint. mean  $\pm$  SEM. Two-way ANOVA using Tukey's multiple comparisons test. \*\*\*\*p  $\leq$  0.0001.

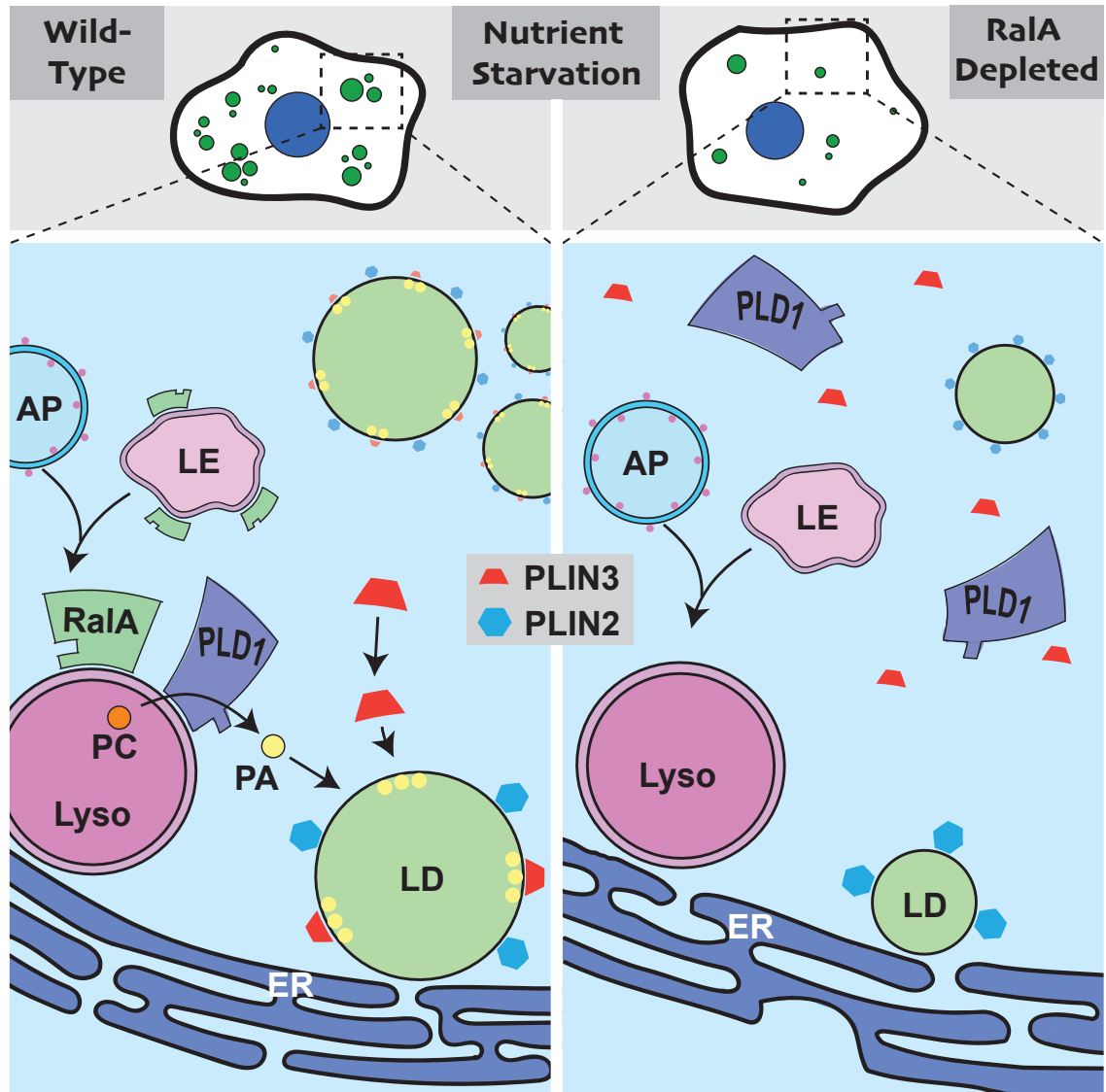


**Figure 2.18 Model for RaIA-dependent starvation induced LD accumulation**

The current model for how RaIA facilitates LD accumulation in response to nutrient starvation. Our data indicate that RaIA promotes LD accumulation through PLD1 by recruiting PLD1 to lysosomes. At the lysosomes, PLD1 generates PA, a molecule necessary for PLIN3 recruitment to LDs and LD growth.

## **Chapter 3: Perspectives and Future Directions**

### **3.1 Introduction**

Successful completion of this thesis and studies herein have uncovered a novel function for the small GTPase RalA. The current understanding how cells respond to environmental stress has taken years to uncover. Our understanding of RalA's regulation of LDs adds some insight to the mechanism by which cells respond to nutrient starvation. While this work builds on this evolving field, it also presents additional questions and further work is needed to understand the full mechanism by which RalA and PLD1 are regulating LDs. In this chapter, I will focus on discussing future studies that would expand on the foundation of work that we have completed for this thesis and the insight that we have gained from our experiments. In the first part of the chapter, I will discuss the upstream signaling to RalA during nutrient starvation. Additionally, I will discuss utilization of new tools and reagents generated for this study that may further our understanding of RalA biology. In the second part of the chapter, I will focus my discussion towards understanding the mechanism by which RalA and PLD1 dependent PA is influencing LD accumulation during nutrient starvation. Lastly, I will conclude this chapter with a discussion on the broader implications of this study with focus on addressing the physiological relevance and models best studied to test the relevance of these findings.

### **3.2 Identifying how RalA senses nutrient starvation**

As discussed in detail in the first chapter, RalA is a multifaceted protein involved in various cellular functions. The spatial and temporal regulation of RalA is driven by upstream signals that dictate its cellular functions. For example, RalA is phosphorylated on S194 by Aurora-A Kinase during mitosis. This phosphorylation causes RalA to relocalize to the

mitochondria, where it recruits RalBP1 and in turn DRP1 for mitochondrial fission. RalA can be regulated in a number of ways. In addition to phosphorylation, RalA is ubiquitinated, acted upon by RalGEFs and RalGAPs and is potentially regulated by calcium. It is unlikely that RalA is engaged in LD regulation under nutrient replete conditions. Depletion of RalA in our studies has no effect at the level of LDs in basal conditions or in conditions of fatty acid stimulation. These findings suggest that RalA is only involved LD regulation under specific conditions, such as nutrient starvation. The identity of the upstream signals that regulate RalA during HBSS starvation are not currently known and can be useful in fully understanding how RalA regulates LD accumulation.

We initially hypothesized that RalA was acting in a nucleotide dependent manner to facilitate LD accumulation. However, this was proven less likely when RalA GTP status was relatively unchanged upon nutrient starvation and when GTP and GDP locked RalA mutants were able to rescue LD accumulation (Figure 2.11C-E). These findings suggest that a more likely scenario is that RalA is being regulated at the level of post translational modifications (PTMs). We began our investigation of RalA PTMs by focusing on phosphorylation. Currently, only two confirmed phosphorylation sites have been identified on RalA. RalA Serine 194 is a well-studied phosphorylation site that can be phosphorylated by Aurora-A Kinase and Protein Kinase A (PKA). RalA is also phosphorylated on Serine 183 by a yet to be identified kinase but is dephosphorylated by Protein Phosphatase 2a. S194 was of particular interest due to its reported phosphorylation by PKA, which is a kinase involved in nutrient sensing pathways. We investigated if either phosphorylation site was necessary for RalA-dependent starvation-induced LD accumulation. To do this, we utilized site directed mutagenesis to create phospho-inactive mutants (serine to alanine mutations) of RalA at S194A and S183A. We then stably expressed WT RalA, RalA S194A or RalA S183A constructs into RalA KO MEFs and determined whether these phosphorylation sites were necessary for LD accumulation during HBSS starvation. Both RalA S194A and S183A were able to rescue LD accumulation in RalA

KO MEFs to levels comparable to WT RalA, suggesting that these phosphorylation sites are likely not involved in LD accumulation. In addition to S183 and S194, other putative phosphorylation sites exist on RalA that have not been explored (Table 3.1). Many of these sites are intriguing because they are within key RalA domains, including the proposed PLD1 binding domain and switch I and switch II regions important for effector binding. To investigate whether any of these sites are involved in LD accumulation during nutrient starvation, future investigators can utilize a strategy similar to the one I used for studying S183 and S194 with phospho-inactive mutants can be repeated for these putative sites. However, this type of experiment is tedious and inefficient. Additionally, it is possible that RalA is phosphorylated at multiple sites during nutrient starvation. Phosphorylation specific RalA antibodies are not well-validated and prevent us from probing for phosphorylated RalA via western blot, ELISA, or immunofluorescence. Therefore, an alternative and perhaps more informative approach is to use liquid chromatography tandem mass spectrometry-based analysis to determine sites of RalA phosphorylation (if any) during HBSS nutrient deprivation.

Equally important to determining the site(s) of phosphorylation on RalA during nutrient starvation is identifying which kinase phosphorylates it. In fact, it may be more informative to determine the kinase before investigating which site is phosphorylated. Many kinases have known consensus recognition sites and there are now many available computational tools that can examine consensus sites on proteins of interest. Matching kinase consensus recognition sites with mapped phosphorylation sites of RalA could narrow which site, if any, is phosphorylated during nutrient starvation. Interestingly, utilizing one of these computational tools reveals a number of potential kinases that may phosphorylate RalA (Table 3.1). The reliability of this analysis is strengthened by its finding that PKA phosphorylates RalA at S194 with a confidence score of 0.86 (on a scale of 0-1). A few kinases of interest with high confidence scores for multiple putative RalA phosphorylation sites include PKA, protein kinase

C (PKC), glycogen synthase kinase 3 (GSK3), and Ca<sup>2+</sup>/calmodulin-dependent protein kinase II (CaMKII).

Calcium-dependent CaMKII is an intriguing kinase to consider, in part due to Ca<sup>2+</sup> signaling during nutrient starvation. Ca<sup>2+</sup> signaling has a complex and heavily debated role in autophagy regulation. Numerous studies have reported that increased Ca<sup>2+</sup> signaling leads to initiation of autophagy, mainly through the CaMKII-AMPK signaling pathway (Gao et al., 2008; Ghislat et al., 2012; Høyer-Hansen et al., 2007; Lam et al., 2008; Wang et al., 2008). Equally so, substantial studies have reported that Ca<sup>2+</sup> is a negative regulator of autophagy (Criollo et al., 2007; Harr et al., 2010; Sarkar et al., 2005; Vicencio et al., 2009). While the precise Ca<sup>2+</sup> regulation of autophagy is far from understood, these studies have been informative. Cytosolic Ca<sup>2+</sup> levels have been reported to increase during nutrient starvation, both from extracellular influx as well as intracellular stores (Ghislat et al., 2012). This increased Ca<sup>2+</sup> signaling activates the CaMKII-AMPK pathway, ultimately leading to the phosphorylation and activation of ULK1, a protein that initiates autophagy (Ghislat et al., 2012; Høyer-Hansen et al., 2007). This finding is interesting because RalA is able to bind to Ca<sup>2+</sup> as well as calmodulin (discussed in more detail in Chapter 1), both of which regulate CaMKII. It is possible that Ca<sup>2+</sup> signaling and CaMKII could directly regulate RalA during nutrient starvation, perhaps by phosphorylation in the case of CaMKII.

The PKC family of serine/threonine kinases has important functions in regulating cell growth and signal transduction (Newton, 2018). Several PKC isoforms of PKC are activated upon stress conditions. Raveh-Amit and coauthors report that PKC $\eta$  protein expression is increased by sevenfold upon amino acid starvation in MCF-7 cells (Raveh-Amit et al., 2009). PKC $\theta$  is activated during and required for ER stress-induced autophagy, though dispensable for amino acid-induced autophagy (Sakaki et al., 2008). PKC $\gamma$  and PKC $\epsilon$  have related functions in protecting neural and cardiac cells during oxidative stress (Gopalakrishna and

Jaken, 2000). Several PKC isoforms are also able to localize to LDs. Upon oleic acid stimulation, PKC $\alpha$ , PKC  $\beta$ I, and PKC  $\delta$  rapidly translocate from the cytosol onto LDs (Chen et al., 2002). In another study, members of the novel subfamily of PKC (PKC $\eta$ , PKC $\delta$  and PKC $\epsilon$ ) are found on LDs in Huh-7 cells (Suzuki et al., 2013). Most PKC isoforms are regulated by DAG while some are additionally regulated by Ca<sup>2+</sup>, both of which are important molecules during nutrient stress (Newton, 2018).

Genetic depletion can be used to investigate whether any of these candidate kinases are involved in RalA mediated LD accumulation during nutrient starvation. We can knockdown each kinase in WT MEFs and determine if loss of protein expression leads to a defect in LD accumulation similar to that of loss of RalA. Follow up experiments such as in vitro kinase assays can be done to determine if kinases of interest are able to phosphorylate RalA. A drawback to this candidate-based approach is that none of the investigated kinases may be involved in regulating RalA during nutrient stress. An alternative, unbiased approach would be to utilize mass spectrometry to identify if any kinases may be binding to RalA during nutrient starvation.

Aside from phosphorylation, Ral GTPases can undergo non-degradative mono-ubiquitination on lysine residues which regulate their localization and effector binding (Neyraud et al., 2012; Simicek et al., 2013). It's possible that ubiquitination of RalA could also govern its function during nutrient starvation. RalB is deubiquitinated during starvation conditions, which allows it to selectively engage with Exo84 to carry out autophagy initiation. Both Ral proteins have multiple predicted ubiquitination sites but only one site has been reported on RalB (lys47) where no sites have been identified on RalA. Given that very little is currently known about ubiquitination sites on RalA, a mass spectrometry-based proteomic approach may be the most informative way to determine which sites of RalA are ubiquitinated during nutrient starvation. If one or more sites are identified, further studies can be done to determine if ubiquitination of these sites is necessary for starvation-induced LD

accumulation. Ra1A ubiquitination-resistant mutants can be generated for identified sites by mutating lysine residues to arginine and then expressed in Ra1A KO MEFs to determine which site is necessary for LD accumulation. An alternative approach would be to generate ubiquitination-resistant mutants on predicted Ra1A ubiquitination residues, express these mutants in Ra1A KO MEFs and then determine whether any are unable to rescue LD accumulation during nutrient starvation.

### **3.3 Uncovering mechanism of Ra1A trafficking to endosomal system**

Critical to Ra1A's ability to facilitating LD accumulation is relocalizing to the lysosomes upon starvation. We detect a dramatic shift in Ra1A localization from the plasma membrane and late endosomes to the lysosomes upon nutrient starvation. Furthermore, we see a similar shift in PLD1 localization to lysosomes upon starvation and this relocalization is dependent on Ra1A. Given this finding, we hypothesize that Ra1A is functioning to recruit PLD1 to lysosomes during nutrient starvation. How Ra1A and in turn PLD1 are able to relocate to the lysosomes is not known. Ra1A is a membrane bound protein and terminates with a CAAX motif that is geranylgeranylated and further processed by two enzymes, RCE1 and ICMT at the ER. Processing by both enzymes is critical for proper Ra1A localization. RCE1 processing is necessary for proper Ra1A localization to the plasma membrane where as ICMT is necessary for Ra1A to localize to endosomes (Gentry et al., 2015). Based on our findings and other reports in the literature, among the various cellular residence of Ra1A is the late endosome. We detected that Ra1A colocalized with the late endosomal marker Rab7 during basal conditions. While others have reported Ra1A to be on early endosomes, we did not see Ra1A colocalize with the early endosomal marker, EEA1. It is likely that Ra1A is making its way to the late endosomes after trafficking through the early endosomal compartment. This movement is likely rapid, thus not easy to detect. Given that Ra1A is already present on late endosomes during basal conditions, we hypothesize that Ra1A localizes to the lysosomes by

endosomal trafficking and maturation of late endosomes into lysosomes during nutrient starvation. RalA has been linked to several endosomal functions in different cell types, which further strengthens the likelihood of this scenario.

To test whether RalA is indeed translocating to the lysosome via the endosomal pathway, we can genetically prevent RalA trafficking to the endosomes in one of two ways. We can knockdown/knockout ICMT in our cells, which should prevent GFP-RalA from trafficking to the late endosomes in basal and starvation conditions as well as prevent RalA from localizing to the lysosome during starvation conditions (Gentry et al., 2015). As a complement, we can use site directed mutagenesis to modify the CAAX motif of GFP-RalA, preventing it from being processed by ICMT and resulting in a failure to localize to the late endosome. Related to these studies is gaining a better understanding of the mechanism by which RalA makes its way from the plasma membrane to endosomes. We speculate that one mechanism by which RalA makes its way to the endosomal membranes is via clathrin-mediated endocytosis (CME). CME is a vesicular transport process that transports various cargo from outside the cell into the interior. CME is the major endocytic route for uptake of extracellular cargo. Transferrin is a protein that is taken up into the cell by CME and is routinely used to study the process. RalA has been shown to colocalize with transferrin labeled endosomes (Gentry et al., 2015; Pollock et al., 2019). Additionally, CME is required for RalA localization to the mitochondria upon mitochondrial depolarization (Pollock et al., 2019). Pollock and coauthors demonstrated that either genetic or pharmacological inhibition of CME prevents RalA relocalization to the mitochondria (Pollock et al., 2019). A similar strategy can be employed (using Pitstop2 or knocking down AP2 complex to prevent CME) to determine if CME is involved in RalA localization to late endosomes and lysosomes.

It is entirely possible that RalA makes its way to the lysosome in an endosomal-independent manner. Another route that RalA may take to lysosomes is via autophagosomes. Identifying the origin of autophagosomal membranes has long been an interest in the field and

many questions still remain about its exact source. Studies suggest that autophagosomal membranes are likely derived from multiple sources, including the ER, mitochondria, and plasma membrane. It is possible that RalA makes its way onto autophagosomes prior to fusion with lysosomes. Though this is not likely in the case for HeLa cells as RalA was not detected on LC3 positive autophagosomes during nutrient starvation. However, this possibility can also be ruled out by blocking fusion of autophagosomes with lysosomes and then determining whether RalA is still present on lysosomes during nutrient starvation. Fusion of autophagosomes with lysosomes is mediated by the SNARE proteins syntaxin17 (stx17) and VAMP8 and knockdown of stx17 prevents autophagosomal-lysosomal fusion (Hikita et al., 2018; Itakura et al., 2012). We can monitor the localization of GFP-RalA in cells with stx17 knockdown to determine if RalA utilizes autophagosomal membranes to localize to lysosomes.

### **3.4 Elucidating the role of PA in starvation-induced LD accumulation**

Central to our findings and model is PA, the enzymatic product of PLD1. Our data strongly suggest that PA is playing an important function in promoting LD accumulation during HBSS starvation. While WT PLD1 is able to rescue LD accumulation in cells lacking RalA, the catalytically inactive mutant of PLD1 is unable to do so. Likewise, inhibition of PLD1 using FIPI, which binds to the catalytic domain of PLD1 also prevents LD accumulation, even in the presence of RalA. However, our understanding of the precise role of PA is far from understood and a number of questions remain, including: 1) what is the precise function of PA in LD accumulation, 2) where does PA localize during nutrient starvation, 3) what is the biological advantage for PA production at the lysosome, and 4) how PA is trafficking from its place of production, the lysosome to its final destination?

### 3.4.1 Understanding the precise function of PA in LD accumulation

While our data consistently support the involvement of PA in LD accumulation, our studies did not provide direct evidence of what PA is doing. We believe there are two ways that PA could influence LD growth, both of which are consistent with our findings. PA could be used for generating TAGs and packed into LDs or it could be used as a recruiting molecule to bring PLIN3 or other important proteins necessary for LD budding or growth.

PA can be utilized as a precursor for the biosynthesis of many different lipids in the cell, including TAGs. One possibility is that PLD1 produced PA gets shuttled into the Kennedy pathway for triglyceride synthesis and is used as a precursor for DAG production (Figure 3.1). This DAG can subsequently be converted into TAG and stored into LDs (Figure 3.1). In this manner, the PA would be used as packaging material during nutrient starvation. However, PA would likely need to be the major source of TAG biosynthetic material in order for a significant difference to manifest in the form of LD accumulation in cells with and without *RalA*. Furthermore, this possibility would predict that there would be a large, detectable increase in cellular PA levels upon nutrient starvation. However, we did not detect significant change in PA levels upon nutrient starvation or significant differences between WT and *RalA* deficient cells. There remains the possibility that detectable differences in PA may go unnoticed due to rapid conversion into DAG or other lipid species. However, we believe this is unlikely and that the effect of PA is not due to how much is being produced. Instead, we hypothesize that PA is being enriched at specific compartments in the cell to facilitate LD growth during starvation and that this enrichment may go undetected at a global level. This is also consistent with the finding that *RalA* has no influence on PLD1 activity, further supporting a hypothesis for compartmentalized PA production instead of a global increase in PA production upon nutrient starvation.

Our data strongly suggests that PA is being produced at the lysosomes. *RalA* recruits PLD1 to lysosomes upon nutrient starvation. Furthermore, forced lysosomal localization of

PLD1 rescues LD accumulation as well as PLIN3 relocalization of LDs in cells lacking Ra1A. Importantly, forced localization of a PA phosphatase, Lipin1, prevents LD accumulation and PLIN3 relocalization to LDs in cells expressing Ra1A. Once produced, we hypothesize that PA is transferred either to the ER to assist in LD budding or the LD to assist in LD growth (Figure 3.2). In addition to being utilized as a precursor for other lipids, PA has recognized functions in changing the physical properties of membranes as well as acting as a signaling molecule and recruiting proteins. Growing evidence suggests that changes in phospholipid membrane composition is an important contributor to LD budding from the ER and phospholipids such as PA, PE and DAG are generating wide interest in this function. Furthermore, there is evidence to suggest that PA is acting to recruit PLIN3 to the ER or LDs. Experiments utilizing model phospholipid monolayers enriched with PA showed increased PLIN3 interaction and insertion into the monolayer compared to those enriched with other phospholipids, such as PC. PLIN3 has additionally been detected to be among the first proteins to be recruited to nascent LDs upon LD stimulation conditions. Further elucidation of the precise function of PA requires understanding the localization of PA during nutrient starvation.

### **3.4.2 Determining the localization of PA during nutrient starvation**

Understanding the subcellular localization of PA during HBSS starvation is an important but difficult task. While there appear to be insightful approaches to answering this question, each approach has limitations that may prevent us from reliably uncovering the true localization of PA. We hypothesize that PA is being generated at the lysosome and being transferred to either the ER or LDs during nutrient starvation (Figure 3.2).

The first method to detect intracellular PA levels is to utilize PA specific biosensors, referred to as PA probes. PA probes are genetically engineered fusion proteins that consist of a fluorescent tag attached to the minimal PA binding domain of PA binding proteins. Traditionally, the PA binding domain of proteins such as spo20, Opi1p, and PDE4A1 were

utilized. While studies have confirmed that these probes can detect intracellular pools of PA, these PA probes were found to localize to different subcellular compartments. Spo20-PA probes appear to detect nuclear and plasma membrane PA, whereas Opi1p-PA probes detect nuclear and ER PA and PDE4A1-PA probe detects PA at the golgi. These findings suggest that PA probes detect different pools of PA, likely by binding to different PA species among other possibilities. Dozens of PA probes exist currently and more proteins that contain PA binding domains have been identified. We have access to 10 different PA probes from the Nicolas Vitale lab, whose focus is developing a better understanding of PA cellular functions and with expertise in detecting subcellular PA. To detect whether PA is being enriched at lysosomes, ER or LDs, we can express these 10 probes in either WT or RalA deficient cells and determine if they have significant overlap with either lysosomes (limp2 antibody), ER (calnexin antibody), or LDs (Bodipy 493/503) during basal and nutrient starvation conditions. Indeed these studies have already been attempted for a subset of these probes. While some probes showed promise, their localization was difficult to interpret and reproduce and ultimately made utilization of these probes unreliable for making accurate conclusions.

A second approach to determining the intracellular localization of PA is to use subcellular fractionation to isolate pure organelle compartments of the lysosome, ER and LDs and then utilize mass spectrometry to detect the amount of PA at each compartment. This can be done in unstarved and starved cells and the distribution of PA can be compared between conditions. Pure isolation of organelles is difficult to achieve, especially when attempting to separate multiple organelles from the cell sample. For various biological and technical reasons, there is often significant cross-contamination of organelles, making pure organelle isolation difficult. We utilized several methods of subcellular fractionation in MEFs using different gradients and consistently were unable to remove ER cross-contamination into other organelle fractions, for example.

### **3.4.3 Understanding the rationale for PA production at the lysosome**

Related to uncovering the localization of PA during nutrient starvation is rationalizing why PA is produced at the lysosome rather than directly at the ER or LDs. We hypothesize that PLD1 is recruited to lysosomes so that it has access to phosphatidylcholine, which is recycled from membranes during autophagy at the lysosome. PC is a substrate of PLD1 that is used to generate PA. Important questions remain about how PLD1 get access to these liberated PC molecules. Autophagy derived PC is in the lumen of lysosomes and PLD1 is presumably recruited to the outer membrane of lysosomes. One hypothesis is that the liberated PC is added onto outer lysosomal membranes through the actions of phospholipid flippases. Flippases facilitate the movement of phospholipids from one leaflet of a bilayer, through the hydrophobic core and onto the other leaflet. Flippases can generate membrane asymmetry and are found in many different organelle membranes (Sebastian et al., 2012). It's possible that a flippase binds to PC on the luminal side of the lysosome and transfers it to the outer leaflet of lysosomes, allowing PLD1 access to PC.

### **3.4.4 Determining how PA is trafficking from the lysosome to its final destination**

While significant work is needed in dissecting PA's function and localization, something in common about all of the presented possibilities is that they are likely happening at or involving the ER. The ER is the site of neutral lipid synthesis, the location of LD biogenesis and even involved in LD growth. If the ER is central to PA's involvement, there needs to be a way for lysosomal generated PA to get to the ER. We reasoned that one mechanism of PA transfer may be through direct transfer via membrane contact sites (MCS) (Figure 3.2). MCS are defined as areas of close juxtaposition of membranes from two different organelles and are important ways for inter-organelle exchange of lipids and other metabolites. For example, ER-PM contact sites facilitate the exchange of PM derived PtdIns4P for ER derived phosphatidylserine (Filseck et al., 2015). In recent years, a number

of studies have reported lipid exchange at ER-endolysosomal pathway. Lim and coauthors showed that oxysterol binding protein (OSBP) and vamp-associated proteins (VAP) mediate the transfer of cholesterol from the ER to the lysosome across MCS (Lim et al., 2019). Similarly, another sterol transport protein, StAR-related lipid transfer domain-3 (STARD3) and VAP also facilitates exchange of cholesterol between the ER and late endosomes (Wilhelm et al., 2017). We used high resolution confocal microscopy as well as electron microscopy to determine the proximity of lysosomes, ER and LDs to each other. We saw clear evidence of close apposition of all three organelles during nutrient starvation, even in the absence of RalA. Furthermore, high resolution confocal imaging also showed PLIN3 ring-like structures in close apposition to the ER upon nutrient starvation in wild-type cells, supporting the involvement of the ER.

The ER-endolysosomal MCS has been most extensively studied in yeast, an organism that contains a vacuole that acts similar to mammalian late endosomes and lysosomes. A number of proteins involved in tethering ER-endolysosomal contacts have been discovered, many of which are conserved in multicellular organisms. These proteins include the yeast protein *mdm1*, which is part of the Sorting Nexin family of proteins in mammals, as well as *Vsp13* (Henne et al., 2015; Lang et al., 2015; Wang et al., 2014). Additionally, other proteins identified in mammals include protrudin, annexin A1, and NPC1 (Eden et al., 2016; Höglinger et al., 2019; Raiborg et al., 2015).

To test the hypothesis that PA transfers from the lysosome to the ER via MCS, we can disrupt ER-endolysosomal MCS by knocking down one of the tethers listed above and then determine if this inhibition leads to loss of LD accumulation and PLIN3 recruitment to LDs during nutrient starvation in cells with intact RalA and PLD1. If PA is being transferred from lysosomes to the ER through MCS, it is unlikely that its doing so by simple diffusion. It is likely happening with assistance from lipid transfer proteins (LTPs), which have been shown to play

a pivotal role in movement of lipids between other ER-organelle MCS (Hanada, 2018; Muallem et al., 2017; Peretti et al., 2020).

LTPs facilitate the intracellular movement of lipids by non-vesicular transport (Wong et al., 2019). This means of trafficking lipids is used to maintain membrane composition. LTPs carry out lipid transfer across aqueous phases by providing lipids with a hydrophobic environment, usually in the form of a cavity lined with hydrophobic residues (Sha et al., 1998; Tsujishita and Hurley, 2000). LTPs show selectivity for lipids, both for their head group and acyl chain length. Some LTPs are able to bind two different lipid species and function to exchange species between cellular compartments, or transfer two species from one compartment to another. LTPs have been found for all kinds of lipid species (Wong et al., 2019). LTPs that are able to bind to PA include two members of the Phosphatidylinositol transfer proteins (PITPs) family, Nir2 and PITPNC1 (Garner et al., 2012; Kim et al., 2015). Nir2 is able to bind to both PI and PA and is enriched at ER-PM MCS (Kim et al., 2013). Nir2 facilitates the transfer of PI from the ER to the PM and in exchange, transports PA from the PM to the ER (Kim et al., 2015).

Another interesting group of LTPs are members of the GRAMD1 family, GRAMD1A, GRAMD1B, and GRAMD1C. GRAMD1 proteins are localized to the ER and function to transport sterols from the PM and lysosomal membrane (Höglinger et al., 2019; Naito et al., 2019; Sandhu et al., 2018). GRAMD1 proteins contain two functional domains, a StART-like domain that allows it to bind to cholesterol and a GRAM domain, which binds to anionic lipids, including PS and PA (Gatta et al., 2015; Sandhu et al., 2018). A recent study by Trinh and coauthors suggested that GRAMD1b facilitates the exchange of cholesterol from the ER (through its StART domain) for PS at the PM (through its GRAM domain) (Trinh et al., 2020). Fascinatingly, GRAMD1b is required for LD formation; GRAMD1b KO mice have complete loss of cytoplasmic LDs in the adrenal cortex (Sandhu et al., 2018). Given these data, we hypothesize that members of the GRAMD1 family may function at the ER-lysosomal MCS to

facilitate the exchange of ER cholesterol for lysosomal PA generated during nutrient starvation. Future studies to test this hypothesis include performing immunofluorescence and high-resolution imaging to visualize GRAMD1 protein localization during nutrient starvation, which would be predicted to be at ER-lysosomal contacts. In addition, we would genetically deplete GRAMD1 proteins and look to see if loss of GRAMD1 prevents LD accumulation in WT cells during nutrient starvation. These localization and loss of function studies can also be repeated with other candidate proteins, such as the PITP family of transporters discussed above.

### **3.5 Investigating the physiological relevance of RalA mediated LD accumulation**

While the findings in this thesis are of great interest, further studies are needed to develop its physiological relevance and appreciate its full potential. I propose two way that this pathway can be further explored: 1) investigating the relevance of RalA mediated LD accumulation in a disease-based model, such as in cancer and 2) investigating the physiological relevance of RalA mediated LD accumulation in an in vivo animal model.

### **3.6 Investigating the relevance of RalA mediated LD accumulation in cancer cells**

Metabolic reprogramming is recognized as one of the major hallmarks of cancer cells. Given the competitive and harsh environment that many tumor cells adapt to and overcome, it is not surprising that they are able to utilize metabolites beyond glucose for survival. In addition to other metabolites, lipids are important driver of tumorigenesis. Not only are they important as building blocks for generating new membranes, but can also be utilized for energy production via beta-oxidation. Furthermore, individual lipid species are now understood to play additional cellular roles, such as in cellular signaling and protein recruitment. As discussed in chapter 1, LDs are the metabolic hubs that respond to cellular

stress conditions, many of which are the same stress conditions that cancer cells experience. These dynamic organelles are able to respond to the environmental and cellular stress cues and regulate the appropriate release of lipids for a variety of purposes. Given their fundamental role as a source of cellular lipids, LDs have been harnessed by a number of cancer cells to promote tumorigenesis. Cancer cells fuel their increased lipid usage by multiple means. Some cancers increase fatty acid synthesis, others increase fatty acid uptake from the environment, and others still increase autophagy to recycle membranes and mobilize the lipids within. No matter which of these a cancer cell uses or any combination of, they need to be able to store these lipids and the various means of sourcing lipids all converge on storage at LDs. Playing such a central role, it is not surprising that elevated TAG levels and LD accumulation have become noteworthy features of many tumors including those of pancreatic, breast, lung, kidney, liver, ovarian, prostate, brain, colorectal cancer and more (Berndt et al., 2019; Grachan et al., 2021; Jin and Yuan, 2020; Petan et al., 2018; Qiu et al., 2015; Roman et al., 2020; Rozeveld et al., 2020; Sunami et al., 2017; Wu et al., 2020; Zhao et al., 2019).

Downstream of the oncogenic Ras pathway, RalA's involvement in tumorigenesis has been of considerable interest. RalA has been implicated in pancreatic, lung, bladder, colorectal, prostate, ovarian, and liver (Ezzeldin et al., 2014; Guin et al., 2013; Lim et al., 2005, 2006; Martin et al., 2011; Peschard et al., 2012; Smith et al., 2007; Theodorescu, 2017). However, it is not completely understood how RalA contributes to tumorigenesis. Our studies identify RalA as an important regulator of nutrient stress induced LD accumulation. Given that many cancer cells undergo similar stress conditions and rely on lipids for growth, one hypothesis is that RalA drives tumorigenesis through its regulation of LDs. We can test this hypothesis in a tumor model for Ras driven cancer cells that depend on RalA for survival, such as non-small cell lung cancer (NSCLC). Male and coauthors report that depletion of RalA leads to reduced proliferation and invasiveness alongside increased apoptosis in KRas-dependent A549 cells (Male et al., 2012). Peschard et al. demonstrate that expression of

either RalA or RalB is sufficient for tumor growth and that genetic depletion of both leads to loss of NSCLC tumorigenesis in a KRas<sup>G12D</sup>-driven mouse model (Peschard et al., 2012). To test whether RalA mediates NSCLC through its functions in regulating LDs, we will utilize an orthotopic NSCLC mouse model. For this study, we will utilize 4 different A549 cell lines, WT A549, RalA KO A549, PLIN3 KO A549 and RalA/PLIN3 DKO A549 cells. We will orthotopically implant these cell lines into immunocompromised mice and compare lung tumor formation across the 4 cell lines. We would expect RalA KO A549 orthotopic mice to have significantly reduced tumor formation as compared to WT A549 orthotopic mice. If RalA is mediating tumorigenesis through LD growth, then PLIN3 KO A549 cells should also generate less tumors than WT A549 cells and the level of tumor formation should be similar to that of tumor formation in RalA KO A549. Importantly, the RalA/PLIN3 DKO A549 orthotopic mice should have tumor formation equivalent to that of the single RalA KO or single PLIN3 KO orthotopic mice. If the DKO orthotopic mice produce significantly fewer tumors than either of the single KO mice, that would suggest that RalA and PLIN3 are promoting tumor formation by independent means. If tumor formation is reduced in RalA KO orthotopic mice but unchanged in PLIN3 KO mice, this would suggest that RalA influences tumor formation through one of other functions such as exocytosis.

Further mouse studies can be done to test whether RalA's regulation of LDs influences cancer in other ways, including studies on the metastatic potential of cells lacking RalA. Additionally, this study can be further expanded to other cancers that depend on RalA signaling for survival, such as pancreatic ductal adenocarcinomas (Lim et al., 2005, 2010). Ultimately, these studies may help identify the mechanism by which RalA is contributing to tumorigenesis and establish new therapeutic targets.

### **3.7 Investigating the physiological relevance of starvation-induced LD accumulation in a skeletal muscle mouse model**

An interesting tissue to study the physiological relevance of Ra1A during nutrient stress conditions is the skeletal muscle. At the organismal level, important tissues involved in nutrient stress are white adipose tissue (WAT), the liver and skeletal muscles. WAT function as nutrient reservoirs for the entire organism. During times of sufficient or excess nutrient, WAT stores energy in the form of TAGs in a large unilocular LD. During prolonged nutrient starvation, WAT releases fatty acids from its LD stores into the circulation for other tissue to utilize for energy. Skeletal muscle tissue takes up a major portion of these released FAs through upregulation of FA import processes and  $\beta$ -oxidation in order to shift to FAs utilization as a source of energy. Ultimately, this process is important in preserving the glucose levels in blood circulation for the brain. Skeletal muscle cells contain multiple, small LDs, similar to those in MEFs. During another form of nutrient stress, intense exercise, skeletal muscles also increase FA import. These increased FAs have to be stored and sequestered into LDs to prevent lipotoxicity and studies that shown that skeletal muscles increase LD accumulation upon nutrient stress (Kanaley et al., 2009). Given that Ra1A functions to promote LD accumulation during nutrient starvation in cultured cells, we hypothesize that Ra1A functions to promote LD accumulation in skeletal muscle cells upon nutrient stress.

To test this hypothesis, we would knock out Ra1A in mice. Global knockout of Ra1A is embryonically lethal and therefore we would use a skeletal muscle conditional KO of Ra1A. We would utilize a cre recombinase system under the control of the muscle-specific muscle creatine kinase (MCK) promoter to generate a skeletal muscle specific Ra1A KO mice (Figure 3.3). Given that Ra1A has numerous functions in the cell, appropriate controls will be required to attribute any observed changes on whole mouse physiology or skeletal muscles to Ra1A mediating LD growth. Therefore, a skeletal muscle specific KO of a protein that prevents LD growth, such as PLIN3 will be utilized for comparison. It is expected that changes in

conditional Ra1A KO mice mimic that of conditional PLIN3 KO mice in this case. Therefore, the mice utilized in this study would be WT mice, conditional Ra1A KO mice, and conditional PLIN3 KO mice.

After confirming conditional KO of Ra1A and PLIN3 by western blot, we would perform a series of murine experiments to investigate the consequences of Ra1A or PLIN3 KO in skeletal muscles in underfed and 24 hours fasting conditions. Our experiments would comprise a thorough investigation of whole-body physiological differences between WT and Ra1A KO mice as well as skeletal muscle specific difference in response to fasting. At the organismal level, key measurements of interest would be body weight in fed and fasted state, glucose tolerance and insulin sensitivity, rate of fatty acid oxidation, respiratory exchange rate, and energy expenditure. At the skeletal muscle level, we would compare differences in LDs, as well as fatty acid uptake into skeletal muscles in fed and fasted states. Furthermore, we would compare the mRNA and protein expression of proteins involved in fatty acid import into the cell as well as  $\beta$ -oxidation.

The summary of my expected results is outlined in table 3.2. As mentioned previously, skeletal muscle undergoes a shift from glucose to fatty acids as a source for generating energy during nutrient starvation. This shift is mediated both by increased uptake of fatty acids as well as increased  $\beta$ -oxidation. Expression of genes involved in both of these processes is upregulated in starvation conditions (Holst et al., 2003; Lange et al., 2004). These imported fatty acids need to be stored in LDs prior to utilization for  $\beta$ -oxidation. I predict that skeletal muscle in conditional Ra1A KO as well as conditional PLIN3 KO mice will be unable to store these fatty acids due impaired LD growth during 24 hours of starvation. Therefore, I expect to see less LDs and TAGs in skeletal muscle from conditional Ra1A KO and conditional PLIN3 KO mice compared to WT mice after 24 hours of starvation. Furthermore, compared to skeletal muscle in WT mice, I expect skeletal muscle in conditional Ra1A KO and conditional

PLIN3 mice to have decreased mRNA and protein expression of both fatty acid import genes as well as  $\beta$ -oxidation genes.

Given that skeletal muscle tissue consumes a sizeable share of blood glucose in the fed state and is a primary recipient of fatty acids released into circulation by white adipocytes during starvation, I expect the effects of skeletal muscle Ra1A and PLIN3 KO to have whole body physiological consequences. If conditional Ra1A and PLIN3 KO mice are unable to properly store fatty acids in skeletal muscle, I expect their serum levels to have higher non-esterified fatty acids as compared to WT mice. Additionally, I expect conditional Ra1A and PLIN3 KO mice to have decreased  $\beta$ -oxidation. I also hypothesize skeletal muscle in Ra1A and PLIN3 KO mice to have increased glucose uptake and oxidative phosphorylation compared to starved WT mice. This increase in glucose uptake will result in decreased serum glucose levels.

If Ra1A is found to have significant impact on skeletal muscles and whole mouse physiology during fasting conditions, follow up studies could explore the relevance of Ra1A in a metabolic disease model. In conclusion, both the investigation of Ra1A in tumor cells as well as in mice will begin to address the physiological relevance of our findings presented in chapter 2 of this thesis.

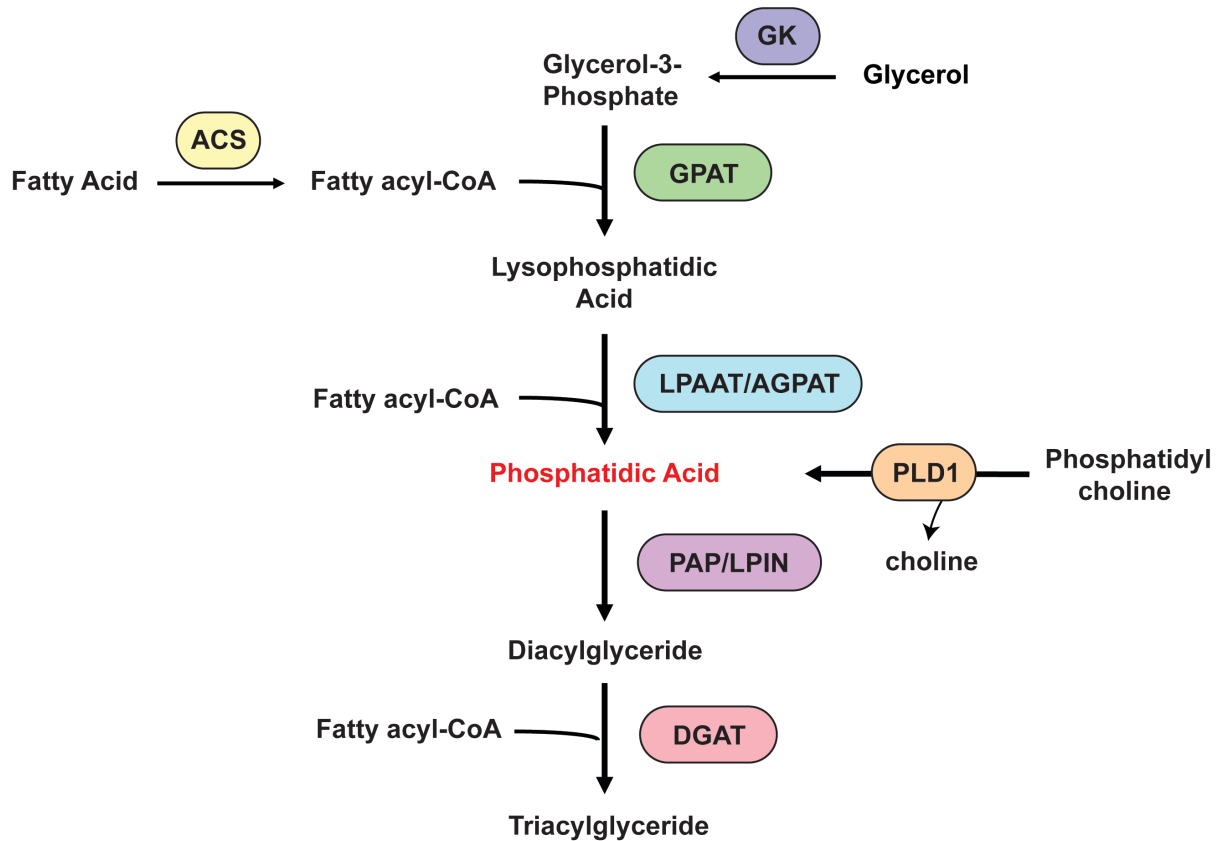


**Figure 3.1 Kennedy Pathway for Triacylglyceride Synthesis**

This pathway outlines the sequential addition of a fatty acyl chain onto a glycerol backbone to generate TAG. Phosphatidic Acid is an intermediate lipid in this pathway and may be shuttled into and out of this pathway.

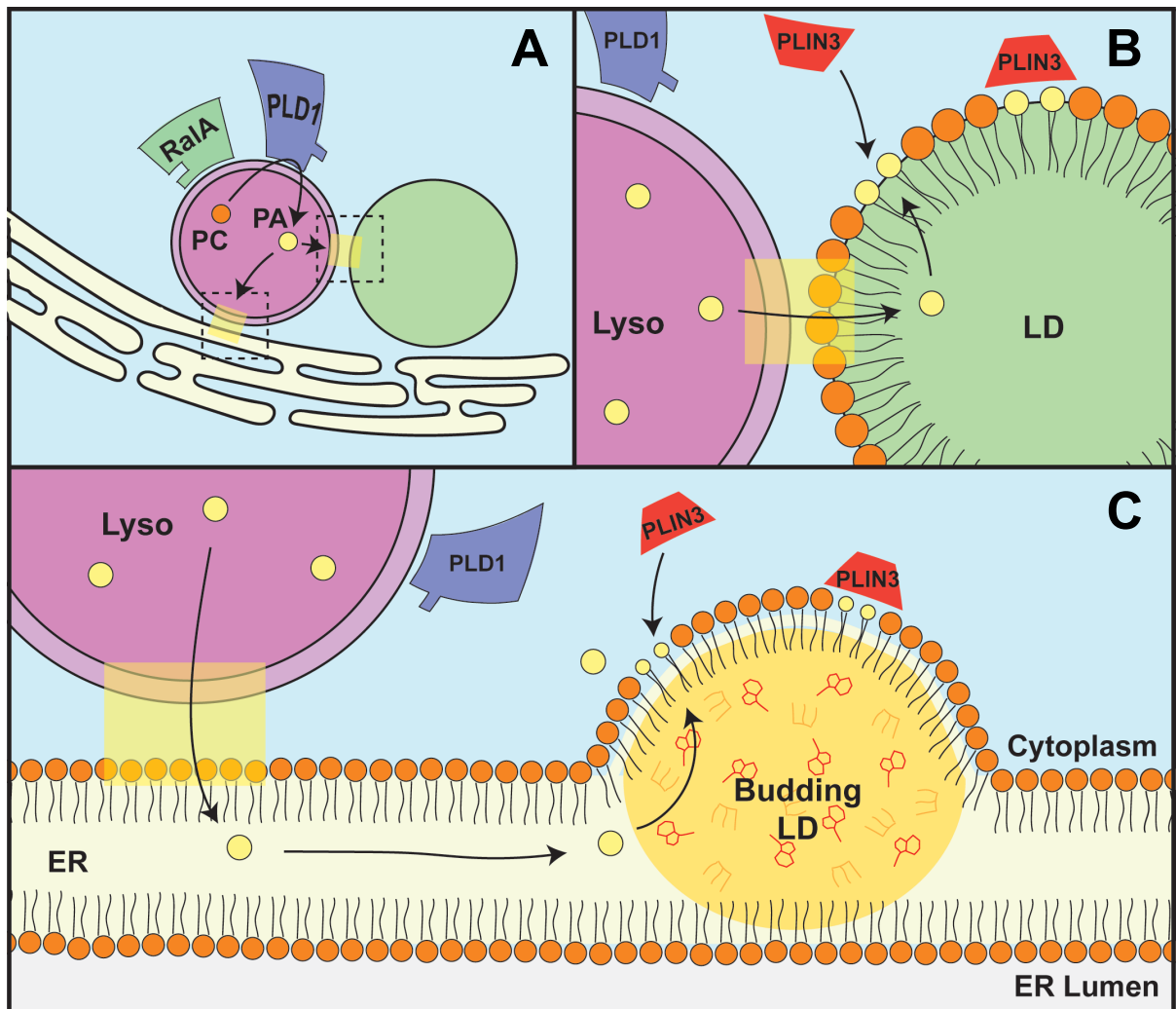


**Figure 3.2 Model for phosphatidic acid trafficking during nutrient starvation**

Our data indicate that PA is produced at the lysosome during nutrient starvation. We hypothesize that the PA moves from the lysosome to either the ER or LD to facilitate LD growth (Panel A). PA sent to the ER can be utilized for TAG synthesis or for insertion into the ER membrane for PLIN3 recruitment (Panel C). Similarly, PA transfer to the LD may function in PLIN3 recruitment (Panel B). PA transfer into either organelle is likely to occur through membrane contact sites.

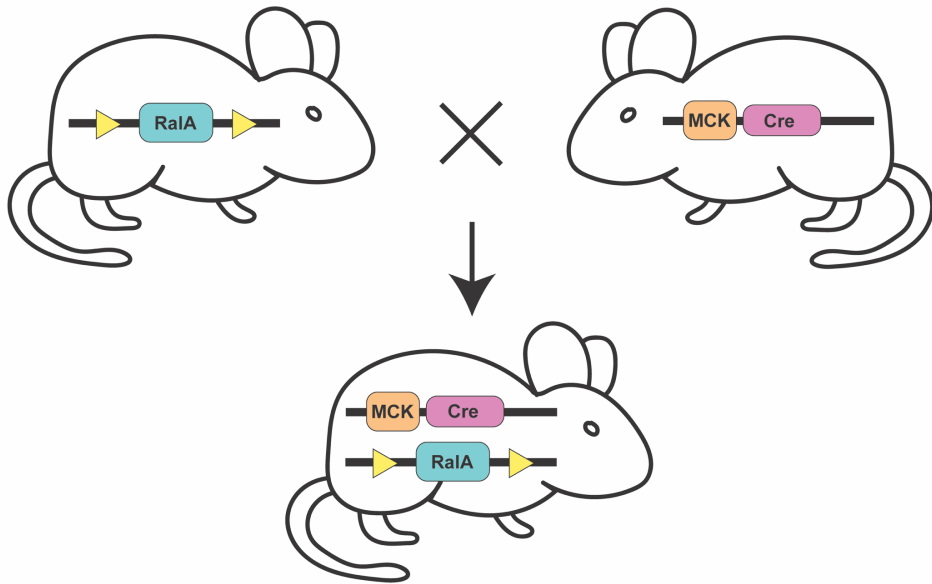


**Figure 3.3 Skeletal muscle conditional KO of RalA in mice**

Residue	Sequence	Predicted Kinase	Score	Residue	Sequence	Predicted Kinase	Score
S11	KGQNSLALH	PKA	.590	S94	LCVFSITEM	unsp	0.701
		DNAPK	.541			CKII	0.543
		CaM-II	.446			CaM-II	0.478
S22	IMVGS GG VG	PKC	0.511	T96	VFSITEMES	CKII	0.637
		GSK3	0.479			Cdc2	0.448
		CaM-II	0.421			GSK3	0.440
S28	GVGKSALTL	CaM-II	0.455	S100	TEMESFAAT	CKII	0.488
		GSK3	0.439			CaM-II	0.447
		PKA	0.425			GSK3	0.441
T31	KSALTLQFM	Cdc2	0.480	T104	SFAATADFR	CKII	0.471
		GSK3	0.453			Cdc2	0.470
		CaM-II	0.443			CaM-II	0.459
Y36	LQFMYDEFV	INSR	0.378	S129	VGNKSDLED	unsp	0.888
		EGFR	0.347			CKII	0.655
		SRC	0.336			CaM-II	0.436
Y43	FVEDYEPTK	unsp	0.378	S138	KRQVSVEEA	unsp	0.998
		EGFR	0.347			RSK	0.531
		SRC	0.336			CKII	0.501
T46	DYEPTKADS	unsp	0.692	Y153	WNVNYVETS	unsp	0.807
		GSK3	0.471			INSR	0.419
		CKII	0.428			EGFR	0.395
S50	TKADSYRKK	unsp	0.992	T156	NYVETSAKT	unsp	0.703
		PKC	0.851			PKC	0.536
		GSK3	0.465			GSK3	0.444
Y51	KADSYRKKV	INSR	0.434	S157	YVETSAKTR	Cdc2	0.461
		unsp	0.373			CaM-II	0.441
		EGFR	0.357			GSK3	0.440
T69	DILDTAGQE	CKII	0.501	T160	TSAKTRANV	CKI	0.497
		GSK3	0.451			GSK3	0.474
		CaM-II	0.446			CaM-II	0.465
Y75	GQEDYAAIR	unsp	0.906	S183	KMEDSKEKN	unsp	0.987
		INSR	0.451			CKI	0.510
		SRC	0.415			GSK3	0.441
Y82	IRDNYFRSG	unsp	0.449	S194	KKRKSLAKR	unsp	0.985
		INSR	0.443			PKA	0.859
		SRC	0.348			PKC	0.783
S85	NYFRSGEGF	CaM-II	0.411				
		Cdc2	0.439				
		GSK3	0.435				

### **Table 3.1 Predicted RalA Phosphorylation Sites and Kinases**

Computational analysis of RalA sequence to determine predicted phosphorylation sites. Analysis of kinase consensus recognition sites indicate top 3 kinases that may phosphorylate RalA at each site. Reference for data on table: Blom N, Sicheritz-Ponten T, Gupta R, Gammeltoft S, Brunak S. Prediction of post-translational glycosylation and phosphorylation of proteins from the amino acid sequence. *Proteomics*: Jun;4(6):1633-49, review 2004.

	WT Mice	Skeletal Muscle Conditional Rala KO Mice	Skeletal Muscle Conditional PLIN3 KO Mice
	24h Fast	24h Fast	24h Fast
<b>Whole Mouse Physiology</b>			
Body Weight	-	-	-
Serum Glucose	-	↓	↓
Serum NEFA	-	↑	↑
Oxidative Phosphorylation	-	↑	↑
β-oxidation	-	↓	↓
<b>Skeletal Muscle</b>			
mRNA expression of β-oxidation	-	↓	↓
Protein expression of β-oxidation	-	↓	↓
mRNA expression of fatty acid import	-	↓	↓
Protein expression of fatty acid import	-	↓	↓
Lipid Droplets	-	↓	↓
TAGs	-	↓	↓

**Table 3.2 Predicted outcome of conditional Rala or PLIN3 knockout in mice skeletal muscle during 24 hours of fasting**

## References

- Adebonojo, F.O., Bensch, K.G., and King, D.W. (1961). The effect of nitrogen on the enzymatic pattern of strain L cells. *Cancer Res* *21*, 252–256.
- Adeyo, O., Horn, P.J., Lee, S., Binns, D.D., Chandrabhas, A., Chapman, K.D., and Goodman, J.M. (2011). The yeast lipin orthologue Pah1p is important for biogenesis of lipid droplets. *J Cell Biology* *192*, 1043–1055.
- Ahmadian, M., Abbott, M.J., Tang, T., Hudak, C.S.S., Kim, Y., Bruss, M., Hellerstein, M.K., Lee, H.-Y., Samuel, V.T., Shulman, G.I., et al. (2011). Desnutrin/ATGL Is Regulated by AMPK and Is Required for a Brown Adipose Phenotype. *Cell Metab* *13*, 739–748.
- Albright, C.F., Giddings, B.W., Liu, J., Vito, M., and Weinberg, R.A. (1993). Characterization of a guanine nucleotide dissociation stimulator for a ras-related GTPase. *Embo J* *12*, 339–347.
- Alpy, F., Rousseau, A., Schwab, Y., Legueux, F., Stoll, I., Wendling, C., Spiegelhalter, C., Kessler, P., Mathelin, C., Rio, M.-C., et al. (2013). STARD3 or STARD3NL and VAP form a novel molecular tether between late endosomes and the ER. *J Cell Sci* *126*, 5500–5512.
- Andersson, L., Bostrom, P., Ericson, J., Rutberg, M., Magnusson, B., Marchesan, D., Ruiz, M., Asp, L., Huang, P., Frohman, M.A., et al. (2006). PLD1 and ERK2 regulate cytosolic lipid droplet formation. *Journal of Cell Science* *119*, 2246–2257.
- Anding, A.L., and Baehrecke, E.H. (2017). Cleaning House: Selective Autophagy of Organelles. *Dev Cell* *41*, 10–22.
- Athenstaedt, K., and Daum, G. (1999). Phosphatidic acid , a key intermediate in lipid metabolism. *European Journal of Biochemistry* *266*, 1–16.
- Awasthi, S., Tompkins, J., Singhal, J., Riggs, A.D., Yadav, S., Wu, X., Singh, S., Warden, C., Liu, Z., Wang, J., et al. (2018). Rlip depletion prevents spontaneous neoplasia in TP53 null mice. *Proc National Acad Sci* *115*, 201719586.
- Balasubramanian, N., Meier, J.A., Scott, D.W., Norambuena, A., White, M.A., and Schwartz, M.A. (2010). RalA-Exocyst Complex Regulates Integrin-Dependent Membrane Raft Exocytosis and Growth Signaling. *Current Biology* *20*, 75–79.
- Barneda, D., Planas-Iglesias, J., Gaspar, M.L., Mohammadyani, D., Prasannan, S., Dormann, D., Han, G.-S., Jesch, S.A., Carman, G.M., Kagan, V., et al. (2015). The brown adipocyte protein CIDEA promotes lipid droplet fusion via a phosphatidic acid-binding amphipathic helix. *Elife* *4*, e07485.
- Becuwe, M., Bond, L.M., Pinto, A.F.M., Boland, S., Mejhert, N., Elliott, S.D., Cicconet, M., Graham, M.M., Liu, X.N., Ilkayeva, O., et al. (2020). FIT2 is an acyl-coenzyme A diphosphatase crucial for endoplasmic reticulum homeostasis. *J Cell Biol* *219*, e202006111.

- Bell, M., Wang, H., Chen, H., McLenithan, J.C., Gong, D.-W., Yang, R.-Z., Yu, D., Fried, S.K., Quon, M.J., Londos, C., et al. (2008). Consequences of Lipid Droplet Coat Protein Downregulation in Liver Cells. *Diabetes* 57, 2037–2045.
- Benador, I.Y., Veliova, M., Mahdavian, K., Petcherski, A., Wikstrom, J.D., Assali, E.A., Acín-Pérez, R., Shum, M., Oliveira, M.F., Cinti, S., et al. (2018). Mitochondria Bound to Lipid Droplets Have Unique Bioenergetics, Composition, and Dynamics that Support Lipid Droplet Expansion. *Cell Metab* 27, 869-885.e6.
- Bensaad, K., Favaro, E., Lewis, C.A., Peck, B., Lord, S., Collins, J.M., Pinnick, K.E., Wigfield, S., Buffa, F.M., Li, J.-L., et al. (2014). Fatty Acid Uptake and Lipid Storage Induced by HIF-1 $\alpha$  Contribute to Cell Growth and Survival after Hypoxia-Reoxygenation. *Cell Reports* 9, 349–365.
- Berg, M.C.W. van den, Gogh, I.J.A. van, Smits, A.M.M., Triest, M. van, Dansen, T.B., Visscher, M., Polderman, P.E., Vliem, M.J., Rehmann, H., and Burgering, B.M.T. (2013). The Small GTPase RALA Controls c-Jun N-terminal Kinase-mediated FOXO Activation by Regulation of a JIP1 Scaffold Complex\*. *J Biol Chem* 288, 21729–21741.
- Berndt, N., Eckstein, J., Heucke, N., Gajowski, R., Stockmann, M., Meierhofer, D., and Holzhütter, H.-G. (2019). Characterization of Lipid and Lipid Droplet Metabolism in Human HCC. *Cells* 8, 512.
- Bersuker, K., Peterson, C.W.H., To, M., Sahl, S.J., Savikhin, V., Grossman, E.A., Nomura, D.K., and Olzmann, J.A. (2018). A Proximity Labeling Strategy Provides Insights into the Composition and Dynamics of Lipid Droplet Proteomes. *DEVCEL* 44, 97-112.e7.
- Bielinski, D.F., Pyun, H.Y., Linko-Stentz, K., Macara, I.G., and Fine, R.E. (1993). Ra1 and Rab3a are major GTP-binding proteins of axonal rapid transport and synaptic vesicles and do not redistribute following depolarization stimulated synaptosomal exocytosis. *Biochimica Et Biophysica Acta Bba - Biomembr* 1151, 246–256.
- Bjedov, I., Toivonen, J.M., Kerr, F., Slack, C., Jacobson, J., Foley, A., and Partridge, L. (2010). Mechanisms of Life Span Extension by Rapamycin in the Fruit Fly *Drosophila melanogaster*. *Cell Metab* 11, 35–46.
- Bodemann, B.O., Orvedahl, A., Cheng, T., Ram, R.R., Ou, Y.-H., Formstecher, E., Maiti, M., Hazelett, C.C., Wauson, E.M., Balakireva, M., et al. (2011). RalB and the Exocyst Mediate the Cellular Starvation Response by Direct Activation of Autophagosome Assembly. *Cell* 144, 253–267.
- Bohnert, M. (2020). Tethering Fat: Tethers in Lipid Droplet Contact Sites. *Contact* 3, 2515256420908142.
- Bose, C., Yadav, S., Singhal, S.S., Singhal, J., Hindle, A., Lee, J., Cheedella, N.K.S., Rehman, S., Rahman, R.L., Jones, C., et al. (2020). Rlip Depletion Suppresses Growth of Breast Cancer. *Cancers* 12, 1446.
- Bougnères, L., Helft, J., Tiwari, S., Vargas, P., Chang, B.H.-J., Chan, L., Campisi, L., Lauvau, G., Hugues, S., Kumar, P., et al. (2009). A Role for Lipid Bodies in the Cross-presentation of Phagocytosed Antigens by MHC Class I in Dendritic Cells. *Immunity* 31, 232–244.

- Boulant, S., Targett-Adams, P., and McLauchlan, J. (2007). Disrupting the association of hepatitis C virus core protein with lipid droplets correlates with a loss in production of infectious virus. *J Gen Virol* 88, 2204–2213.
- Boutant, M., Kulkarni, S.S., Joffraud, M., Ratajczak, J., Valera-Alberni, M., Combe, R., Zorzano, A., and Cantó, C. (2017). Mfn2 is critical for brown adipose tissue thermogenic function. *Embo J* 36, 1543–1558.
- Brasaemle, D.L., Barber, T., Wolins, N.E., Serrero, G., Blanchette-Mackie, E.J., and Londos, C. (1997). Adipose differentiation-related protein is an ubiquitously expressed lipid storage droplet-associated protein. *J Lipid Res* 38, 2249–2263.
- Brown, F.D., Thompson, N., Saqib, K.M., Clark, J.M., Powner, D., Thompson, N.T., Solari, R., and Wakelam, M.J.O. (1998). Phospholipase D1 localises to secretory granules and lysosomes and is plasma-membrane translocated on cellular stimulation. *Curr Biol* 8, 835–838.
- Brown, H.A., Gutowski, S., Moomaw, C.R., Slaughter, C., and Sternwels, P.C. (1993). ADP-ribosylation factor, a small GTP-dependent regulatory protein, stimulates phospholipase D activity. *Cell* 75, 1137–1144.
- Bruyn, K.M.T. de, Rooij, J. de, Wolthuis, R.M.F., Rehmann, H., Wesenbeek, J., Cool, R.H., Wittinghofer, A.H., and Bos, J.L. (2000). RalGEF2, a Pleckstrin Homology Domain Containing Guanine Nucleotide Exchange Factor for Ral\*. *J Biol Chem* 275, 29761–29766.
- Buers, I., Robenek, H., Lorkowski, S., Nitschke, Y., Severs, N.J., and Hofnagel, O. (2009). TIP47, a Lipid Cargo Protein Involved in Macrophage Triglyceride Metabolism. *Arteriosclerosis Thrombosis Vasc Biology* 29, 767–773.
- Bulankina, A.V., Deggerich, A., Wenzel, D., Mutenda, K., Wittmann, J.G., Rudolph, M.G., Burger, K.N.J., and Höning, S. (2009). TIP47 functions in the biogenesis of lipid droplets. *The Journal of Cell Biology* 185, 641–655.
- Cantor, S.B., Urano, T., and Feig, L.A. (1995). Identification and characterization of Ral-binding protein 1, a potential downstream target of Ral GTPases. *Mol Cell Biol* 15, 4578–4584.
- Cascone, I., Selimoglu, R., Ozdemir, C., Nery, E.D., Yeaman, C., White, M., and Camonis, J. (2008). Distinct roles of RalA and RalB in the progression of cytokinesis are supported by distinct RalGEFs. *The EMBO Journal* 27, 2375–2387.
- Ceriani, M., Scanduzzi, C., Amigoni, L., Tisi, R., Berruti, G., and Martegani, E. (2007). Functional analysis of RalGPS2, a murine guanine nucleotide exchange factor for RalA GTPase. *Exp Cell Res* 313, 2293–2307.
- Chardin, P., and Tavitian, A. (1986). The ral gene: a new ras related gene isolated by the use of a synthetic probe. *Embo J* 5, 2203–2208.
- Chardin, P., and Tavitian, A. (1989). Coding sequences of human ralA and ralB cDNAs. *Nucleic Acid Research* 17, 4380.

- Chen, F., Yan, B., Ren, J., Lyu, R., Wu, Y., Guo, Y., Li, D., Zhang, H., and Hu, J. (2021). FIT2 organizes lipid droplet biogenesis with ER tubule-forming proteins and septins. *J Cell Biol* *220*, e201907183.
- Chen, J., Greenberg, A.S., and Wang, S. (2002). Oleic acid-induced PKC isozyme translocation in RAW 264.7 macrophages. *J Cell Biochem* *86*, 784–791.
- Chen, X.-W., Inoue, M., Hsu, S.C., and Saltiel, A.R. (2006). RalA-exocyst-dependent Recycling Endosome Trafficking Is Required for the Completion of Cytokinesis\*. *J Biol Chem* *281*, 38609–38616.
- Chen, X.-W., Leto, D., Chiang, S.-H., Wang, Q., and Saltiel, A.R. (2007). Activation of RalA Is Required for Insulin-Stimulated Glut4 Trafficking to the Plasma Membrane via the Exocyst and the Motor Protein Myo1c. *Developmental Cell* *13*, 391–404.
- Cheung, W., Gill, M., Esposito, A., Kaminski, C.F., Courousse, N., Chwetzoff, S., Trugnan, G., Keshavan, N., Lever, A., and Desselberger, U. (2010). Rotaviruses Associate with Cellular Lipid Droplet Components To Replicate in Viroplasms, and Compounds Disrupting or Blocking Lipid Droplets Inhibit Viroplasm Formation and Viral Replication  $\nabla$  †. *J Virol* *84*, 6782–6798.
- Chien, Y., Kim, S., Bumeister, R., Loo, Y.-M., Kwon, S.W., Johnson, C.L., Balakireva, M.G., Romeo, Y., Kopelovich, L., Gale, M., et al. (2006). RalB GTPase-Mediated Activation of the I $\kappa$ B Family Kinase TBK1 Couples Innate Immune Signaling to Tumor Cell Survival. *Cell* *127*, 157–170.
- Chorlay, A., and Thiam, A.R. (2018). An Asymmetry in Monolayer Tension Regulates Lipid Droplet Budding Direction. *Biophysj* *114*, 631–640.
- Chorlay, A., Monticelli, L., Ferreira, J.V., M'barek, K.B., Ajjaji, D., Wang, S., Johnson, E., Beck, R., Omrane, M., Beller, M., et al. (2019). Membrane Asymmetry Imposes Directionality on Lipid Droplet Emergence from the ER. *DEVCEL* *50*, 25-42.e7.
- Choudhary, V., Ojha, N., Golden, A., and Prinz, W.A. (2015). A conserved family of proteins facilitates nascent lipid droplet budding from the ER. *The Journal of Cell Biology* *211*, 261–271.
- Choudhary, V., Golani, G., Joshi, A.S., Cottier, S., Schneiter, R., Prinz, W.A., and Kozlov, M.M. (2018). Architecture of Lipid Droplets in Endoplasmic Reticulum Is Determined by Phospholipid Intrinsic Curvature. *Current Biology : CB* *28*, 915-926.e9.
- Clough, R.R., Sidhu, R.S., and Bhullar, R.P. (2002). Calmodulin binds RalA and RalB and is required for the thrombin-induced activation of Ral in human platelets. *Journal of Biological Chemistry* *277*, 28972–28980.
- Connerth, M., Tatsuta, T., Haag, M., Klecker, T., Westermann, B., and Langer, T. (2012). Intramitochondrial Transport of Phosphatidic Acid in Yeast by a Lipid Transfer Protein. *Science* *338*, 815–818.
- Corrotte, M., Nguyen, A.P.T., Harlay, M.L., Vitale, N., Bader, M.-F., and Grant, N.J. (2010). Ral Isoforms Are Implicated in Fc $\gamma$ R-Mediated Phagocytosis: Activation of Phospholipase D by RalA. *J Immunol* *185*, 2942–2950.

- Criollo, A., Maiuri, M.C., Tasdemir, E., Vitale, I., Fiebig, A.A., Andrews, D., Molgó, J., Díaz, J., Lavandero, S., Harper, F., et al. (2007). Regulation of autophagy by the inositol trisphosphate receptor. *Cell Death Differ* 14, 1029–1039.
- D'Adamo, D.R., Novick, S., Kahn, J.M., Leonardi, P., and Pellicer, A. (1997). rsc: a novel oncogene with structural and functional homology with the gene family of exchange factors for Ral. *Oncogene* 14, 1295–1305.
- Dall'Armi, C., Hurtado-Lorenzo, A., Tian, H., Morel, E., Nezu, A., Chan, R.B., Yu, W.H., Robinson, K.S., Yeku, O., Small, S.A., et al. (2010). The phospholipase D1 pathway modulates macroautophagy. *Nature Communications* 1, 142–11.
- Dam, T.J.P. van, Bos, J., and Snel, B. (2011). Evolution of the Ras-like small GTPases and their regulators. *Small Gtpases* 2, 4–16.
- Daniel, J., Maamar, H., Deb, C., Sirakova, T.D., and Kolattukudy, P.E. (2011). Mycobacterium tuberculosis Uses Host Triacylglycerol to Accumulate Lipid Droplets and Acquires a Dormancy-Like Phenotype in Lipid-Loaded Macrophages. *Plos Pathog* 7, e1002093.
- Datta, S., Liu, Y., Hariri, H., Bowerman, J., and Henne, W.M. (2019). Cerebellar ataxia disease-associated Snx14 promotes lipid droplet growth at ER–droplet contacts. *J Cell Biol* 218, 1335–1351.
- Drizyte-Miller, K., Schott, M.B., and McNiven, M.A. (2020). Lipid Droplet Contacts With Autophagosomes, Lysosomes, and Other Degradative Vesicles. *Contact* 3, 2515256420910892.
- Du, G., Altshuler, Y.M., Vitale, N., Huang, P., Chasserot-Golaz, S., Morris, A.J., Bader, M.-F., and Frohman, M.A. (2003). Regulation of phospholipase D1 subcellular cycling through coordination of multiple membrane association motifs. *Journal of Cell Biology* 162, 305–315.
- Du, H., Heur, M., Duanmu, M., Grabowski, G.A., Hui, D.Y., Witte, D.P., and Mishra, J. (2001). Lysosomal acid lipase-deficient mice: depletion of white and brown fat, severe hepatosplenomegaly, and shortened life span. *J Lipid Res* 42, 489–500.
- Dubland, J.A., and Francis, G.A. (2015). Lysosomal acid lipase: at the crossroads of normal and atherogenic cholesterol metabolism. *Frontiers Cell Dev Biology* 3, 3.
- Duelund, L., Jensen, G.V., Hannibal-Bach, H.K., Ejsing, C.S., Pedersen, J.S., Pakkanen, K.I., and Ipsen, J.H. (2013). Composition, structure and properties of POPC–triolein mixtures. Evidence of triglyceride domains in phospholipid bilayers. *Biochimica Et Biophysica Acta Bba - Biomembr* 1828, 1909–1917.
- Eden, E.R., Sanchez-Heras, E., Tsapara, A., Sobota, A., Levine, T.P., and Futter, C.E. (2016). Annexin A1 Tethers Membrane Contact Sites that Mediate ER to Endosome Cholesterol Transport. *Dev Cell* 37, 473–483.
- Egan, J.J., Greenberg, A.S., Chang, M.K., Wek, S.A., Moos, M.C., and Londos, C. (1992). Mechanism of hormone-stimulated lipolysis in adipocytes: translocation of hormone-sensitive lipase to the lipid storage droplet. *Proc National Acad Sci* 89, 8537–8541.

- Eichmann, T.O., Kumari, M., Haas, J.T., Farese, R.V., Zimmermann, R., Lass, A., and Zechner, R. (2012). Studies on the Substrate and Stereo/Regioselectivity of Adipose Triglyceride Lipase, Hormone-sensitive Lipase, and Diacylglycerol-O-acyltransferases\*. *J Biol Chem* 287, 41446–41457.
- Eisenberg-Bord, M., Mari, M., Weill, U., Rosenfeld-Gur, E., Moldavski, O., Castro, I.G., Soni, K.G., Harpaz, N., Levine, T.P., Futerman, A.H., et al. (2018). Identification of seipin-linked factors that act as determinants of a lipid droplet subpopulation. *J Cell Biol* 217, 269–282.
- Ezzeldin, M., Borrego-Diaz, E., Taha, M., Esfandyari, T., Wise, A.L., Peng, W., Rouyanian, A., Kermani, A.A., Soleimani, M., Patrad, E., et al. (2014). RalA signaling pathway as a therapeutic target in hepatocellular carcinoma (HCC). *Mol Oncol* 8, 1043–1053.
- Falk, J., Rohde, M., Bekhite, M.M., Neugebauer, S., Hemmerich, P., Kiehnopf, M., Deufel, T., Hübner, C.A., and Beetz, C. (2014). Functional Mutation Analysis Provides Evidence for a Role of REEP1 in Lipid Droplet Biology. *Hum Mutat* 35, 497–504.
- Falsetti, S.C., Wang, D., Peng, H., Carrico, D., Cox, A.D., Der, C.J., Hamilton, A.D., and Sebt, S.M. (2007). Geranylgeranyltransferase I Inhibitors Target RalB To Inhibit Anchorage-Dependent Growth and Induce Apoptosis and RalA To Inhibit Anchorage-Independent Growth  $\nabla$ . *Mol Cell Biol* 27, 8003–8014.
- Faugaret, D., Chouinard, F.C., Harbour, D., azreq, M.-A.E., and Bourgoïn, S.G. (2011). An essential role for phospholipase D in the recruitment of vesicle amine transport protein-1 to membranes in human neutrophils. *Biochem Pharmacol* 81, 144–156.
- Fei, W., Shui, G., Gaeta, B., Du, X., Kuerschner, L., Li, P., Brown, A.J., Wenk, M.R., Parton, R.G., and Yang, H. (2008). Fld1p, a functional homologue of human seipin, regulates the size of lipid droplets in yeast. *The Journal of Cell Biology* 180, 473–482.
- Fei, W., Shui, G., Zhang, Y., Krahmer, N., Ferguson, C., Kapterian, T.S., Lin, R.C., Dawes, I.W., Brown, A.J., Li, P., et al. (2011). A Role for Phosphatidic Acid in the Formation of “Supersized” Lipid Droplets. *PLoS Genetics* 7, e1002201-11.
- Fenwick, R.B., Prasanna, S., Campbell, L.J., Nietlispach, D., Evetts, K.A., Camonis, J., Mott, H.R., and Owen, D. (2009). Solution Structure and Dynamics of the Small GTPase RalB in Its Active Conformation: Significance for Effector Protein Binding  $\dagger$   $\ddagger$ . *Biochemistry-Us* 48, 2192–2206.
- Fenwick, R.B., Campbell, L.J., Rajasekar, K., Prasanna, S., Nietlispach, D., Camonis, J., Owen, D., and Mott, H.R. (2010). The RalB-RLIP76 Complex Reveals a Novel Mode of Ral-Effector Interaction. *Structure* 18, 985–995.
- Filseck, J.M. von, Čopič, A., Delfosse, V., Vanni, S., Jackson, C.L., Bourguet, W., and Drin, G. (2015). Phosphatidylserine transport by ORP/Osh proteins is driven by phosphatidylinositol 4-phosphate. *Science* 349, 432–436.
- Finegold, A.A., Johnson, D.I., Farnsworth, C.C., Gelb, M.H., Judd, S.R., Glomset, J.A., and Tamanoi, F. (1991). Protein geranylgeranyltransferase of *Saccharomyces cerevisiae* is specific for Cys-Xaa-Xaa-Leu motif proteins and requires the CDC43 gene product but not the DPR1 gene product. *Proc National Acad Sci* 88, 4448–4452.

- Frankel, P., Aronheim, A., Kavanagh, E., Balda, M.S., Matter, K., Bunney, T.D., and Marshall, C.J. (2005). RalA interacts with ZONAB in a cell density-dependent manner and regulates its transcriptional activity. *Embo J* 24, 54–62.
- Fredrikson, G., Strålfors, P., Nilsson, N.O., and Belfrage, P. (1981). Hormone-sensitive lipase of rat adipose tissue. Purification and some properties. *J Biol Chem* 256, 6311–6320.
- Freyberg, Z., Sweeney, D., Siddhanta, A., Bourgoïn, S., Frohman, M., and Shields, D. (2001). Intracellular Localization of Phospholipase D1 in Mammalian Cells. 1–13.
- Freyre, C.A.C., Rauher, P.C., Ejsing, C.S., and Klemm, R.W. (2019). MIGA2 Links Mitochondria, the ER, and Lipid Droplets and Promotes De Novo Lipogenesis in Adipocytes. *Mol Cell* 76, 811–825.e14.
- Frias, M.A., Mukhopadhyay, S., Lehman, E., Walasek, A., Utter, M., Menon, D., and Foster, D.A. (2020). Phosphatidic acid drives mTORC1 lysosomal translocation in the absence of amino acids. *J Biol Chem* 295, 263–274.
- Frische, E.W., Berkel, W.P., Haafte, G. van, Cuppen, E., Plasterk, R.H., Tijsterman, M., Bos, J.L., and Zwartkruis, F.J.T. (2007). RAP-1 and the RAL-1/exocyst pathway coordinate hypodermal cell organization in *Caenorhabditis elegans*. *Embo J* 26, 5083–5092.
- Gallardo-Montejano, V.I., Yang, C., Hahner, L., McAfee, J.L., Johnson, J.A., Holland, W.L., Fernandez-Valdivia, R., and Bickel, P.E. (2021). Perilipin 5 links mitochondrial uncoupled respiration in brown fat to healthy white fat remodeling and systemic glucose tolerance. *Nat Commun* 12, 3320.
- Ganesan, S., Shabits, B.N., and Zaremberg, V. (2015). Tracking Diacylglycerol and Phosphatidic Acid Pools in Budding Yeast. *Lipid Insights* 8*sl*, LPI.S31781-11.
- Gao, G., Chen, F.-J., Zhou, L., Su, L., Xu, D., Xu, L., and Li, P. (2017a). Control of lipid droplet fusion and growth by CIDE family proteins. *Biochimica Et Biophysica Acta Bba - Mol Cell Biology Lipids* 1862, 1197–1204.
- Gao, Q., Binns, D.D., Kinch, L.N., Grishin, N.V., Ortiz, N., Chen, X., and Goodman, J.M. (2017b). Pet10p is a yeast perilipin that stabilizes lipid droplets and promotes their assembly. *J Cell Biol* 216, 3199–3217.
- Gao, W., Ding, W.-X., Stolz, D.B., and Yin, X.-M. (2008). Induction of macroautophagy by exogenously introduced calcium. *Autophagy* 4, 754–761.
- Garner, K., Hunt, A.N., Koster, G., Somerharju, P., Groves, E., Li, M., Raghu, P., Holic, R., and Cockcroft, S. (2012). Phosphatidylinositol Transfer Protein, Cytoplasmic 1 (PITPNC1) Binds and Transfers Phosphatidic Acid\*. *J Biol Chem* 287, 32263–32276.
- Gatta, A.T., Wong, L.H., Sere, Y.Y., Calderón-Noreña, D.M., Cockcroft, S., Menon, A.K., and Levine, T.P. (2015). A new family of StART domain proteins at membrane contact sites has a role in ER-PM sterol transport. *Elife* 4, e07253.

- Gentry, L.R., Martin, T.D., Reiner, D.J., and Der, C.J. (2014). Ral small GTPase signaling and oncogenesis: More than just 15minutes of fame. *BBA - Molecular Cell Research* 1843, 2976–2988.
- Gentry, L.R., Nishimura, A., Cox, A.D., Martin, T.D., Tsygankov, D., Nishida, M., Elston, T.C., and Der, C.J. (2015). Divergent roles of CAAX motif-signaled posttranslational modifications in the regulation and subcellular localization of Ral GTPases. *Journal of Biological Chemistry* 290, 22851–22861.
- Ghislat, G., Patron, M., Rizzuto, R., and Knecht, E. (2012). Withdrawal of Essential Amino Acids Increases Autophagy by a Pathway Involving Ca<sup>2+</sup>/Calmodulin-dependent Kinase Kinase- $\beta$  (CaMKK- $\beta$ ). *Journal of Biological Chemistry* 287, 38625–38636.
- Ghoroghi, S., Mary, B., Larnicol, A., Asokan, N., Klein, A., Osmani, N., Busnelli, I., Delalande, F., Paul, N., Halary, S., et al. (2021). Ral GTPases promote breast cancer metastasis by controlling biogenesis and organ targeting of exosomes. *Elife* 10, e61539.
- Gimm, T., Wiese, M., Teschemacher, B., Deggerich, A., Schödel, J., Knaup, K.X., Hackenbeck, T., Hellerbrand, C., Amann, K., Wiesener, M.S., et al. (2010). Hypoxia-inducible protein 2 is a novel lipid droplet protein and a specific target gene of hypoxia-inducible factor-1. *Faseb J* 24, 4443–4458.
- Goi, T., Shipitsin, M., Lu, Z., Foster, D.A., Klinz, S.G., and Feig, L.A. (2000). An EGF receptor/Ral-GTPase signaling cascade regulates c-Src activity and substrate specificity. *Embo J* 19, 623–630.
- Gong, J., Sun, Z., Wu, L., Xu, W., Schieber, N., Xu, D., Shui, G., Yang, H., Parton, R.G., and Li, P. (2011). Fsp27 promotes lipid droplet growth by lipid exchange and transfer at lipid droplet contact sites. *J Cell Biology* 195, 953–963.
- Gopalakrishna, R., and Jaken, S. (2000). Protein kinase C signaling and oxidative stress. *Free Radical Bio Med* 28, 1349–1361.
- Gordon, G.B., Barcza, M.A., and Bush, M.E. (1977). Lipid accumulation of hypoxic tissue culture cells. *Am J Pathology* 88, 663–678.
- Grachan, J.J., Kery, M., Giaccia, A.J., Denko, N.C., and Papandreou, I. (2021). Lipid droplet storage promotes murine pancreatic tumor growth. *Oncol Rep* 45, 21.
- Greenberg, A.S., Shen, W.-J., Muliro, K., Patel, S., Souza, S.C., Roth, R.A., and Kraemer, F.B. (2001). Stimulation of Lipolysis and Hormone-sensitive Lipase via the Extracellular Signal-regulated Kinase Pathway\*. *J Biol Chem* 276, 45456–45461.
- Grippa, A., Buxó, L., Mora, G., Funaya, C., Idrissi, F.-Z., Mancuso, F., Gomez, R., Muntanyà, J., Sabidó, E., and Carvalho, P. (2015). The seipin complex Fld1/Ldb16 stabilizes ER–lipid droplet contact sites. *J Cell Biol* 211, 829–844.
- Gross, D.A., Zhan, C., and Silver, D.L. (2011). Direct binding of triglyceride to fat storage-inducing transmembrane proteins 1 and 2 is important for lipid droplet formation. *Proc National Acad Sci* 108, 19581–19586.

- Grujic, O., and Bhullar, R.P. (2009). Ral GTPase interacts with the N-terminal in addition to the C-terminal region of PLC- $\delta$ 1. *Biochemical and Biophysical Research Communications* 383, 401–405.
- Gu, J.-Q., Wang, D.-F., Yan, X.-G., Zhong, W.-L., Zhang, J., Fan, B., and Ikuyama, S. (2010). A Toll-like receptor 9-mediated pathway stimulates perilipin 3 (TIP47) expression and induces lipid accumulation in macrophages. *Am J Physiol-Endoc M* 299, E593–E600.
- Guin, S., Ru, Y., Wynes, M.W., Mishra, R., Lu, X., Owens, C., Barón, A.E., Vasu, V.T., Hirsch, F.R., Kern, J.A., et al. (2013). Contributions of KRAS and RAL in Non-Small-Cell Lung Cancer Growth and Progression. *J Thorac Oncol* 8, 1492–1501.
- Haemmerle, G., Zimmermann, R., Hayn, M., Theussl, C., Waeg, G., Wagner, E., Sattler, W., Magin, T.M., Wagner, E.F., and Zechner, R. (2002). Hormone-sensitive Lipase Deficiency in Mice Causes Diglyceride Accumulation in Adipose Tissue, Muscle, and Testis\*. *J Biol Chem* 277, 4806–4815.
- Haemmerle, G., Lass, A., Zimmermann, R., Gorkiewicz, G., Meyer, C., Rozman, J., Heldmaier, G., Maier, R., Theussl, C., Eder, S., et al. (2006). Defective Lipolysis and Altered Energy Metabolism in Mice Lacking Adipose Triglyceride Lipase. *Science* 312, 734–737.
- Han, J.M., Kim, Y., Lee, J.S., Lee, C.S., Lee, B.D., Ohba, M., Kuroki, T., Suh, P.-G., and Ryu, S.H. (2002). Localization of Phospholipase D1 to Caveolin-enriched Membrane via Palmitoylation: Implications for Epidermal Growth Factor Signaling. 1–13.
- Han, K., Kim, M.-H., Seeburg, D., Seo, J., Verpelli, C., Han, S., Chung, H.S., Ko, J., Lee, H.W., Kim, K., et al. (2009). Regulated RalBP1 Binding to RalA and PSD-95 Controls AMPA Receptor Endocytosis and LTD. *Plos Biol* 7, e1000187.
- Hanada, K. (2018). Lipid transfer proteins rectify inter-organelle flux and accurately deliver lipids at membrane contact sites. *J Lipid Res* 59, 1341–1366.
- Hariri, H., Rogers, S., Ugrankar, R., Liu, Y.L., Feathers, J.R., and Henne, W.M. (2017). Lipid droplet biogenesis is spatially coordinated at ER–vacuole contacts under nutritional stress. 1–16.
- Hariri, H., Speer, N., Bowerman, J., Rogers, S., Fu, G., Reetz, E., Datta, S., Feathers, J.R., Ugrankar, R., Nicastro, D., et al. (2019). Mdm1 maintains endoplasmic reticulum homeostasis by spatially regulating lipid droplet biogenesis. *J Cell Biol* 218, 1319–1334.
- Harr, M.W., McColl, K.S., Zhong, F., Molitoris, J.K., and Distelhorst, C.W. (2010). Glucocorticoids downregulate Fyn and inhibit IP3-mediated calcium signaling to promote autophagy in T lymphocytes. *Autophagy* 6, 912–921.
- Harris, C., Herker, E., Farese, R.V., and Ott, M. (2011). Hepatitis C Virus Core Protein Decreases Lipid Droplet Turnover A MECHANISM FOR CORE-INDUCED STEATOSIS\*. *J Biol Chem* 286, 42615–42625.
- Hazelett, C.C., Sheff, D., and Yeaman, C. (2011). RalA and RalB differentially regulate development of epithelial tight junctions. *Mol Biol Cell* 22, 4787–4800.

- Henne, W.M., Zhu, L., Balogi, Z., Stefan, C., Pleiss, J.A., and Emr, S.D. (2015). Mdm1/Snx13 is a novel ER–endolysosomal interorganelle tethering protein. *J Cell Biol* 210, 541–551.
- Hikita, H., Sakane, S., and Takehara, T. (2018). Mechanisms of the autophagosome-lysosome fusion step and its relation to non-alcoholic fatty liver disease. *Liver Res* 2, 120–124.
- Hinson, E.R., and Cresswell, P. (2009). The antiviral protein, viperin, localizes to lipid droplets via its N-terminal amphipathic  $\alpha$ -helix. *Proc National Acad Sci* 106, 20452–20457.
- Hodgkin, M.N., Masson, M.R., Powner, D., Saqib, K.M., Ponting, C.P., and Wakelam, M.J.O. (2000). Phospholipase D regulation and localisation is dependent upon a phosphatidylinositol 4,5-bisphosphate-specific PH domain. 1–4.
- Hofer, F., Berdeaux, R., and Martin, G.S. (1998). Ras-independent activation of Ral by a Ca<sup>2+</sup>-dependent pathway. *Curr Biol* 8, 839–844.
- Höglinger, D., Burgoyne, T., Sanchez-Heras, E., Hartwig, P., Colaco, A., Newton, J., Futter, C.E., Spiegel, S., Platt, F.M., and Eden, E.R. (2019). NPC1 regulates ER contacts with endocytic organelles to mediate cholesterol egress. *Nat Commun* 10, 4276.
- Holly, R.M., Mavor, L.M., Zuo, Z., and Blankenship, J.T. (2015). A rapid, membrane-dependent pathway directs furrow formation through RalA in the early *Drosophila* embryo. *Development* 142, 2316–2328.
- Holst, D., Luquet, S., Nogueira, V., Kristiansen, K., Leverve, X., and Grimaldi, P.A. (2003). Nutritional regulation and role of peroxisome proliferator-activated receptor  $\delta$  in fatty acid catabolism in skeletal muscle. *Biochimica Et Biophysica Acta Bba - Mol Cell Biology Lipids* 1633, 43–50.
- Hope, R.G., Murphy, D.J., and McLauchlan, J. (2002). The Domains Required to Direct Core Proteins of Hepatitis C Virus and GB Virus-B to Lipid Droplets Share Common Features with Plant Oleosin Proteins\*. *J Biol Chem* 277, 4261–4270.
- Høyer-Hansen, M., Bastholm, L., Szyniarowski, P., Campanella, M., Szabadkai, G., Farkas, T., Bianchi, K., Fehrenbacher, N., Elling, F., Rizzuto, R., et al. (2007). Control of Macroautophagy by Calcium, Calmodulin-Dependent Kinase Kinase- $\beta$ , and Bcl-2. *Mol Cell* 25, 193–205.
- Hudson, M.E., Pozdnyakova, I., Haines, K., Mor, G., and Snyder, M. (2007). Identification of differentially expressed proteins in ovarian cancer using high-density protein microarrays. *Proc National Acad Sci* 104, 17494–17499.
- Hugenroth, M., and Bohnert, M. (2019). Come a little bit closer! Lipid droplet-ER contact sites are getting crowded. *Biochimica Et Biophysica Acta Bba - Mol Cell Res* 1867, 118603.
- Inoue, M., Akama, T., Jiang, Y., and Chun, T.-H. (2015). The Exocyst Complex Regulates Free Fatty Acid Uptake by Adipocytes. *Plos One* 10, e0120289.
- Isomura, M., Okui, K., Fujiwara, T., Shin, S., and Nakamura, Y. (1996). Isolation and mapping of RAB2L, a human cDNA that encodes a protein homologous to RalGDS. *Cytogenet Genome Res* 74, 263–265.

- Itabe, H., Yamaguchi, T., Nimura, S., and Sasabe, N. (2017). Perilipins: a diversity of intracellular lipid droplet proteins. *Lipids in Health and Disease* 16, 1–11.
- Itakura, E., Kishi-Itakura, C., and Mizushima, N. (2012). The Hairpin-type Tail-Anchored SNARE Syntaxin 17 Targets to Autophagosomes for Fusion with Endosomes/Lysosomes. *Cell* 151, 1256–1269.
- Jacquier, N., Choudhary, V., Mari, M., Toulmay, A., Reggiori, F., and Schneiter, R. (2011). Lipid droplets are functionally connected to the endoplasmic reticulum in *Saccharomyces cerevisiae*. *J Cell Sci* 124, 2424–2437.
- Jägerström, S., Polesie, S., Wickström, Y., Johansson, B.R., Schröder, H.D., Højlund, K., and Boström, P. (2009). Lipid droplets interact with mitochondria using SNAP23. *Cell Biol Int* 33, 934–940.
- Jambunathan, S., Yin, J., Khan, W., Tamori, Y., and Puri, V. (2011). FSP27 Promotes Lipid Droplet Clustering and Then Fusion to Regulate Triglyceride Accumulation. *Plos One* 6, e28614.
- Jenkins, G.M., and Frohman, M.A. (2005). Phospholipase D: a lipid centric review. *Cellular and Molecular Life Sciences* 62, 2305–2316.
- Jenkins, C.M., Mancuso, D.J., Yan, W., Sims, H.F., Gibson, B., and Gross, R.W. (2004). Identification, Cloning, Expression, and Purification of Three Novel Human Calcium-independent Phospholipase A2 Family Members Possessing Triacylglycerol Lipase and Acylglycerol Transacylase Activities\*. *J Biol Chem* 279, 48968–48975.
- Jiang, H., Luo, J.-Q., Urano, T., Frankel, P., Lu, Z., Foster, D.A., and Feig, L.A. (1995). Involvement of Ral GTPase in v-Src-induced phospholipase D activation. *Nature* 378, 409–412.
- Jin, C., and Yuan, P. (2020). Implications of lipid droplets in lung cancer: Associations with drug resistance. *Oncol Lett* 20, 2091–2104.
- Johansson, J., Naszai, M., Hodder, M.C., Pickering, K.A., Miller, B.W., Ridgway, R.A., Yu, Y., Peschard, P., Brachmann, S., Campbell, A.D., et al. (2019). RAL GTPases Drive Intestinal Stem Cell Function and Regeneration through Internalization of WNT Signalosomes. *Stem Cell* 1–24.
- Jullien-Flores, V., Dorseuil, O., Romero, F., Letourneur, F., Saragosti, S., Berger, R., Tavitian, A., Gacon, G., and Camonis, J.H. (1995). Bridging Ral GTPase to Rho Pathways RLIP76, A Ral EFFECTOR WITH CDC42/Rac GTPase-ACTIVATING PROTEIN ACTIVITY (\*). *J Biol Chem* 270, 22473–22477.
- Jung, C.H., Jun, C.B., Ro, S.-H., Kim, Y.-M., Otto, N.M., Cao, J., Kundu, M., and Kim, D.-H. (2009). ULK-Atg13-FIP200 Complexes Mediate mTOR Signaling to the Autophagy Machinery. *Mol Biol Cell* 20, 1992–2003.
- Kadereit, B., Kumar, P., Wang, W.-J., Miranda, D., Snapp, E.L., Severina, N., Torregroza, I., Evans, T., and Silver, D.L. (2008). Evolutionarily conserved gene family important for fat storage. *Proc National Acad Sci* 105, 94–99.

- Kamphorst, J.J., Nofal, M., Commisso, C., Hackett, S.R., Lu, W., Grabocka, E., Heiden, M.G.V., Miller, G., Drebin, J.A., Bar-Sagi, D., et al. (2015). Human Pancreatic Cancer Tumors Are Nutrient Poor and Tumor Cells Actively Scavenge Extracellular Protein. *Cancer Res* 75, 544–553.
- Kanaley, J.A., Shadid, S., Sheehan, M.T., Guo, Z., and Jensen, M.D. (2009). Relationship between plasma free fatty acid, intramyocellular triglycerides and long-chain acylcarnitines in resting humans. *J Physiology* 587, 5939–5950.
- Kashatus, D.F., Lim, K.-H., Brady, D.C., Pershing, N.L.K., Cox, A.D., and Counter, C.M. (2011). RALA and RALBP1 regulate mitochondrial fission at mitosis. *Nature Cell Biology* 13, 1108–1115.
- Kassan, A., Herms, A., Fernández-Vidal, A., Bosch, M., Schieber, N.L., Reddy, B.J.N., Fajardo, A., Gelabert-Baldrich, M., Tebar, F., Enrich, C., et al. (2013). Acyl-CoA synthetase 3 promotes lipid droplet biogenesis in ER microdomains. *The Journal of Cell Biology* 203, 985–1001.
- Kassas, N., Tanguy, E., Thahouly, T., Fouillen, L., Heintz, D., Chasserot-Golaz, S., Bader, M.-F., Grant, N.J., and Vitale, N. (2017). Comparative Characterization of Phosphatidic Acid Sensors and Their Localization during Frustrated Phagocytosis. *Journal of Biological Chemistry* 292, 4266–4279.
- Kaushik, S., and Cuervo, A.M. (2015). Degradation of lipid droplet-associated proteins by chaperone-mediated autophagy facilitates lipolysis. *Nat Cell Biol* 17, 759–770.
- Kikuchi, A., Demo, S.D., Ye, Z.H., Chen, Y.W., and Williams, L.T. (1994). ralGDS family members interact with the effector loop of ras p21. *Mol Cell Biol* 14, 7483–7491.
- Kim, S., Kedan, A., Marom, M., Gavert, N., Keinan, O., Selitrennik, M., Laufman, O., and Lev, S. (2013). The phosphatidylinositol-transfer protein Nir2 binds phosphatidic acid and positively regulates phosphoinositide signalling. *Embo Rep* 14, 891–899.
- Kim, Y.J., Guzman-Hernandez, M.-L., Wisniewski, E., and Balla, T. (2015). Phosphatidylinositol-Phosphatidic Acid Exchange by Nir2 at ER-PM Contact Sites Maintains Phosphoinositide Signaling Competence. *Dev Cell* 33, 549–561.
- Kinsella, B.T., Erdman, R.A., and Maltese, W.A. (1991). Carboxyl-terminal isoprenylation of ras-related GTP-binding proteins encoded by rac1, rac2, and ralA. *J Biol Chem* 266, 9786–9794.
- Klemm, R.W., Norton, J.P., Cole, R.A., Li, C.S., Park, S.H., Crane, M.M., Li, L., Jin, D., Boye-Doe, A., Liu, T.Y., et al. (2013). A Conserved Role for Atlastin GTPases in Regulating Lipid Droplet Size. *Cell Reports* 3, 1465–1475.
- Kooijman, E.E., Chupin, V., Kruijff, B. de, and Burger, K.N.J. (2003). Modulation of Membrane Curvature by Phosphatidic Acid and Lysophosphatidic Acid. *Traffic* 4, 162–174.
- Krahmer, N., Guo, Y., Wilfling, F., Hilger, M., Lingrell, S., Heger, K., Newman, H.W., Schmidt-Supprian, M., Vance, D.E., Mann, M., et al. (2011). Phosphatidylcholine Synthesis for Lipid Droplet Expansion Is Mediated by Localized Activation of CTP:Phosphocholine Cytidylyltransferase. *Cell Metab* 14, 504–515.

- Kroemer, G., Mariño, G., and Levine, B. (2010). Autophagy and the Integrated Stress Response. *Molecular Cell* *40*, 280–293.
- Kuerschner, L., Moessinger, C., and Thiele, C. (2008). Imaging of Lipid Biosynthesis: How a Neutral Lipid Enters Lipid Droplets. *Traffic* *9*, 338–352.
- Kumar, N., Leonzino, M., Hancock-Cerutti, W., Horenkamp, F.A., Li, P., Lees, J.A., Wheeler, H., Reinisch, K.M., and Camilli, P.D. (2018). VPS13A and VPS13C are lipid transport proteins differentially localized at ER contact sites. *J Cell Biol* *217*, 3625–3639.
- Kumar, Y., Cocchiaro, J., and Valdivia, R.H. (2006). The Obligate Intracellular Pathogen *Chlamydia trachomatis* Targets Host Lipid Droplets. *Curr Biol* *16*, 1646–1651.
- Kuribara, H., Tago, K., Yokozeki, T., Sasaki, T., Takai, Y., Morii, N., Narumiya, S., Katada, T., and Kanaho, Y. (1995). Synergistic Activation of Rat Brain Phospholipase D by ADP-ribosylation Factor and rhoA p21, and Its Inhibition by Clostridium botulinum C3 Exoenzyme (\*). *J Biol Chem* *270*, 25667–25671.
- Kvam, E., and Goldfarb, D.S. (2004). Nvj1p is the outer-nuclear-membrane receptor for oxysterol-binding protein homolog Osh1p in *Saccharomyces cerevisiae*. *J Cell Sci* *117*, 4959–4968.
- Lafontan, M., and Langin, D. (2009). Lipolysis and lipid mobilization in human adipose tissue. *Prog Lipid Res* *48*, 275–297.
- Lalli, G. (2009). RalA and the exocyst complex influence neuronal polarity through PAR-3 and aPKC. *J Cell Sci* *122*, 1499–1506.
- Lam, D., Kosta, A., Luciani, M.-F., and Golstein, P. (2008). The Inositol 1,4,5-Trisphosphate Receptor Is Required to Signal Autophagic Cell Death. *Mol Biol Cell* *19*, 691–700.
- Lang, A.B., Peter, A.T.J., Walter, P., and Kornmann, B. (2015). ER–mitochondrial junctions can be bypassed by dominant mutations in the endosomal protein Vps13. *J Cell Biol* *210*, 883–890.
- Lange, P., Ragni, M., Silvestri, E., Moreno, M., Schiavo, L., Lombardi, A., Farina, P., Feola, A., Goglia, F., and Lanni, A. (2004). Combined cDNA array/RT-PCR analysis of gene expression profile in rat gastrocnemius muscle: relation to its adaptive function in energy metabolism during fasting. *Faseb J* *18*, 1–22.
- Lass, A., Zimmermann, R., Haemmerle, G., Riederer, M., Schoiswohl, G., Schweiger, M., Kienesberger, P., Strauss, J.G., Gorkiewicz, G., and Zechner, R. (2006). Adipose triglyceride lipase-mediated lipolysis of cellular fat stores is activated by CGI-58 and defective in Chanarin-Dorfman Syndrome. *Cell Metab* *3*, 309–319.
- Lee, S., Wurtzel, J.G.T., Singhal, S.S., Awasthi, S., and Goldfinger, L.E. (2012). RALBP1/RLIP76 Depletion in Mice Suppresses Tumor Growth by Inhibiting Tumor Neovascularization. *Cancer Res* *72*, 5165–5173.

- Li, D., Zhao, Y.G., Li, D., Zhao, H., Huang, J., Miao, G., Feng, D., Liu, P., Li, D., and Zhang, H. (2019). The ER-Localized Protein DFCEP1 Modulates ER-Lipid Droplet Contact Formation. *Cell Reports* 27, 343-358.e5.
- Li, G., Han, L., Chou, T.-C., Fujita, Y., Arunachalam, L., Xu, A., Wong, A., Chiew, S.-K., Wan, Q., Wang, L., et al. (2007). RalA and RalB Function as the Critical GTP Sensors for GTP-Dependent Exocytosis. *J Neurosci* 27, 190–202.
- Li, Z., Schulze, R.J., Weller, S.G., Krueger, E.W., Schott, M.B., Zhang, X., Casey, C.A., Liu, J., Stöckli, J., James, D.E., et al. (2016). A novel Rab10-EHBP1-EHD2 complex essential for the autophagic engulfment of lipid droplets. *Sci Adv* 2, e1601470.
- Lim, C.-Y., Davis, O.B., Shin, H.R., Zhang, J., Berdan, C.A., Jiang, X., Counihan, J.L., Ory, D.S., Nomura, D.K., and Zoncu, R. (2019). ER–lysosome contacts enable cholesterol sensing by mTORC1 and drive aberrant growth signalling in Niemann–Pick type C. *Nat Cell Biol* 21, 1206–1218.
- Lim, K.-H., Baines, A.T., Fiordalisi, J.J., Shipitsin, M., Feig, L.A., Cox, A.D., Der, C.J., and Counter, C.M. (2005). Activation of RalA is critical for Ras-induced tumorigenesis of human cells. *Cancer Cell* 7, 533–545.
- Lim, K.-H., O’Hayer, K., Adams, S.J., Kendall, S.D., Campbell, P.M., Der, C.J., and Counter, C.M. (2006). Divergent Roles for RalA and RalB in Malignant Growth of Human Pancreatic Carcinoma Cells. *Current Biology* 16, 2385–2394.
- Lim, K.H., Brady, D.C., Kashatus, D.F., Ancrile, B.B., Der, C.J., Cox, A.D., and Counter, C.M. (2010). Aurora-A Phosphorylates, Activates, and Relocalizes the Small GTPase RalA. *Molecular and Cellular Biology* 30, 508–523.
- Listenberger, L.L., Han, X., Lewis, S.E., Cases, S., Farese, R.V., Ory, D.S., and Schaffer, J.E. (2003). Triglyceride accumulation protects against fatty acid-induced lipotoxicity. *Proceedings of the National Academy of Sciences* 100, 3077–3082.
- Liu, K., Zhou, S., Kim, J.-Y., Tillison, K., Majors, D., Rearick, D., Lee, J.H., Fernandez-Boyanapalli, R.F., Barricklow, K., Houston, M.S., et al. (2009). Functional analysis of FSP27 protein regions for lipid droplet localization, caspase-dependent apoptosis, and dimerization with CIDEA. *Am J Physiol-Endoc M* 297, E1395–E1413.
- Liu, P., Ying, Y., Zhao, Y., Mundy, D.I., Zhu, M., and Anderson, R.G.W. (2004). Chinese Hamster Ovary K2 Cell Lipid Droplets Appear to Be Metabolic Organelles Involved in Membrane Traffic. *Journal of Biological Chemistry* 279, 3787–3792.
- Lizaso, A., Tan, K.-T., and Lee, Y.-H. (2013).  $\beta$ -adrenergic receptor-stimulated lipolysis requires the RAB7-mediated autolysosomal lipid degradation. *Autophagy* 9, 1228–1243.
- Ljubcic, S., Bezzi, P., Vitale, N., and Regazzi, R. (2009). The GTPase RalA regulates different steps of the secretory process in pancreatic beta-cells. *PLoS ONE* 4, e7770-10.

- Lopez-Andreo, M.J., Gomez-Fernandez, J.C., and Corbalan-Garcia, S. (2003). The Simultaneous Production of Phosphatidic Acid and Diacylglycerol Is Essential for the Translocation of Protein Kinase C $\epsilon$  to the Plasma Membrane in RBL-2H3 Cells. *Mol Biol Cell* *14*, 4885–4895.
- Lu, Z., Hornia, A., Joseph, T., Sukezane, T., Frankel, P., Zhong, M., Bychenok, S., Xu, L., Feig, L.A., and Foster, D.A. (2000). Phospholipase D and RalA Cooperate with the Epidermal Growth Factor Receptor To Transform 3Y1 Rat Fibroblasts. *Mol Cell Biol* *20*, 462–467.
- Luo, J.-Q., Liu, X., Hammond, S.M., Colley, W.C., Feig, L.A., Frohman, M.A., Morris, A.J., and Foster, D.A. (1997). RalA Interacts Directly with the Arf-Responsive, PIP2-Dependent Phospholipase D1. *Biochem Biophys Res Commun* *235*, 854–859.
- Luo, J.-Q., Liu, X., Frankel, P., Rotunda, T., Ramos, M., Flom, J., Jiang, H., Feig, L.A., Morris, A.J., Kahn, R.A., et al. (1998). Functional association between Arf and RalA in active phospholipase D complex. *PNAS* *95*, 3632–3637.
- Maehama, T., Tanaka, M., Nishina, H., Murakami, M., Kanaho, Y., and Hanada, K. (2008). RalA Functions as an Indispensable Signal Mediator for the Nutrient-sensing System. *Journal of Biological Chemistry* *283*, 35053–35059.
- Maier, A., Wu, H., Cordasic, N., Oefner, P., Dietel, B., Thiele, C., Weidemann, A., Eckardt, K., and Warnecke, C. (2017). Hypoxia-inducible protein 2 Hig2/Hilpda mediates neutral lipid accumulation in macrophages and contributes to atherosclerosis in apolipoprotein E-deficient mice. *FASEB J* *31*, 4971–4984.
- Male, H., Patel, V., Jacob, M.A., Borrego-Diaz, E., Wang, K., Young, D.A., Wise, A.L., Huang, C., Veldhuizen, P.V., O'Brien-Ladner, A., et al. (2012). Inhibition of RalA signaling pathway in treatment of non-small cell lung cancer. *Lung Cancer (Amsterdam, Netherlands)* *77*, 252–259.
- Manifava, M., Thuring, J.W.J.F., Lim, Z.-Y., Packman, L., Holmes, A.B., and Ktistakis, N.T. (2001). Differential Binding of Traffic-related Proteins to Phosphatidic Acid- or Phosphatidylinositol (4,5)-Bisphosphate-coupled Affinity Reagents\*. *J Biol Chem* *276*, 8987–8994.
- Marchesan, D., Rutberg, M., Andersson, L., Asp, L., Larsson, T., Borén, J., Johansson, B.R., and Olofsson, S.-O. (2003). A Phospholipase D-dependent Process Forms Lipid Droplets Containing Caveolin, Adipocyte Differentiation-related Protein, and Vimentin in a Cell-free System. *Journal of Biological Chemistry* *278*, 27293–27300.
- Mark, B.L., Jilkina, O., and Bhullar, R.P. (1996). Association of RalGTP-Binding Protein with Human Platelet Dense Granules. *Biochem Biophys Res Commun* *225*, 40–46.
- Martin, T.D., Samuel, J.C., Routh, E.D., Der, C.J., and Yeh, J.J. (2011). Activation and involvement of Ral GTPases in colorectal cancer. *Cancer Research* *71*, 206–215.
- Martin, T.D., Mitin, N., Cox, A.D., Yeh, J.J., and Der, C.J. (2012). Phosphorylation by Protein Kinase C $\alpha$  Regulates RalB Small GTPase Protein Activation, Subcellular Localization, and Effector Utilization\*. *J Biol Chem* *287*, 14827–14836.

- Martin, T.D., Chen, X.-W., Kaplan, R.E.W., Saltiel, A.R., Walker, C.L., Reiner, D.J., and Der, C.J. (2014). Ral and Rheb GTPase Activating Proteins Integrate mTOR and GTPase Signaling in Aging, Autophagy, and Tumor Cell Invasion. *Mol Cell* 53, 209–220.
- Martinez-Lopez, N., Garcia-Macia, M., Sahu, S., Athonvarangkul, D., Liebling, E., Merlo, P., Cecconi, F., Schwartz, G.J., and Singh, R. (2016). Autophagy in the CNS and Periphery Coordinate Lipophagy and Lipolysis in the Brown Adipose Tissue and Liver. *Cell Metab* 23, 113–127.
- Mattos, K.A., D'Avila, H., Rodrigues, L.S., Oliveira, V.G.C., Sarno, E.N., Atella, G.C., Pereira, G.M., Bozza, P.T., and Pessolani, M.C.V. (2010). Lipid droplet formation in leprosy: Toll-like receptor-regulated organelles involved in eicosanoid formation and Mycobacterium leprae pathogenesis. *J Leukocyte Biol* 87, 371–384.
- M'barek, K.B., Ajjaji, D., Chorlay, A., Vanni, S., Forêt, L., and Thiam, A.R. (2017). ER Membrane Phospholipids and Surface Tension Control Cellular Lipid Droplet Formation. *Dev Cell* 41, 591-604.e7.
- Melo, R.C.N., Fabrino, D.L., Dias, F.F., and Parreira, G.G. (2006). Lipid bodies: structural markers of inflammatory macrophages in innate immunity. *Inflamm Res* 55, 342–348.
- Michaelson, D., Ali, W., Chiu, V.K., Bergo, M., Silletti, J., Wright, L., Young, S.G., and Philips, M. (2005). Postprenylation CAAX Processing Is Required for Proper Localization of Ras but Not Rho GTPases. *Mol Biol Cell* 16, 1606–1616.
- Mirheydari, M., Rathnayake, S.S., Frederick, H., Arhar, T., Mann, E.K., Cocklin, S., and Kooijman, E.E. (2016). Insertion of perilipin 3 into a glycerol(phospho)lipid monolayer depends on lipid headgroup and acyl chain species. 1–12.
- Miyanari, Y., Atsuzawa, K., Usuda, N., Watashi, K., Hishiki, T., Zayas, M., Bartenschlager, R., Wakita, T., Hijikata, M., and Shimotohno, K. (2007). The lipid droplet is an important organelle for hepatitis C virus production. *Nat Cell Biol* 9, 1089–1097.
- Mizushima, N., Yamamoto, A., Hatano, M., Kobayashi, Y., Kabeya, Y., Suzuki, K., Tokuhiya, T., Ohsumi, Y., and Yoshimori, T. (2001). Dissection of Autophagosome Formation Using Apg5-Deficient Mouse Embryonic Stem Cells. *J Cell Biology* 152, 657–668.
- Moradpour, D., Englert, C., Wakita, T., and Wands, J.R. (1996). Characterization of Cell Lines Allowing Tightly Regulated Expression of Hepatitis C Virus Core Protein. *Virology* 222, 51–63.
- Moskalenko, S., Henry, D.O., Rosse, C., Mirey, G., Camonis, J.H., and White, M.A. (2002). The exocyst is a Ral effector complex. *Nat Cell Biol* 4, 66–72.
- Moskalenko, S., Tong, C., Rosse, C., Mirey, G., Formstecher, E., Daviet, L., Camonis, J., and White, M.A. (2003). Ral GTPases Regulate Exocyst Assembly through Dual Subunit Interactions\*. *J Biol Chem* 278, 51743–51748.
- Muallem, S., Chung, W.Y., Jha, A., and Ahuja, M. (2017). Lipids at membrane contact sites: cell signaling and ion transport. *Embo Rep* 18, 1893–1904.

- Murphy, S.E., and Levine, T.P. (2016). VAP, a Versatile Access Point for the Endoplasmic Reticulum: Review and analysis of FFAT-like motifs in the VAPome. *Biochimica Et Biophysica Acta Bba - Mol Cell Biology Lipids* 1861, 952–961.
- Mylonis, I., Sembongi, H., Befani, C., Liakos, P., Siniosoglou, S., and Simos, G. (2012). Hypoxia causes triglyceride accumulation by HIF-1-mediated stimulation of lipin 1 expression. *J Cell Sci* 125, 3485–3493.
- Na, T., Shin, Y.K., Roh, K.J., Kang, S., Hong, I., Oh, S.J., Seong, J.K., Park, C.K., Choi, Y.L., and Lee, M. (2009). Liver X receptor mediates hepatitis B virus X protein–induced lipogenesis in hepatitis B virus–associated hepatocellular carcinoma. *Hepatology* 49, 1122–1131.
- Naito, T., Ercan, B., Krshnan, L., Triebl, A., Koh, D.H.Z., Wei, F.-Y., Tomizawa, K., Torta, F.T., Wenk, M.R., and Saheki, Y. (2019). Movement of accessible plasma membrane cholesterol by the GRAMD1 lipid transfer protein complex. *Elife* 8, e51401.
- Nakamura, N., Banno, Y., and Tamiya-Koizumi, K. (2005). Arf1-dependent PLD1 is localized to oleic acid-induced lipid droplets in NIH3T3 cells. *Biochemical and Biophysical Research Communications* 335, 117–123.
- Neel, N.F., Rossman, K.L., Martin, T.D., Hayes, T.K., Yeh, J.J., and Der, C.J. (2012). The RalB Small GTPase Mediates Formation of Invadopodia through a GTPase-Activating Protein-Independent Function of the RalBP1/RLIP76 Effector. *Mol Cell Biol* 32, 1374–1386.
- Newton, A.C. (2018). Protein kinase C: perfectly balanced. *Crit Rev Biochem Mol* 53, 208–230.
- Neyraud, V., Aushev, V.N., Hatzoglou, A., Meunier, B., Cascone, I., and Camonis, J. (2012). RalA and RalB Proteins Are Ubiquitinated GTPases, and Ubiquitinated RalA Increases Lipid Raft Exposure at the Plasma Membrane. *Journal of Biological Chemistry* 287, 29397–29405.
- Nguyen, T.B., Louie, S.M., Daniele, J.R., Tran, Q., Dillin, A., Zoncu, R., Nomura, D.K., and Olzmann, J.A. (2017). DGAT1-Dependent Lipid Droplet Biogenesis Protects Mitochondrial Function during Starvation- Induced Autophagy. *Developmental Cell* 42, 1–19.
- Nicely, N.I., Kosak, J., Serrano, V. de, and Mattos, C. (2004). Crystal Structures of Ral-GppNHp and Ral-GDP Reveal Two Binding Sites that Are Also Present in Ras and Rap. *Structure* 12, 2025–2036.
- Nishimura, A., and Linder, M.E. (2013). Identification of a Novel Prenyl and Palmitoyl Modification at the CaaX Motif of Cdc42 That Regulates RhoGDI Binding. *Mol Cell Biol* 33, 1417–1429.
- Nishino, N., Tamori, Y., Tateya, S., Kawaguchi, T., Shibakusa, T., Mizunoya, W., Inoue, K., Kitazawa, R., Kitazawa, S., Matsuki, Y., et al. (2008). FSP27 contributes to efficient energy storage in murine white adipocytes by promoting the formation of unilocular lipid droplets. *J Clin Invest* 118, 2808–2821.
- Noda, T., and Ohsumi, Y. (1998). Tor, a Phosphatidylinositol Kinase Homologue, Controls Autophagy in Yeast\*. *J Biol Chem* 273, 3963–3966.

- Nose, F., Yamaguchi, T., Kato, R., Aiuchi, T., Obama, T., Hara, S., Yamamoto, M., and Itabe, H. (2013). Crucial Role of Perilipin-3 (TIP47) in Formation of Lipid Droplets and PGE2 Production in HL-60-Derived Neutrophils. *PLoS ONE* *8*, e71542-9.
- Ohsaki, Y., Kawai, T., Yoshikawa, Y., Cheng, J., Jokitalo, E., and Fujimoto, T. (2016). PML isoform II plays a critical role in nuclear lipid droplet formation. *J Cell Biol* *212*, 29–38.
- Ohta, Y., SUZUKI, N., NAKAMURA, S., HARTWIG, J.H., and STOSSEL, T.P. (1999). The small GTPase RalA targets filamin to induce filopodia. 1–7.
- Olzmann, J.A., and Carvalho, P. (2019). Dynamics and functions of lipid droplets. *Nat Rev Mol Cell Bio* *20*, 137–155.
- Ouimet, M., Hennessy, E.J., Solingen, C. van, Koelwyn, G.J., Hussein, M.A., Ramkhelawon, B., Rayner, K.J., Temel, R.E., Perisic, L., Hedin, U., et al. (2016). miRNA Targeting of Oxysterol-Binding Protein-Like 6 Regulates Cholesterol Trafficking and Efflux. *Arteriosclerosis Thrombosis Vasc Biology* *36*, 942–951.
- Ozanne, D.M., Brady, M.E., Cook, S., Gaughan, L., Neal, D.E., and Robson, C.N. (2000). Androgen Receptor Nuclear Translocation Is Facilitated by the f-Actin Cross-Linking Protein Filamin. *Mol Endocrinol* *14*, 1618–1626.
- Ozeki, S., Cheng, J., Tauchi-Sato, K., Hatano, N., Taniguchi, H., and Fujimoto, T. (2005). Rab18 localizes to lipid droplets and induces their close apposition to the endoplasmic reticulum-derived membrane. *J Cell Sci* *118*, 2601–2611.
- Pagac, M., Cooper, D.E., Qi, Y., Lukmantara, I.E., Mak, H.Y., Wu, Z., Tian, Y., Liu, Z., Lei, M., Du, X., et al. (2016). SEIPIN Regulates Lipid Droplet Expansion and Adipocyte Development by Modulating the Activity of Glycerol-3-phosphate Acyltransferase. *CellReports* *17*, 1546–1559.
- Pagnon, J., Matzaris, M., Stark, R., Meex, R.C.R., Macaulay, S.L., Brown, W., O'Brien, P.E., Tiganis, T., and Watt, M.J. (2012). Identification and Functional Characterization of Protein Kinase A Phosphorylation Sites in the Major Lipolytic Protein, Adipose Triglyceride Lipase. *Endocrinology* *153*, 4278–4289.
- Palacios-Moreno, J., Foltz, L., Guo, A., Stokes, M.P., Kuehn, E.D., George, L., Comb, M., and Grimes, M.L. (2015). Neuroblastoma Tyrosine Kinase Signaling Networks Involve FYN and LYN in Endosomes and Lipid Rafts. *Plos Comput Biol* *11*, e1004130.
- Pan, X., Roberts, P., Chen, Y., Kvam, E., Shulga, N., Huang, K., Lemmon, S., and Goldfarb, D.S. (2000). Nucleus–Vacuole Junctions in *Saccharomyces cerevisiae* Are Formed Through the Direct Interaction of Vac8p with Nvj1p. *Mol Biol Cell* *11*, 2445–2457.
- Pankiv, S., Clausen, T.H., Lamark, T., Brech, A., Bruun, J.-A., Outzen, H., Øvervatn, A., Bjørkøy, G., and Johansen, T. (2007). p62/SQSTM1 Binds Directly to Atg8/LC3 to Facilitate Degradation of Ubiquitinated Protein Aggregates by Autophagy\*. *J Biol Chem* *282*, 24131–24145.
- Park, J.-B. (2001). Regulation of GTP-binding state in RalA through Ca<sup>2+</sup> and calmodulin. *Exp Mol Medicine* *33*, 54–58.

- Park, S.H., and Weinberg, R.A. (1995). A putative effector of Ral has homology to Rho/Rac GTPase activating proteins. *Oncogene* *11*, 2349–2355.
- Peretti, D., Kim, S., Tufi, R., and Lev, S. (2020). Lipid Transfer Proteins and Membrane Contact Sites in Human Cancer. *Frontiers Cell Dev Biology* *7*, 371.
- Peschard, P., McCarthy, A., Leblanc-Dominguez, V., Yeo, M., Guichard, S., Stamp, G., and Marshall, C.J. (2012). Genetic deletion of RALA and RALB small GTPases reveals redundant functions in development and tumorigenesis. *Current Biology : CB* *22*, 2063–2068.
- Petan, T., Jarc, E., and Jusović, M. (2018). Lipid Droplets in Cancer: Guardians of Fat in a Stressful World. *Molecules* *23*, 1941.
- Pollock, S.R., Schinlever, A.R., Rohani, A., Kashatus, J.A., and Kashatus, D.F. (2019). RalA and RalB relocalization to depolarized mitochondria depends on clathrin-mediated endocytosis and facilitates TBK1 activation. *PLoS ONE* *14*, e0214764-22.
- Potocký, M., Pleskot, R., Pejchar, P., Vitale, N., Kost, B., and Žárský, V. (2014). Live-cell imaging of phosphatidic acid dynamics in pollen tubes visualized by Spo20p-derived biosensor. *New Phytol* *203*, 483–494.
- Puri, V., Konda, S., Ranjit, S., Aouadi, M., Chawla, A., Chouinard, M., Chakladar, A., and Czech, M.P. (2007). Fat-specific Protein 27, a Novel Lipid Droplet Protein That Enhances Triglyceride Storage. *J Biol Chem* *282*, 34213–34218.
- Qiu, B., Ackerman, D., Sanchez, D.J., Li, B., Ochocki, J.D., Grazioli, A., Bobrovnikova-Marjon, E., Diehl, J.A., Keith, B., and Simon, M.C. (2015). HIF2 $\alpha$ -Dependent Lipid Storage Promotes Endoplasmic Reticulum Homeostasis in Clear-Cell Renal Cell Carcinoma. *Cancer Discov* *5*, 652–667.
- Quilliam, L.A., Rebhun, J.F., and Castro, A.F. (2002). A growing family of guanine nucleotide exchange factors is responsible for activation of ras-family GTPases. *Prog Nucleic Acid Re* *71*, 391–444.
- Raiborg, C., Wenzel, E.M., Pedersen, N.M., Olsvik, H., Schink, K.O., Schultz, S.W., Vietri, M., Nisi, V., Bucci, C., Brech, A., et al. (2015). Repeated ER–endosome contacts promote endosome translocation and neurite outgrowth. *Nature* *520*, 234–238.
- Rambold, A.S., Kostecky, B., Elia, N., and Lippincott-Schwartz, J. (2011). Tubular network formation protects mitochondria from autophagosomal degradation during nutrient starvation. *1–6*.
- Rambold, A.S., Cohen, S., and Lippincott-Schwartz, J. (2015). Fatty Acid Trafficking in Starved Cells: Regulation by Lipid Droplet Lipolysis, Autophagy, and Mitochondrial Fusion Dynamics. *DEVCEL* *32*, 678–692.
- Raveh-Amit, H., Maissel, A., Poller, J., Marom, L., Elroy-Stein, O., Shapira, M., and Livneh, E. (2009). Translational Control of Protein Kinase C $\eta$  by Two Upstream Open Reading Frames  $\nabla$ . *Mol Cell Biol* *29*, 6140–6148.

- Rebhun, J.F., Chen, H., and Quilliam, L.A. (2000). Identification and Characterization of a New Family of Guanine Nucleotide Exchange Factors for the Ras-related GTPase Ral\*. *J Biol Chem* 275, 13406–13410.
- Rizzo, M.A., Shome, K., Watkins, S.C., and Romero, G. (2000). The Recruitment of Raf-1 to Membranes Is Mediated by Direct Interaction with Phosphatidic Acid and Is Independent of Association with Ras\*. *J Biol Chem* 275, 23911–23918.
- Robenek, H., Lorkowski, S., Schnoor, M., and Troyer, D. (2005). Spatial Integration of TIP47 and Adipophilin in Macrophage Lipid Bodies\*. *J Biol Chem* 280, 5789–5794.
- Rocha, N., Kuijl, C., Kant, R. van der, Janssen, L., Houben, D., Janssen, H., Zwart, W., and Neeffjes, J. (2009). Cholesterol sensor ORP1L contacts the ER protein VAP to control Rab7–RILP–p150Glued and late endosome positioning. *J Cell Biology* 185, 1209–1225.
- Rohwedder, A., Zhang, Q., Rudge, S.A., and Wakelam, M.J.O. (2014). Lipid droplet formation in response to oleic acid in Huh-7 cells is mediated by the fatty acid receptor FFAR4. *Journal of Cell Science* 127, 3104–3115.
- Roman, M., Wrobel, T.P., Panek, A., Paluszkiewicz, C., and Kwiatek, W.M. (2020). Lipid droplets in prostate cancer cells and effect of irradiation studied by Raman microspectroscopy. *Biochimica Et Biophysica Acta Bba - Mol Cell Biology Lipids* 1865, 158753.
- Rossé, C., L'Hoste, S., Offner, N., Picard, A., and Camonis, J. (2003). RLIP, an Effector of the Ral GTPases, Is a Platform for Cdk1 to Phosphorylate Epsin during the Switch Off of Endocytosis in Mitosis\*. *J Biol Chem* 278, 30597–30604.
- Rozeveld, C.N., Johnson, K.M., Zhang, L., and Razidlo, G.L. (2020). KRAS Controls Pancreatic Cancer Cell Lipid Metabolism and Invasive Potential through the Lipase HSL. *Cancer Res* 80, 4932–4945.
- Rudoni, S., Colombo, S., Coccetti, P., and Martegani, E. (2001). Role of guanine nucleotides in the regulation of the Ras/cAMP pathway in *Saccharomyces cerevisiae*. 1–9.
- Ruiter, N.D. de, Wolthuis, R.M.F., Dam, H. van, Burgering, B.M.T., and Bos, J.L. (2000). Ras-Dependent Regulation of c-Jun Phosphorylation Is Mediated by the Ral Guanine Nucleotide Exchange Factor-Ral Pathway. *Mol Cell Biol* 20, 8480–8488.
- Sablina, A.A., Chen, W., Arroyo, J.D., Corral, L., Hector, M., Bulmer, S.E., DeCaprio, J.A., and Hahn, W.C. (2007). The Tumor Suppressor PP2A A $\beta$  Regulates the RalA GTPase. *Cell* 129, 969–982.
- Saka, H.A., and Valdivia, R. (2012). Emerging Roles for Lipid Droplets in Immunity and Host-Pathogen Interactions. *Annu Rev Cell Dev Bi* 28, 411–437.
- Sakaki, K., Wu, J., and Kaufman, R.J. (2008). Protein Kinase C $\theta$  Is Required for Autophagy in Response to Stress in the Endoplasmic Reticulum\*. *J Biol Chem* 283, 15370–15380.

- Salo, V.T., Belevich, I., Li, S., Karhinen, L., Vihinen, H., Vigouroux, C., Magré, J., Thiele, C., Hölttä-Vuori, M., Jokitalo, E., et al. (2016). Seipin regulates ER–lipid droplet contacts and cargo delivery. *Embo J* 35, 2699–2716.
- Salo, V.T., Li, S., Vihinen, H., Hölttä-Vuori, M., Szkalicity, A., Horvath, P., Belevich, I., Peränen, J., Thiele, C., Somerharju, P., et al. (2019). Seipin Facilitates Triglyceride Flow to Lipid Droplet and Counteracts Droplet Ripening via Endoplasmic Reticulum Contact. *Dev Cell* 50, 478-493.e9.
- Samsa, M.M., Mondotte, J.A., Iglesias, N.G., Assunção-Miranda, I., Barbosa-Lima, G., Poian, A.T.D., Bozza, P.T., and Gamarnik, A.V. (2009). Dengue Virus Capsid Protein Usurps Lipid Droplets for Viral Particle Formation. *Plos Pathog* 5, e1000632.
- Sandhu, J., Li, S., Fairall, L., Pfisterer, S.G., Gurnett, J.E., Xiao, X., Weston, T.A., Vashi, D., Ferrari, A., Orozco, J.L., et al. (2018). Aster Proteins Facilitate Nonvesicular Plasma Membrane to ER Cholesterol Transport in Mammalian Cells. *Cell* 175, 514-529.e20.
- Sarkar, S., Floto, R.A., Berger, Z., Imarisio, S., Cordenier, A., Pasco, M., Cook, L.J., and Rubinsztein, D.C. (2005). Lithium induces autophagy by inhibiting inositol monophosphatase. *J Cell Biology* 170, 1101–1111.
- Sawamoto, K., Winge, P., Koyama, S., Hirota, Y., Yamada, C., Miyao, S., Yoshikawa, S., Jin, M., Kikuchi, A., and Okano, H. (1999). The Drosophila Ral GTPase Regulates Developmental Cell Shape Changes through the Jun NH2-terminal Kinase Pathway. *J Cell Biology* 146, 361–372.
- Schroeder, B., Schulze, R.J., Weller, S.G., Sletten, A.C., Casey, C.A., and McNiven, M.A. (2015). The small GTPase Rab7 as a central regulator of hepatocellular lipophagy. *Hepatology* 61, 1896–1907.
- Schuldiner, M., and Bohnert, M. (2017). A different kind of love – lipid droplet contact sites. *BBA - Molecular and Cell Biology of Lipids* 1862, 1188–1196.
- Schulze, R.J., Krueger, E.W., Weller, S.G., Johnson, K.M., Casey, C.A., Schott, M.B., and McNiven, M.A. (2020). Direct lysosome-based autophagy of lipid droplets in hepatocytes. *Proc National Acad Sci* 117, 32443–32452.
- Schweiger, M., Paar, M., Eder, C., Brandis, J., Moser, E., Gorkiewicz, G., Grond, S., Radner, F.P.W., Cerk, I., Cornaciu, I., et al. (2012). G0/G1 switch gene-2 regulates human adipocyte lipolysis by affecting activity and localization of adipose triglyceride lipase. *J Lipid Res* 53, 2307–2317.
- Sebastian, T.T., Baldrige, R.D., Xu, P., and Graham, T.R. (2012). Phospholipid flippases: Building asymmetric membranes and transport vesicles. *Biochimica Et Biophysica Acta Bba - Mol Cell Biology Lipids* 1821, 1068–1077.
- Sha, B., Phillips, S.E., Bankaitis, V.A., and Luo, M. (1998). Crystal structure of the *Saccharomyces cerevisiae* phosphatidylinositol- transfer protein. *Nature* 391, 506–510.
- Shao, H., and Andres, D.A. (2000). A Novel RalGEF-like Protein, RGL3, as a Candidate Effector for Rit and Ras\*. *J Biol Chem* 275, 26914–26924.

- Sharma, K., D'Souza, R.C.J., Tyanova, S., Schaab, C., Wiśniewski, J.R., Cox, J., and Mann, M. (2014). Ultradeep Human Phosphoproteome Reveals a Distinct Regulatory Nature of Tyr and Ser/Thr-Based Signaling. *Cell Reports* 8, 1583–1594.
- Shaw, C.S., Jones, D.A., and Wagenmakers, A.J.M. (2008). Network distribution of mitochondria and lipid droplets in human muscle fibres. *Histochem Cell Biol* 129, 65–72.
- Shipitsin, M., and Feig, L.A. (2004). RalA but Not RalB Enhances Polarized Delivery of Membrane Proteins to the Basolateral Surface of Epithelial Cells. *Molecular and Cellular Biology* 24, 5746–5756.
- Shirakawa, R., Fukai, S., Kawato, M., Higashi, T., Kondo, H., Ikeda, T., Nakayama, E., Okawa, K., Nureki, O., Kimura, T., et al. (2009). Tuberos Sclerosis Tumor Suppressor Complex-like Complexes Act as GTPase-activating Proteins for Ral GTPases\*. *J Biol Chem* 284, 21580–21588.
- Sidhu, R.S., Clough, R.R., and Bhullar, R.P. (2005a). Regulation of Phospholipase C- $\delta$ 1 through Direct Interactions with the Small GTPase Ral and Calmodulin\*. *J Biol Chem* 280, 21933–21941.
- Sidhu, R.S., Elsaraj, S.M., Grujic, O., and Bhullar, R.P. (2005b). Calmodulin binding to the small GTPase Ral requires isoprenylated Ral. *Biochemical and Biophysical Research Communications* 336, 105–109.
- Simicek, M., Lievens, S., Laga, M., Guzenko, D., Aushev, V.N., Kalev, P., Baietti, M.F., Strelkov, S.V., Gevaert, K., Tavernier, J., et al. (2013). The deubiquitylase USP33 discriminates between RALB functions in autophagy and innate immune response. *Nature Cell Biology* 15, 1220–1230.
- Singer, W.D., Brown, H.A., Jiang, X., and Sternweis, P.C. (1996). Regulation of Phospholipase D by Protein Kinase C Is Synergistic with ADP-ribosylation Factor and Independent of Protein Kinase Activity (\*). *J Biol Chem* 271, 4504–4510.
- Singh, M.K., Martin, A.P.J., Joffre, C., Zago, G., Camonis, J., Coppey, M., and Parrini, M.C. (2019). Localization of RalB signaling at endomembrane compartments and its modulation by autophagy. *Nature Publishing Group* 9, 8910–8913.
- Singh, R., Kaushik, S., Wang, Y., Xiang, Y., Novak, I., Komatsu, M., Tanaka, K., Cuervo, A.M., and Czaja, M.J. (2009). Autophagy regulates lipid metabolism. *Nature* 458, 1131–1135.
- Singhal, S.S., Wickramarachchi, D., Yadav, S., Singhal, J., Leake, K., Vatsyayan, R., Chaudhary, P., Lelsani, P., Suzuki, S., Yang, S., et al. (2011). Glutathione-Conjugate Transport by RLIP76 Is Required for Clathrin-Dependent Endocytosis and Chemical Carcinogenesis. *Mol Cancer Ther* 10, 16–28.
- Skinner, J.R., Shew, T.M., Schwartz, D.M., Tzekov, A., Lopus, C.M., Abumrad, N.A., and Wolins, N.E. (2009). Diacylglycerol Enrichment of Endoplasmic Reticulum or Lipid Droplets Recruits Perilipin 3/TIP47 during Lipid Storage and Mobilization. 1–8.
- Skorobogatko, Y., Dragan, M., Cordon, C., Reilly, S.M., Hung, C.-W., Xia, W., Zhao, P., Wallace, M., Lackey, D.E., Chen, X.-W., et al. (2018). RalA controls glucose homeostasis by regulating glucose uptake in brown fat. *Proceedings of the National Academy of Sciences* 115, 7819–7824.

- Smith, S.C., Oxford, G., Baras, A.S., Owens, C., Havaleshko, D., Brautigan, D.L., Safo, M.K., and Theodorescu, D. (2007). Expression of Ral GTPases, Their Effectors, and Activators in Human Bladder Cancer. *Clin Cancer Res* 13, 3803–3813.
- Spiczka, K.S., and Yeaman, C. (2008). Ral-regulated interaction between Sec5 and paxillin targets Exocyst to focal complexes during cell migration. *J Cell Sci* 121, 2880–2891.
- Stahelin, R.V., Ananthanarayanan, B., Blatner, N.R., Singh, S., Bruzik, K.S., Murray, D., and Cho, W. (2004). Mechanism of Membrane Binding of the Phospholipase D1 PX Domain. *Journal of Biological Chemistry* 279, 54918–54926.
- Steinberg, G.R., Kemp, B.E., and Watt, M.J. (2007). Adipocyte triglyceride lipase expression in human obesity. *Am J Physiol-Endoc M* 293, E958–E964.
- Su, W., Yeku, O., Olepu, S., Genna, A., Park, J.-S., Ren, H., Du, G., Gelb, M.H., Morris, A.J., and Frohman, M.A. (2009). 5-Fluoro-2-indolyl des-chlorohalopemide (FIPI), a phospholipase D pharmacological inhibitor that alters cell spreading and inhibits chemotaxis. *Molecular Pharmacology* 75, 437–446.
- Sugihara, K., Asano, S., Tanaka, K., Iwamatsu, A., Okawa, K., and Ohta, Y. (2001). The exocyst complex binds the small GTPase RalA to mediate filopodia formation. *Nature Cell Biology* 4, 73–78.
- Sullivan, M.R., Danai, L.V., Lewis, C.A., Chan, S.H., Gui, D.Y., Kunchok, T., Dennstedt, E.A., Heiden, M.G.V., and Muir, A. (2019). Quantification of microenvironmental metabolites in murine cancers reveals determinants of tumor nutrient availability. *Elife* 8, e44235.
- Sunami, Y., Rebelo, A., and Kleeff, J. (2017). Lipid Metabolism and Lipid Droplets in Pancreatic Cancer and Stellate Cells. *Cancers* 10, 3.
- Sung, T.C. (1997). Mutagenesis of phospholipase D defines a superfamily including a trans-Golgi viral protein required for poxvirus pathogenicity. *The EMBO Journal* 16, 4519–4530.
- Sung, T.-C., Roper, R.L., Zhang, Y., Rudge, S.A., Temel, R., Hammond, S.M., Morris, A.J., Moss, B., Engebrecht, J., and Frohman, M.A. (1997). Mutagenesis of phospholipase D defines a superfamily including a trans-Golgi viral protein required for poxvirus pathogenicity. 1–12.
- Suzuki, M., Iio, Y., Saito, N., and Fujimoto, T. (2013). Protein kinase C $\eta$  is targeted to lipid droplets. *Histochem Cell Biol* 139, 505–511.
- Sztalryd, C., Bell, M., Lu, X., Mertz, P., Hickenbottom, S., Chang, B.H.-J., Chan, L., Kimmel, A.R., and Londos, C. (2006). Functional Compensation for Adipose Differentiation-related Protein (ADFP) by Tip47 in an ADFP Null Embryonic Cell Line\*. *J Biol Chem* 281, 34341–34348.
- Szymanski, K.M., Binns, D., Bartz, R., Grishin, N.V., Li, W.-P., Agarwal, A.K., Garg, A., Anderson, R.G.W., and Goodman, J.M. (2007). The lipodystrophy protein seipin is found at endoplasmic reticulum lipid droplet junctions and is important for droplet morphology. *Proc National Acad Sci* 104, 20890–20895.

- Tanguy, E., Kassas, N., and Vitale, N. (2018). Protein–Phospholipid Interaction Motifs: A Focus on Phosphatidic Acid. *Biomolecules* 8, 20–29.
- Tanguy, E., Wang, Q., Moine, H., and Vitale, N. (2019). Phosphatidic Acid: From Pleiotropic Functions to Neuronal Pathology. *Frontiers in Cellular Neuroscience* 13, 19470–19478.
- Tanguy, E., Bagneaux, P.C. de, Kassas, N., Ammar, M.-R., Wang, Q., Haeberlé, A.-M., Raheirindratsara, J., Fouillen, L., Renard, P.-Y., Montero-Hadjadje, M., et al. (2020). Mono- and Polyunsaturated Phosphatidic Acid Regulate Distinct Steps of Regulated Exocytosis in Neuroendocrine Cells. *Cell Reports* 32, 108026.
- Tarnopolsky, M.A., Rennie, C.D., Robertshaw, H.A., Fedak-Tarnopolsky, S.N., Devries, M.C., and Hamadeh, M.J. (2007). Influence of endurance exercise training and sex on intramyocellular lipid and mitochondrial ultrastructure, substrate use, and mitochondrial enzyme activity. *Am J Physiology-Regulatory Integr Comp Physiology* 292, R1271–R1278.
- Taschler, U., Radner, F.P.W., Heier, C., Schreiber, R., Schweiger, M., Schoiswohl, G., Preiss-Landl, K., Jaeger, D., Reiter, B., Koefeler, H.C., et al. (2011). Monoglyceride Lipase Deficiency in Mice Impairs Lipolysis and Attenuates Diet-induced Insulin Resistance\*. *J Biol Chem* 286, 17467–17477.
- Theodorescu, D. (2017). RAL GTPases: Biology and potential as therapeutic targets in cancer. 1–38.
- Thiam, A.R., and Forêt, L. (2016). The physics of lipid droplet nucleation, growth and budding. *Biochimica Et Biophysica Acta Bba - Mol Cell Biology Lipids* 1861, 715–722.
- Toda, K., Nogami, M., Murakami, K., Kanaho, Y., and Nakayama, K. (1999). Colocalization of phospholipase D1 and GTP-binding-defective mutant of ADP-ribosylation factor 6 to endosomes and lysosomes. *Febs Lett* 442, 221–225.
- Toh, S.Y., Gong, J., Du, G., Li, J.Z., Yang, S., Ye, J., Yao, H., Zhang, Y., Xue, B., Li, Q., et al. (2008). Up-Regulation of Mitochondrial Activity and Acquirement of Brown Adipose Tissue-Like Property in the White Adipose Tissue of Fsp27 Deficient Mice. *Plos One* 3, e2890.
- Trinh, M.N., Brown, M.S., Goldstein, J.L., Han, J., Vale, G., McDonald, J.G., Seemann, J., Mendell, J.T., and Lu, F. (2020). Last step in the path of LDL cholesterol from lysosome to plasma membrane to ER is governed by phosphatidylserine. *Proc National Acad Sci* 117, 18521–18529.
- Tsujishita, Y., and Hurley, J.H. (2000). Structure and lipid transport mechanism of a StAR-related domain. *Nat Struct Biol* 7, 408–414.
- Vaughan, M., and Steinberg, D. (1963). Effect of hormones on lipolysis and esterification of free fatty acids during incubation of adipose tissue in vitro \*. *J Lipid Res* 4, 193–199.
- Vaughan, M., Berger, J.E., and Steinberg, D. (1964). Hormone-sensitive Lipase and Monoglyceride Lipase Activities in Adipose Tissue. *J Biol Chem* 239, 401–409.
- Vicencio, J.M., Ortiz, C., Criollo, A., Jones, A.W.E., Kepp, O., Galluzzi, L., Joza, N., Vitale, I., Morselli, E., Tailler, M., et al. (2009). The inositol 1,4,5-trisphosphate receptor regulates autophagy through its interaction with Beclin 1. *Cell Death Differ* 16, 1006–1017.

- Villena, J.A., Roy, S., Sarkadi-Nagy, E., Kim, K.-H., and Sul, H.S. (2004). Desnutrin, an Adipocyte Gene Encoding a Novel Patatin Domain-containing Protein, Is Induced by Fasting and Glucocorticoids ECTOPIC EXPRESSION OF DESNUTRIN INCREASES TRIGLYCERIDE HYDROLYSIS\*. *J Biol Chem* 279, 47066–47075.
- Vitale, N., Mawet, J., Camonis, J., Regazzi, R., Bader, M.-F., and Chasserot-Golaz, S. (2005). The Small GTPase RalA Controls Exocytosis of Large Dense Core Secretory Granules by Interacting with ARF6-dependent Phospholipase D1\*. *J Biol Chem* 280, 29921–29928.
- Vries, J.E. de, Vork, M.M., Roemen, T.H., Jong, Y.F. de, Cleutjens, J.P., Vusse, G.J. van der, and Bilsen, M. van (1997). Saturated but not mono-unsaturated fatty acids induce apoptotic cell death in neonatal rat ventricular myocytes. *J Lipid Res* 38, 1384–1394.
- Walther, T.C., Chung, J., and Jr, R.V.F. (2017). Lipid Droplet Biogenesis. *Annual Review of Cell and Developmental Biology* 33, 491–510.
- Wang, K.L., and Roufogalis, B.D. (1999). Ca<sup>2+</sup>/Calmodulin Stimulates GTP Binding to the Ras-related Protein Ral-A\*. *J Biol Chem* 274, 14525–14528.
- Wang, C., Liu, Z., and Huang, X. (2012). Rab32 Is Important for Autophagy and Lipid Storage in *Drosophila*. *Plos One* 7, e32086.
- Wang, C.-W., Miao, Y.-H., and Chang, Y.-S. (2014). A sterol-enriched vacuolar microdomain mediates stationary phase lipophagy in budding yeast. *J Cell Biol* 206, 357–366.
- Wang, H., Owens, C., Chandra, N., Conaway, M.R., Brautigam, D.L., and Theodorescu, D. (2010a). Phosphorylation of RalB is important for bladder cancer cell growth and metastasis. *Cancer Research* 70, 8760–8769.
- Wang, H., Wei, E., Quiroga, A.D., Sun, X., Touret, N., and Lehner, R. (2010b). Altered Lipid Droplet Dynamics in Hepatocytes Lacking Triacylglycerol Hydrolase Expression. *Mol Biol Cell* 21, 1991–2000.
- Wang, H., Sreenivasan, U., Hu, H., Saladino, A., Polster, B.M., Lund, L.M., Gong, D., Stanley, W.C., and Sztalryd, C. (2011). Perilipin 5, a lipid droplet-associated protein, provides physical and metabolic linkage to mitochondria. *Journal of Lipid Research* 52, 2159–2168.
- Wang, H., Becuwe, M., Housden, B.E., Chitraju, C., Porras, A.J., Graham, M.M., Liu, X.N., Thiam, A.R., Savage, D.B., Agarwal, A.K., et al. (2016). Seipin is required for converting nascent to mature lipid droplets. *Elife* 5, e16582.
- Wang, K.L., Khan, M.T., and Roufogalis, B.D. (1997). Identification and Characterization of a Calmodulin-binding Domain in Ral-A, a Ras-related GTP-binding Protein Purified from Human Erythrocyte Membrane\*. *J Biol Chem* 272, 16002–16009.
- Wang, L., Li, G., and Sugita, S. (2004). RalA-Exocyst Interaction Mediates GTP-dependent Exocytosis\*. *J Biol Chem* 279, 19875–19881.

- Wang, Q., Wang, J.-Y., Zhang, X.-P., Lv, Z.-W., Fu, D., Lu, Y.-C., Hu, G.-H., Luo, C., and Chen, J.-X. (2013). RLIP76 is overexpressed in human glioblastomas and is required for proliferation, tumorigenesis and suppression of apoptosis. *Carcinogenesis* *34*, 916–926.
- Wang, S.H., Shih, Y.L., Ko, W.C., Wei, Y.H., and Shih, C.M. (2008). Cadmium-induced autophagy and apoptosis are mediated by a calcium signaling pathway. *Cell Mol Life Sci* *65*, 3640–3652.
- Wang, Z.Q., Yu, Y., Zhang, X.H., Floyd, E.Z., and Cefalu, W.T. (2010c). Human adenovirus 36 decreases fatty acid oxidation and increases de novo lipogenesis in primary cultured human skeletal muscle cells by promoting Cidec/FSP27 expression. *Int J Obesity* *34*, 1355–1364.
- Watt, M.J., and Steinberg, G.R. (2008). Regulation and function of triacylglycerol lipases in cellular metabolism. *Biochem J* *414*, 313–325.
- Wilfling, F., Wang, H., Haas, J.T., Krahmer, N., Gould, T.J., Uchida, A., Cheng, J.-X., Graham, M., Christiano, R., Fröhlich, F., et al. (2013). Triacylglycerol Synthesis Enzymes Mediate Lipid Droplet Growth by Relocalizing from the ER to Lipid Droplets. *DEVCEL* *24*, 384–399.
- Wilfling, F., Thiam, A.R., Olarte, M.-J., Wang, J., Beck, R., Gould, T.J., Allgeyer, E.S., Pincet, F., Bewersdorf, J., Jr, R.V.F., et al. (2014). Arf1/COPI machinery acts directly on lipid droplets and enables their connection to the ER for protein targeting. *ELife* *3*, 604–620.
- Wilhelm, L.P., Wendling, C., Védie, B., Kobayashi, T., Chenard, M., Tomasetto, C., Drin, G., and Alpy, F. (2017). STARD3 mediates endoplasmic reticulum-to-endosome cholesterol transport at membrane contact sites. *Embo J* *36*, 1412–1433.
- Wolins, N.E., Rubin, B., and Brasaemle, D.L. (2001). TIP47 Associates with Lipid Droplets\*. *J Biol Chem* *276*, 5101–5108.
- Wolins, N.E., Quaynor, B.K., Skinner, J.R., Schoenfish, M.J., Tzekov, A., and Bickel, P.E. (2005). S3-12, Adipophilin, and TIP47 Package Lipid in Adipocytes\*. *J Biol Chem* *280*, 19146–19155.
- Wolinski, H., Hofbauer, H.F., Hellauer, K., Cristobal-Sarramian, A., Kolb, D., Radulovic, M., Knittelfelder, O.L., Rechberger, G.N., and Kohlwein, Sepp.D. (2015). Seipin is involved in the regulation of phosphatidic acid metabolism at a subdomain of the nuclear envelope in yeast. *Biochimica Et Biophysica Acta Bba - Mol Cell Biology Lipids* *1851*, 1450–1464.
- Wolthuis, R.M., Bauer, B., Veer, L.J. van 't, Vries-Smits, A.M. de, Cool, R.H., Spaargaren, M., Wittinghofer, A., Burgering, B.M., and Bos, J.L. (1996). RalGDS-like factor (Rlf) is a novel Ras and Rap 1A-associating protein. *Oncogene* *13*, 353–362.
- Wong, L.H., Gatta, A.T., and Levine, T.P. (2019). Lipid transfer proteins: the lipid commute via shuttles, bridges and tubes. *Nat Rev Mol Cell Bio* *20*, 85–101.
- Wu, J.C., Chen, T.Y., Yu, C.T.R., Tsai, S.J., Hsu, J.M., Tang, M.J., Chou, C.K., Lin, W.J., Yuan, C.J., and Huang, C.Y.F. (2005). Identification of V23RalA-Ser194 as a Critical Mediator for Aurora-A-induced Cellular Motility and Transformation by Small Pool Expression Screening. *Journal of Biological Chemistry* *280*, 9013–9022.

- Wu, X., Geng, F., Cheng, X., Guo, Q., Zhong, Y., Cloughesy, T.F., Yong, W.H., Chakravarti, A., and Guo, D. (2020). Lipid Droplets Maintain Energy Homeostasis and Glioblastoma Growth via Autophagic Release of Stored Fatty Acids. *Iscience* *23*, 101569.
- Wu, Z., Owens, C., Chandra, N., Popovic, K., Conaway, M., and Theodorescu, D. (2010). RalBP1 Is Necessary for Metastasis of Human Cancer Cell Lines. *Neoplasia* *12*, 1003–1012.
- Xie, X., Langlais, P., Zhang, X., Heckmann, B.L., Saarinen, A.M., Mandarino, L.J., and Liu, J. (2014). Identification of a novel phosphorylation site in adipose triglyceride lipase as a regulator of lipid droplet localization. *Am J Physiol-Endoc M* *306*, E1449–E1459.
- Xu, D., Li, Y., Wu, L., Li, Y., Zhao, D., Yu, J., Huang, T., Ferguson, C., Parton, R.G., Yang, H., et al. (2018). Rab18 promotes lipid droplet (LD) growth by tethering the ER to LDs through SNARE and NRZ interactions. *The Journal of Cell Biology* *217*, 975–995.
- Yan, C., and Theodorescu, D. (2018). RAL GTPases: Biology and Potential as Therapeutic Targets in Cancer. *Pharmacological Reviews* *70*, 1–11.
- Yang, X., Lu, X., Lombès, M., Rha, G.B., Chi, Y.-I., Guerin, T.M., Smart, E.J., and Liu, J. (2010). The G0/G1 Switch Gene 2 Regulates Adipose Lipolysis through Association with Adipose Triglyceride Lipase. *Cell Metab* *11*, 194–205.
- Yoon, M.-S., Du, G., Backer, J.M., Frohman, M.A., and Chen, J. (2011). Class III PI-3-kinase activates phospholipase D in an amino acid-sensing mTORC1 pathway. *Journal of Cell Biology* *195*, 435–447.
- Zechner, R., Madeo, F., and Kratky, D. (2017). Cytosolic lipolysis and lipophagy: two sides of the same coin. *Nature Reviews Molecular Cell Biology* *18*, 671–684.
- Zhang, H., and Li, W. (2016). Dysregulation of micro-143-3p and BALBP1 contributes to the pathogenesis of the development of ovarian carcinoma. *Oncol Rep* *36*, 3605–3610.
- Zhang, X., Saarinen, A.M., Hitosugi, T., Wang, Z., Wang, L., Ho, T.H., and Liu, J. (2017). Inhibition of intracellular lipolysis promotes human cancer cell adaptation to hypoxia. *Elife* *6*, e31132.
- Zhao, G., Cardenas, H., and Matei, D. (2019). Ovarian Cancer—Why Lipids Matter. *Cancers* *11*, 1870.
- Zhao, K., Zhou, H., Zhao, X., Wolff, D.W., Tu, Y., Liu, H., Wei, T., and Yang, F. (2012). Phosphatidic acid mediates the targeting of tBid to induce lysosomal membrane permeabilization and apoptosis. *J Lipid Res* *53*, 2102–2114.
- Zheng, M., Zhang, X., Sun, N., Min, C., Zhang, X., and Kim, K.-M. (2016a). RalA employs GRK2 and  $\beta$ -arrestins for the filamin A-mediated regulation of trafficking and signaling of dopamine D2 and D3 receptor. *Biochimica Et Biophysica Acta Bba - Mol Cell Res* *1863*, 2072–2083.
- Zheng, M., Zhang, X., Guo, S., Zhang, X., Min, C., Cheon, S.H., Oak, M.-H., Kim, Y.R., and Kim, K.-M. (2016b). Agonist-induced changes in RalA activities allows the prediction of the endocytosis of G protein-coupled receptors. *Biochimica Et Biophysica Acta Bba - Mol Cell Res* *1863*, 77–90.

Zimmermann, R., Strauss, J.G., Haemmerle, G., Schoiswohl, G., Birner-Gruenberger, R., Riederer, M., Lass, A., Neuberger, G., Eisenhaber, F., Hermetter, A., et al. (2004). Fat Mobilization in Adipose Tissue Is Promoted by Adipose Triglyceride Lipase. *Science* 306, 1383–1386.

Zutphen, T. van, Todde, V., Boer, R. de, Kreim, M., Hofbauer, H.F., Wolinski, H., Veenhuis, M., Klei, I.J. van der, and Kohlwein, S.D. (2014). Lipid droplet autophagy in the yeast *Saccharomyces cerevisiae*. *Mol Biol Cell* 25, 290–301.